AD NUMBER

ADB204822

NEW LIMITATION CHANGE

TO

Approved for public release, distribution unlimited

FROM

Distribution authorized to DoD only; Proprietary Info; 13 Nov 95. Other requests shall be referred to Army Medical Research and Material Command, Attn: MCMR-RMI-S, Fort Detrick, MD 21702-5012.

AUTHORITY

USAMRMC ltr dtd 21 Jan 2000

AD_____

CONTRACT NUMBER: DAMD17-95-C-5037

TITLE: The MOST - Monitor for Oxygenation of Surface and Tissue

PRINCIPAL INVESTIGATOR: Michael P. Whalen

CONTRACTING ORGANIZATION: Cybernet Systems Corporation
Ann Arbor, Michigan 48105

REPORT DATE: October 1995

TYPE OF REPORT: Final, Phase I

PREPARED FOR: U.S. Army Medical Research and Materiel Command
Fort Detrick, Maryland 21702-5012

REPORT DOCUMENTATION PAGE

Form Approved
OMB No. 0704-0188

1. AGENCY USE ONLY *(Leave blank)*	2. REPORT DATE	3. REPORT TYPE AND DATES COVERED
	October 1995	Final, Phase I 15 Mar 95 - 14 Sep 95

4. TITLE AND SUBTITLE
The MOST - Monitor for Oxygenation of Surface and Tissue

5. FUNDING NUMBERS
DAMD17-95-C-5037

6. AUTHOR(S)
Michael P. Whalen

7. PERFORMING ORGANIZATION NAME(S) AND ADDRESS(ES)
Cybernet Systems Corporation
Ann Arbor, Michigan 48105

8. PERFORMING ORGANIZATION REPORT NUMBER

9. SPONSORING/MONITORING AGENCY NAME(S) AND ADDRESS(ES)
U.S. Army Medical Research and Materiel Command
Fort Detrick, Maryland 21702-5012

10. SPONSORING/MONITORING AGENCY REPORT NUMBER

11. SUPPLEMENTARY NOTES

12a. DISTRIBUTION/AVAILABILITY STATEMENT
Distribution authorized to DoD Components only, Specific Authority. Other requests shall be referred to the Commander, U.S. Army Medical Research and Materiel Command, ATTN: MCMR-RMI-S, Fort Detrick, MD 21702-5012

12b. DISTRIBUTION CODE

13. ABSTRACT *(Maximum 200 words)*

In this Phase I project we developed the design for an optical sensor device that can measure tissue oxygenation at any location on the body, by detection of light reflected back from the tissue. The device also allows for resolution of oxygenation and hemoglobin concentrations within deep tissue (up to depths of 2cm) versus surface tissue. This device therefore avoids the inaccuracies due to peripheral vasocostriction, by measuring at non-peripheral locations and into deeper tissue. The device also has a greater capability for measuring oxygenation of specific physiological structures and systems. Extensive simulations and analyses demonstrated the feasibility of the device, provided for determination of an optimum design, and quantified the capabilities of the device. The design is a uniquely advanced concept which offers capabilities beyond all known commercial, prototype, and research techniques for optical measurement of tissue.

14. SUBJECT TERMS
Tissue Oxygenation, Pulse Oximetry, Non-invasive Sensors, Physiological Monitoring, Remote Monitoring, Optical Sensor, Deep Tissue Measurement, and Hemoglobin Concentration

15. NUMBER OF PAGES
86

16. PRICE CODE

17. SECURITY CLASSIFICATION OF REPORT	18. SECURITY CLASSIFICATION OF THIS PAGE	19. SECURITY CLASSIFICATION OF ABSTRACT	20. LIMITATION OF ABSTRACT
Unclassified	Unclassified	Unclassified	limited

GENERAL INSTRUCTIONS FOR COMPLETING SF 298

The Report Documentation Page (RDP) is used in announcing and cataloging reports. It is important that this information be consistent with the rest of the report, particularly the cover and title page. Instructions for filling in each block of the form follow. It is important to ***stay within the lines*** to meet ***optical scanning requirements***.

Block 1. Agency Use Only *(Leave blank)*.

Block 2. Report Date. Full publication date including day, month, and year, if available (e.g. 1 Jan 88). Must cite at least the year.

Block 3. Type of Report and Dates Covered. State whether report is interim, final, etc. If applicable, enter inclusive report dates (e.g. 10 Jun 87 - 30 Jun 88).

Block 4. Title and Subtitle. A title is taken from the part of the report that provides the most meaningful and complete information. When a report is prepared in more than one volume, repeat the primary title, add volume number, and include subtitle for the specific volume. On classified documents enter the title classification in parentheses.

Block 5. Funding Numbers. To include contract and grant numbers; may include program element number(s), project number(s), task number(s), and work unit number(s). Use the following labels:

C	- Contract	**PR**	- Project
G	- Grant	**TA**	- Task
PE	- Program Element	**WU**	- Work Unit Accession No.

Block 6. Author(s). Name(s) of person(s) responsible for writing the report, performing the research, or credited with the content of the report. If editor or compiler, this should follow the name(s).

Block 7. Performing Organization Name(s) and Address(es). Self-explanatory.

Block 8. Performing Organization Report Number. Enter the unique alphanumeric report number(s) assigned by the organization performing the report.

Block 9. Sponsoring/Monitoring Agency Name(s) and Address(es). Self-explanatory.

Block 10. Sponsoring/Monitoring Agency Report Number. *(If known)*

Block 11. Supplementary Notes. Enter information not included elsewhere such as: Prepared in cooperation with...; Trans. of...; To be published in.... When a report is revised, include a statement whether the new report supersedes or supplements the older report.

Block 12a. Distribution/Availability Statement. Denotes public availability or limitations. Cite any availability to the public. Enter additional limitations or special markings in all capitals (e.g. NOFORN, REL, ITAR).

- **DOD** - See DoDD 5230.24, "Distribution Statements on Technical Documents."
- **DOE** - See authorities.
- **NASA** - See Handbook NHB 2200.2.
- **NTIS** - Leave blank.

Block 12b. Distribution Code.

- **DOD** - Leave blank.
- **DOE** - Enter DOE distribution categories from the Standard Distribution for Unclassified Scientific and Technical Reports.
- **NASA** - Leave blank.
- **NTIS** - Leave blank.

Block 13. Abstract. Include a brief *(Maximum 200 words)* factual summary of the most significant information contained in the report.

Block 14. Subject Terms. Keywords or phrases identifying major subjects in the report.

Block 15. Number of Pages. Enter the total number of pages.

Block 16. Price Code. Enter appropriate price code *(NTIS only)*.

Blocks 17. - 19. Security Classifications. Self-explanatory. Enter U.S. Security Classification in accordance with U.S. Security Regulations (i.e., UNCLASSIFIED). If form contains classified information, stamp classification on the top and bottom of the page.

Block 20. Limitation of Abstract. This block must be completed to assign a limitation to the abstract. Enter either UL (unlimited) or SAR (same as report). An entry in this block is necessary if the abstract is to be limited. If blank, the abstract is assumed to be unlimited.

*U.S.GPO:1993-0-358-779

FOREWORD

Opinions, interpretations, conclusions and recommendations are those of the author and are not necessarily endorsed by the US Army.

N/A Where copyrighted material is quoted, permission has been obtained to use such material.

N/A Where material from documents designated for limited distribution is quoted, permission has been obtained to use the material.

MPW Citations of commercial organizations and trade names in this report do not constitute an official Department of Army endorsement or approval of the products or services of these organizations.

N/A In conducting research using animals, the investigator(s) adhered to the "Guide for the Care and Use of Laboratory Animals," prepared by the Committee on Care and Use of Laboratory Animals of the Institute of Laboratory Resources, National Research Council (NIH Publication No. 86-23, Revised 1985).

____ For the protection of human subjects, the investigator(s) adhered to policies of applicable Federal Law 45 CFR 46.

N/A In conducting research utilizing recombinant DNA technology, the investigator(s) adhered to current guidelines promulgated by the National Institutes of Health.

N/A In the conduct of research utilizing recombinant DNA, the investigator(s) adhered to the NIH Guidelines for Research Involving Recombinant DNA Molecules.

N/A In the conduct of research involving hazardous organisms, the investigator(s) adhered to the CDC-NIH Guide for Biosafety in Microbiological and Biomedical Laboratories.

Accesion For	
NTIS CRA&I	☐
DTIC TAB	☒
Unannounced	☐
Justification	
By	
Distribution /	
Availability Codes	
Dist	Avail and / or Special
E-4	

Michael P. Whalen 10/12/95

PI - Signature Date

Executive Summary

In this Phase I effort we developed the design of a portable, deep tissue oxygenation measurement device, for monitoring the condition of casualty patients. Extensive simulations and analyses demonstrated the feasibility of such a device, provided for determination of an optimum design, and quantified the capabilities of the device. Experimental tests validated the invoked assumptions and results.

The use of this device will provide for more effective monitoring of the soldier's health status both on and off the field and during casualty situations. Currently available commercial devices for assessment of tissue oxygenation can only provide measurement at peripheral locations. However, during trauma-- where it can be most crucial to measure oxygenation-- peripheral vasoconstriction occurs and these devices are inaccurate due to low perfusion. Variations in oxygenation among different locations, tissues, and organs in the body will also go undetected by these devices.

The device designed in this Phase I effort utilizes reflectance and frequency domain techniques to allow for measurement at any location and for extraction of oxygenation information within deep tissues. This methodology will allow for localized measurement of oxygenation which can help assess the status of critical systems and organs such as the liver, or the brain.

The Phase I goal-- development of a device for measurement of deep tissue oxygenation-- was accomplished through a comprehensive series of design processes. Specifically we:

- Performed an extensive review of state of the art technology and ongoing research
- Identified several advanced approaches
- Developed computational models for simulation of light transport in tissue
- Performed extensive simulations to assess the characteristics of light-tissue interaction
- Conducted experiments to validate tissue absorption levels
- Evaluated advanced methodologies for deep tissue measurement
- Demonstrated capabilities for deep tissue measurement (using the frequency domain method)
- Implemented pattern recognition schemes (artificial neural network) for reconstruction of a layered medium
- Analyzed the sensitivity of computed parameters to variable design parameters and measurement noise
- Established detailed requirements and specifications for the Phase II device

Analyses indicate that the designed system will be capable of measuring:

- Tissue oxygenation at depths up to 2 cm
- Hemoglobin concentrations-- oxy-, deoxy-, and total-- up to 2 cm deep

As part of this Phase I effort, the potential for measurement of additional parameters with a single optical sensor was also established. Incorporation of additional measurements into a single, multifunction device would provide a more comprehensive assessment of physiological condition, in a cost-efficient manner. The sensor was also designed for interface with a miniature, portable, physiological measurement and analysis system, previously designed by Cybernet Systems Corpora-

tion, which allows for integration of multiple sensor types. This system has wireless communications capabilities for comprehensive physiological monitoring of remote soldiers in the field.

The designed sensor also has important benefits for commercial applications where accurate measurement of tissue oxygenation is required, such as during anesthesia, surgical procedures, emergency medical treatment, intensive care, critical care, trauma, resuscitation, circulatory conditions, exercise monitoring, etc. Furthermore, by measuring oxygenation in localized, deeper tissues, the proposed device will allow for more effective assessment of the condition of the individual systems within the body.

Keywords:

Tissue Oxygenation
Non-invasive Sensors
Remote Monitoring
Deep Tissue Measurement
Pulse Oximetry
Physiological Monitoring
Optical Sensor
Hemoglobin Concentration

1.0 Identification and Significance of the Problem or Opportunity

Successful trauma management requires accurate monitoring of several important physiological parameters, so that proper action can be taken to help maintain critical functionality. Of most importance are oxygen delivery, oxygen consumption, and cardiac output. Maintaining cardiac output is critical to survival.

Important indicators of cardiac output include HCO_3^-, pH, hemoglobin concentrations, SvO_2 (venous oxygen saturation), SaO_2 (arterial oxygen saturation), pCO_2, pO_2, and hematocrit (% RBCs per volume). With the exception of SaO_2, measurement of these parameters requires invasive techniques, such as from blood gas analysis through a catheter. While the hospital setting may be suitable for such invasive measurement, other settings such as emergency treatment on the battlefield are not suitable for invasive techniques.

A non-invasive alternative is pulse oximetry, which measures SaO_2 by optical methods, and can provide a more suitable means for trauma assessment in the emergency treatment setting. However, current sensors and methodologies for measuring tissue oxygenation, using pulse oximetry, have several limitations. The pulse oximeter uses transmission of light through a thin layer of tissue, at a peripheral location, and measures variations in tissue absorption to determine the oxygen saturation of hemoglobin. Because the transmission of light is used, these devices can only measure at peripheral locations (such as through the finger, the ear lobe, or the foot of infants). This technique must therefore assume uniform oxygenation throughout the body, which is not necessarily the case.

For example, during trauma peripheral vasoconstriction occurs which reduces peripheral perfusion and causes pulse oximeters to supply inaccurate readings (Lawson et al., 1987). In addition, the different systems of the body have different mechanisms for controlling perfusion and will therefore be affected differently during trauma. For example, the body will attempt to maintain perfusion to the brain, at the cost of decreased perfusion to other organs if necessary. It can therefore be important to know the oxygenation status of individual systems/organs for determining the level of injury, and for timely feedback on the effect of actions taken to aid recovery. This assessment requires measurement at non-peripheral locations.

In this phase I project we developed the design for an optical sensor device which can measure tissue oxygenation at any location on the body by measurement of light reflected back from the tissue. The device also allows for resolution of oxygenation within deep tissue (up to 2 cm) versus surface tissue. This device therefore avoids inaccuracies due to peripheral vasoconstriction, by measuring at non-peripheral locations and into deeper tissue. The device also has a greater capability for measuring oxygenation of specific physiological structures and systems.

The optical sensor designed in this Phase I will be compatible with a portable physiological measurement and analysis system designed by Cybernet Systems Corporation in a previous SBIR project. This system allows for highly portable physiological monitoring with multiple sensor types, and has wireless capabilities for communication to a remote medical station. The complete system is shown in Figure 1, which includes the optical oxygenation sensor, the portable physiological measurement system (PPMS), and the portable physiological analysis system (PPAS).

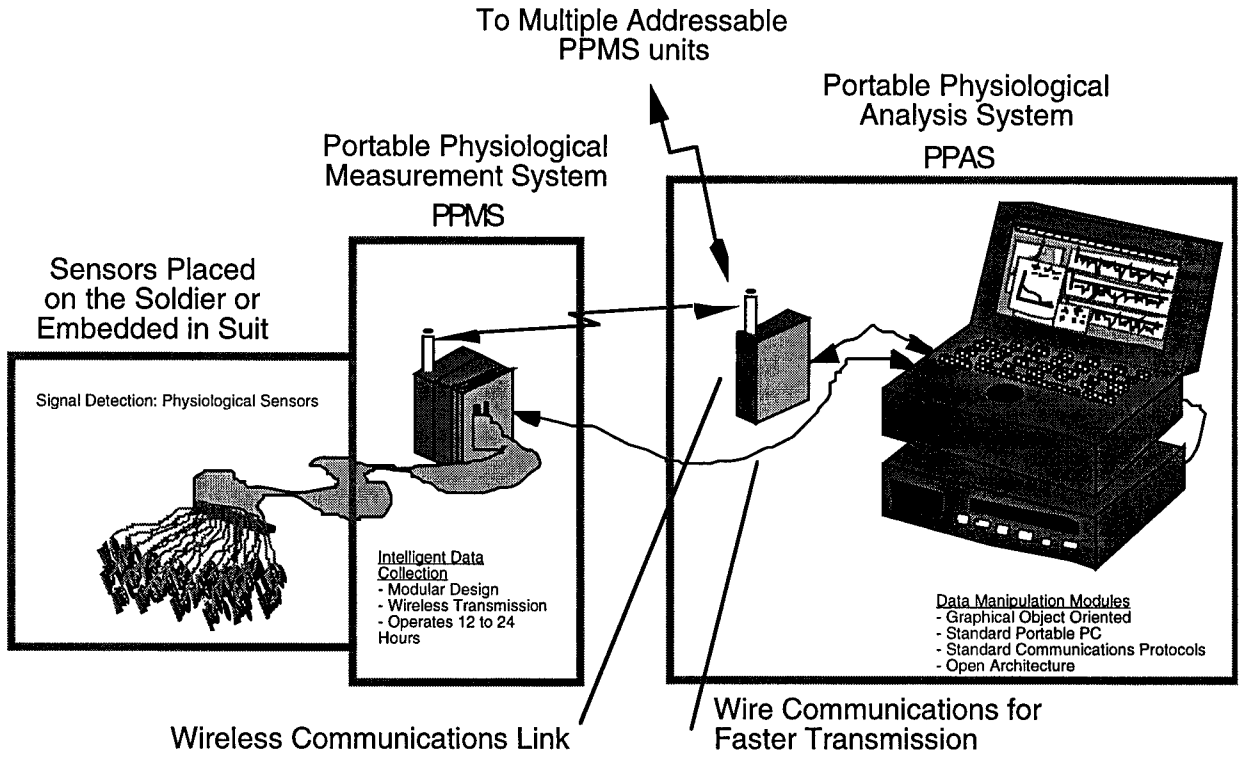

Figure 1: Illustration of the complete portable physiological measurement and analysis system, with interface to the designed optical sensor.

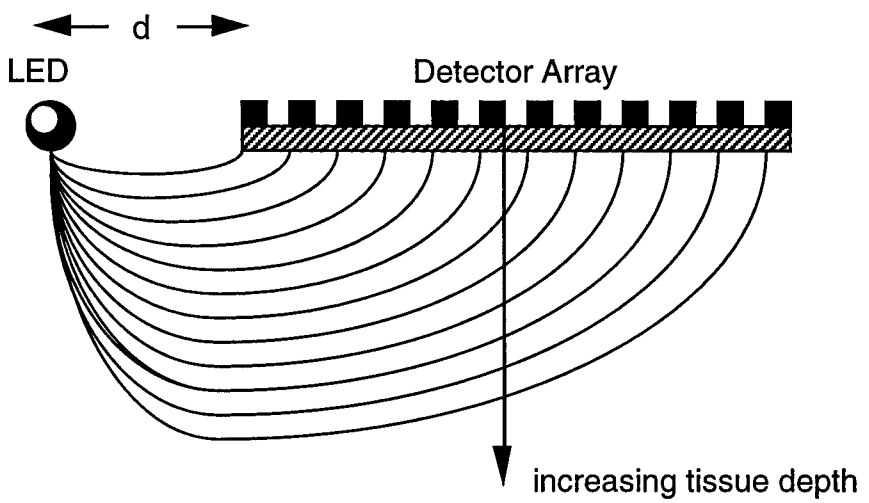

Figure 2: Illustration of depth measurement using the designed optical sensor.

The oxygenation sensor was designed based on a frequency domain methodology. The frequency domain methodology utilizes an intensity modulated light signal and measures the DC level and phase shift of the reflected light, at different distances from the source, to compute the tissue absorption coefficient. Initial research on this methodology for measurement of hemoglobin concentration and oxygen saturation has been reported in recently published papers (Fantini et al., 1995, Fantini et al., 1994). These studies used a few detectors at varying distances from the source and demonstrated the ability to accurately measure hemoglobin concentration (oxy- and deoxy-) and oxygen saturation in a homogeneous medium. A homogeneous medium implies that tissue absorption, and therefore oxygenation, is uniform, which in general is not true for physiological tissue.

Here, we expand upon this methodology by using a large number of detectors, with distance from the source varying by small increments, to address the non-homogenous characteristic of tissue. This is accomplished using an array of detectors, as illustrated in Figure 2.

The detector array provides for high resolution of spatial variations in the amount of light reflected by the tissue. In a non-homogeneous medium, the spatial pattern of light reflected by the tissue will depend on the varying absorption/oxygenation of different layers within the tissue.

Spatial variations of the reflected light therefore translate into depth variations in the oxygenation of tissue. This relationship is complex, as shown from even the case of only two distinct layers which was studied. For the purpose of this Phase I study we implemented a neural network pattern recognition scheme, to attempt to learn this relationship and resolve the depth variations. Training of the neural network from sample simulated data illustrated that the relationship is distinct and neural network is capable of deciphering it.

Extensive simulations were performed to quantify the depth to which measurements can be made. Using assumed worst case values for absorption and scattering, simulations indicate that light is measurable at distances of up to 5 cm or more from the source. This translates to light which has traveled an average of about 4-5 mm deep (for worst case conditions), yet a fraction of light travels to much larger depths. Thus, with reconstruction methods measurement of oxygenation within larger depths is possible. *Indeed, using the neural network the absorption of a deep layer at a depth of 2 cm was determined.*

The designed sensor, extends capabilities beyond all commercial, prototype, and research devices because it:

- Uses a reflectance technique for measurement at any location
- Implements an advanced frequency domain methodology for quantization of hemoglobin concentrations
- Uses an array of detectors, with small increments in source-to-detector distance, for high resolution of spatial variations in reflected light corresponding to resolution of depth variations
- Implements pattern recognition techniques to reconstruct absorption values in a complex layered structure, up to 2 cm deep.

The design is therefore a uniquely advanced concept which offers capabilities beyond all known commercial, prototype, and research techniques for optical measurement of tissue.

Beyond the desired military application, the proposed device has many potential commercial applications. Table 1 lists the uses for pulse oximetry as documented by Severinghaus (1988). The proposed device, by improving upon pulse oximetry capabilities, will add significant benefit to many important medical applications.

Monitoring
Anesthesia, recovery, ICU, NMR, CAT
Reduce need for ICU, low risk groups
Central nursing station
Office procedures: Dentistry, Endoscopy
Monitoring spinal or epidural narcotics
Home or hospital monitoring of SIDS
Critical Care Transport
Circulation
Monitor during microvascular reimplantation
Measure blood pressure (cuff occlusion)
Determine ductus patency
Test circulatory obstruction from cervical reb.
Test patency of arterial grafts
Indicate carotid artery compression during neck surgery
Asses circulatory adequacy in unusual positions
Clinical Tests
Assess hypoxic ventilatory response
Quantitate sleep apnea, adults and infants, SIDS
Measure circulation time with single breath of N_2
Improved Allen's test for radial and ulnar artery patency
Teaching
Physiology during anesthesia
Effectiveness of COR
Bio-feedback for peripheral vasodilation
Relationship of CPAP and PEEP to atelectasis
Waveforms
Diagnosis of irregularities
Absolute amplitude as monitor of circulation
Substitute for arterial line
Monitor circulatory obstruction
Research
Regulation of respiration studies
Exercise physiology
Cardio-pulmonary tests
Mountaineering studies
Animal research

Table 1: Uses for pulse oximetry.

Therapy Control
Maintain deliberate hypoxia in premature infants
Servo-controlled saturation, prematures
Converse O_2 in home O_2 therapy
Determine optimal PEEP and CPAP
Monitor apneic oxygenation during bronchoscopy etc.
Trial of extubation or ending O_2 therapy

Table 1: Uses for pulse oximetry.

2.0 Phase I Technical Objectives

The Phase I effort was aimed at establishing the feasibility of a device for measurement of deep tissue oxygenation, developing an optimum design, and quantifying the capabilities the device. To achieve this goal, the following objectives were established:

1) Evaluate current technologies and ongoing scientific research efforts.

Before approaching an advanced design problem, it is important to first understand the principles of current techniques and their limitations. This process identifies the important issues which must be addressed in the advanced design. The next step is to survey ongoing and past research efforts relevant to the design to identify advanced methodologies and determine their applicability to the design problem.

We therefore performed an extensive review of device specifications and published literature, relevant to the design of a deep tissue oxygenation sensor. This included information on pulse oximetry devices, optical sensors, reflective measurements, time-resolved spectroscopy, photon scattering and migration, diffusion analysis, optical imaging, and optical properties of tissues.

The results of this study, provided a comprehensive knowledge-base on optical measurement of tissue, which identified limitations of current devices, and advanced technologies and methodologies applicable to deep tissue measurement. This study, which is reported in detail in section 3.0, established the rationale and focus for the Phase I design effort.

2) Determine tissue optical characteristics.

In order to analyze the interaction between light and tissue, the properties and characteristics of tissue must first be well understood. Thus, an accurate model for physiological tissue must first be established. This was achieved in the Phase I effort through two means. First, tissue characteristics were established through review of scientific publications and data. This yielded, among other parameters, typical, best-case, and worst-case values for scattering and absorption in human tissue. Results of this study are included in section 4.1.

In addition, scientific data were further validated by performing tests on human tissue, to assess actual absorption levels, using a prototype sensor that was built during the Phase I effort. Measured values were compared to the results obtained from performed simulations. This process val-

idated that tissue models derived from the literature review did indeed reflect typical absorption values seen in the human population. Furthermore, absorption values in the admittedly small population sample, did not vary as greatly as they were expected to. The test procedure and results are reported in detail in section 4.2.

As a whole, this effort resulted in a representative model for physiological tissue which served as the basis for subsequent simulations and analysis of light transport in tissue.

3) Determination of additional substances/parameters for potential optical measurement.

While this Phase I effort was focused on the measurement of tissue oxygenation, there are other significant physiological variables which are important to measure during trauma and other situations. Information on pH, pCO_2, HCO_3^-, Hemoglobin concentration, Hematocrit, glucose/lactate, and other substances in the blood and tissue, for example, can provide for a more comprehensive indication of cardiac output and/or patient status.

Incorporation of these additional measurements into a single, multi-function device would provide a more comprehensive assessment of physiological condition, in a cost-efficient manner. There is also a great need to non-invasively perform many additional measurements, which currently require invasive techniques. Optical methods for non-invasive measurement offer significant advantages because they allow for development of lightweight, portable sensors which can be utilized in highly portable applications.

As part of this Phase I effort we therefore surveyed the potential for measurement of additional parameters, beyond the intended oxygen saturation, with a non-invasive optical sensor. Results of this study are included in section 4.5.

4) Development of a computational model for simulation of light transport in tissue.

To analyze the interaction between light and tissue and to evaluate advanced methodologies for measurement of deep tissue oxygenation, we take advantage of computer simulation techniques. This first requires development of computational models, which accurately represent the migration of photons through physiological tissue. Of particular importance is the highly scattering characteristic of tissue, which makes the migration of photons a non-linear process. Various analysis techniques have been applied to address this characteristic of light transport in tissue.

In this Phase I effort we developed models for simulating light transport in tissue using two different methods: 1) Monte Carlo analysis and 2) Diffusion analysis. The Monte Carlo (MC) technique simulates the path of many individual photons, based on random probabilities, to provide an indication of the total photon migration. The diffusion method represents photon migration as a diffusion process.

Models were constructed on a PC platform, and the performance of each evaluated. MC simulations require large computational time which is not suitable for the large number of simulations which were performed. The majority of simulations were therefore performed using the diffusion based model, which has been demonstrated to provide equivalent results to those obtained from the MC model. Section 4.3 describes, in detail, the model development and validation.

5) Simulate light transport in tissue

Given the developed models for physiological tissue and the migration of photons, simulations were then performed to predict the transport of light through the tissue, and the resulting light measured on the surface. Extensive simulations were performed using the diffusion model to characterize this distribution of light migration. Important characteristics of light-tissue interaction that were studied include:

- Intensity of reflected light as a function of distance from the light source
- Depth of photon path as a function of distance from the light source
- Depth of photon path as a function of transit time

These characteristics are of particular interest for the development of a deep tissue oxygenation sensor, because at greater distances from the source, the measured light has traveled deeper into the tissue. It is therefore important to quantify the distance from the source up to which light is measurable, and to quantify the corresponding depth to which the light has sampled. Photon transit time is also important because time-gating may allow for selection of photons which have traveled to certain depths.

The results of these simulations, which illustrate the important characteristics of light transport in tissue, are reported in section 4.4.1-4.4.3.

6) Analyze advanced methodologies and the capability for deep tissue measurement

After characterization of light-tissue interaction, further simulations then allowed for evaluation and analysis of the advanced methodologies for measurement of deep tissue. The advanced methodologies identified include pulsed light (time-resolved) and intensity modulated (frequency domain) approaches. The frequency domain methodology utilizes an intensity modulated light and measures the DC and phase shift of reflected light, at different distances from the source, to compute the tissue absorption coefficient. The time-resolved methodology utilizes an ultra-short light pulse and measures the decay of the reflected light signal over time to compute the tissue absorption coefficient.

By analyzing the reflected light distribution, based on performed simulations, the capabilities of each method were studied. Analysis results, detailed in sections 4.4.4-4.4.5, indicate that the frequency domain method provides the best approach for deep tissue measurement.

To demonstrate and quantify the capability of this method for measurement of deep tissue oxygenation, we examined a two layer model for tissue. The two layer model studied consists of a surface layer and a deep layer, with three variable parameters: absorption of the surface layer, absorption of the deep layer, and depth of the boundary between layers. Simulations were performed on the two layer model and analyzed using the frequency domain method. The effect of variations in each of the three variables (surface absorption, deep absorption and depth) was individually studied. These results, which demonstrate a relationship between reflected light and the layered structure, are included in section 4.4.6.

To reconstruct the layered information in a unknown medium, pattern recognition methods were

implemented in the Phase I project. Specifically, an artificial neural networked was trained to extract the unknown parameters in a layered medium (i.e. surface absorption, deep absorption, and depth of boundary) based on frequency domain measurement of the reflected light. Section 4.4.7 details results of the neural network implementation, which demonstrates reconstruction of the complex layered structure up to 2 cm deep.

7) Generation of a complete Phase II design.

The performed simulations and analyses served to establish the best methodology for measurement of deep tissue oxygenation. The next step was to translate these results into detailed specifications for the Phase II design. In addition, a comprehensive sensitivity analysis was performed to determine the sensitivity of computed parameters (oxygenation and hemoglobin concentrations) to variable design parameters and measurement noise. The complete Phase II design, detailed in section 5.0, includes specification of the light sources, detectors, driving circuitry, measurement and signal conditioning circuits, signal processing requirements, and sensor interface.

3.0 Review of Related Scientific Research and Current Technologies

Since the introduction of pulse oximetry devices, for non-invasive optical measurement of oxygen saturation (reviewed by Takatani et al., 1994), much research has been directed towards optical methods for non-invasive physiological assessment of oxygen, and other parameters. Optical methods can provide several advantages over other techniques for invasive and non-invasive measurement of chemical substances.

Standard methods for imaging physiological structures such as MRI, CAT, and PET scans use large non-portable equipment, and are not suitable for providing continuous real-time information. More portable, real-time non-invasive methods for physiological assessment include acoustic or ultrasound techniques which can image thermal activity and assess organ function, or measurement of electrical and magnetic fields which can provide a measurement of neural and muscle activity (Godik et al., 1991). These methods however cannot provide a direct measurement of chemical substances in the body-- they can only make inferences about the underlying chemical status.

Chemical status of the blood can be determined by analyzing a sample of blood, but this is invasive and has a limited data response time. By using optical methods, however, a non-invasive measure of chemical concentrations may be possible by determination of the absorptive and scattering properties of the tissue. Optical sensors are lightweight and easily portable; they avoid the ionizing radiation of other imaging techniques, and can provide real-time continuous data.

3.1 Wavelength Considerations

The use of wavelengths in most of the visible range (400-780 nm) has shown some applicability for measurement in brain tissue, but is not effective in skin and other tissue because of high absorption in those media. Furthermore, detection of wavelengths in most of the infra-red (IR) range (780 nm - 1 mm) can allow for measurement of thermal information only. However, wavelengths in the visible red and near infra-red (NIR) (780-1400 nm) range provide an opportunity

for effective optical measurement of various chemical concentrations. This is due to partial transparency of tissue, and to characteristic absorption and scattering properties of chemical substances, in the red and NIR range (Wilson, 1991).

3.2 Pulse Oximetry

3.2.1 Transmission Devices

Currently, most oximetry devices in use are based on optical transmission, where light is transmitted through a thin layer of tissue (either the finger or ear) to measure oxygen saturation of hemoglobin. Functional oxygen saturation is defined as:

$$Functional \quad (SaO_2) = \frac{O_2Hb}{O_2Hb + Hb} x100\ \%$$

However, there are four types of hemoglobin existing in the blood of adults: oxy-hemoglobin (O_2Hb), reduced hemoglobin (Hb), met-hemoglobin (MetHb), and carbooxy-hemoglobin (COHb). The fractional oxygen saturation is defined to include these concentrations:

$$Fractional \quad (SaO_2) = \frac{O_2Hb}{O_2Hb + Hb + COHb + MetHb} x100\ \%$$

MetHb and COHb do not bind oxygen and exist in small concentrations for healthy adults. Therefore, oximetry devices generally assume these concentrations to be negligible and use the functional oxygen saturation. An additional type of hemoglobin-- fetal hemoglobin (FHb)-- is also found in the fetus and early infant and may be of significant concentration.

Oximetry devices measure the absorptive changes in tissue, at two or more wavelengths, to calculate the level of oxygen saturation. Measurement of absorption is based on the Beer-Lambert law, as stated:

$$I_{trans} = I_{in}e^{-A}$$

where:

I_{trans}=intensity of transmitted light
I_{in}=intensity of incident light
$A=DC\varepsilon$,
A=absorption,
D=pathlength,
C=Concentration of solute, and
ε=extinction coefficient of solute.

By measuring the amount of transmitted light, the concentration of an absorbing substance be can determined by application of the Beer-Lambert law. The measured transmitted light will consist

of a DC component and an AC component, where the DC component represents the absorptive properties of the baseline blood and tissue, and the AC component represents the change in absorptive properties due to the arterial pulsation of blood during systole. The AC component is assumed to be due to Hb and O_2Hb absorption only (i.e. all other factors make negligible contribution to AC component).

To compute oxygen saturation oxy- and deoxy- hemoglobin (Hb and HbO_2) need to be distinguished. We therefore consider the absorption characteristics of oxy- and deoxy- hemoglobin (Hb and O_2Hb). There is a large peak in the absorption of Hb below 700 nm; at approximately 805 nm the absorption of Hb and O_2Hb are equal (called the isobestic point); and above 805 nm they are close in value. By application of two different wavelengths (λ_1 and λ_2), where the absorption ratio between Hb and O_2Hb has a large difference (i.e. 660 and 900 nm), the ratio of the AC components at λ_1 and λ_2 provides a measure of SaO_2.

Inaccuracies of this device and methodology may be due to accuracy of the LED wavelength, artifacts from external light and/or motion, the effect of other substances bound to Hb such as MetHb, COHb, FHb, or other physiological factors/conditions in the body (Cysewska-Sobusiak, 1993). Other substances bound to Hb affect accuracy because the above calculations for oxygen saturation use functional oxygen saturation which assumes Total Hb = Hb + O_2Hb. The use of three (or more) wavelengths has been used to provide a more accurate indication of Total Hb (Wickramasinghe et al., 1994). Inaccuracies may also occur due to the effects of photon scattering (scattering is discussed in section 3.5.1).

The transmission devices are also limited in applicability because they may only measure at peripheral locations where light can be transmitted through a thin layer of tissue (such as through the finger, ear, or the foot in infants). This limitation presents problems under conditions where there is peripheral vasoconstriction, causing decreased perfusion of blood. Under conditions of decreased perfusion the pulse oximeter has been shown to produce inaccurate measurements (Lawson et al., 1987). Such vasoconstriction can occur during severe trauma or shock, where measurement of oxygen saturation can be very important. Likewise, there may be situations where it is desirable to measure regional oxygenation differences in non-peripheral areas.

3.2.2 Reflectance Devices

Absorption properties may also be determined by measurement of the light reflected back from the tissue rather than by measurement of the light transmitted through the tissue. Reflectance devices allow for measurement of tissue oxygenation at non-peripheral locations. These devices use the same principles as transmission devices for determination of oxygen saturation levels since the amount of reflected light also provides a measure of optical absorption properties of the tissue, based on the Beer-Lambert law. However, the reflected light is much weaker than the transmitted light (Mendelson et al., 1988).

The main concern of reflective methods is therefore the weakness of the signal. Reflective devices have been used on the forehead with the most success because the signal has been found to be stronger there than other locations (Mendelson, McGinn, 1988). But, studies have also demonstrated the ability to measure tissue oxygenation at other locations, such as the forearm and calf,

using reflective methods (Mendelson et al., 1991). To improve the reflected signal, heating of the skin at the location of the source and detector site has been shown to increase the signal strength (Mendelson, Ochs, 1988).

Advantages of using reflectance methods over transmission include: 1) application to any location on the body, 2) single probe containing both source and detector, and 3) constant source to detector distance.

3.2.3 Qualitative versus Quantitative Measurement

While oxygen saturation may be determined from the ratio of the pulsatile change in absorption at two different wavelengths, knowledge of absolute concentrations of Hb, O_2Hb, and other parameters is also highly desirable. This knowledge may aid in more accurate assessment of oxygen saturation, and can provide further crucial information about physiological status. In general, the methodologies described thus far can provide only a qualitative measure of the concentration of absorbing substances, because the optical pathlength is unknown. To acquire quantitative values for the concentration of specific absorbing substances, using the Beer-Lambert law, the optical pathlength must be known.

3.3 Optical Path Length Determination

Determination of the optical pathlength can allow for quantitative calculation of chemical concentrations, and itself may provide an indication of important changes in the tissue. For example, Maris et al. (1991) report that optical pathlength changes occur in tissue due to hypoxia or other conditions. These changes in pathlength are primarily due to changes in hemoglobin concentration, and as a result can also be indicative of the oxygenation state.

The optical pathlength will not be equal to the source-to-detector distance because of photon scattering. The mean functional pathlength (MFP) is typically expressed as MFP=nL, where L is the source detector length and n is the pathlength factor.

Many studies and implementations for spectrophotometric measurement have initially used an estimation of the optical pathlength, based on averaged experimental results (Faris et al., 1994). However, the optical pathlength may be specifically determined under each situation using one of two methods: 1) Time-resolved or 2) Frequency domain (phase modulation) measurements.

3.3.1 Time-resolved

To perform time-resolved measurement of the optical pathlength, a very narrow pulse of light (on the order of a picosecond) can be applied, rather than a continuous steady-state wave. Then measurement of the time of flight (TOF) for the light to travel from the source to the detector indicates the mean functional pathlength (MFP) (Delpy et al., 1988). This more accurate value may then be applied to the Beer-Lambert equation for quantitative determination of absorbing concentrations.

Time resolved methods to determine pathlength can also aid in depth localization (Chance et al., 1992), and spatial resolution and imaging capabilities (Svaasand et al., 1994), as will be discussed in section 3.5.

3.3.2 Frequency Domain (Phase Modulation)

To measure the optical pathlength using phase modulation, a high frequency light signal (i.e. on the order of 200MHz) is applied. Then measurement of the phase shift between the measured reflected signal and the applied signal provides an indication of the optical pathlength (Hielscher et al., 1993). The phase shift will be directly proportional to the optical pathlength.

Phase modulation methods can also be applied for spatial resolution and imaging capabilities as will be discussed in section 3.5.

3.4 Depth Measurement and Localization

The measurement of absorption properties of particles at depths below the surface, using reflected methods, has been examined and demonstrated but not well quantified. By increasing the distance between the light source and the detector, the light detected will have traveled deeper into the tissue, thus providing an indication of absorption to greater depths (Mendelson, Ochs, 1988; Chance et al., 1992).

However, with increased distance between the source and detector there is more spreading of the light path and the resolution of localization will be decreased (Cui et al., 1991). Also, with increased source to detector distance, a greater intensity of light is required to provide an adequate signal at the detector. Multiple sources have been implemented for increasing the strength of incident light.

Previously reported studies suggest that optical absorption of particles at depths of a few millimeters in tissue, or several centimeters in brain tissue can be measured. However, exact depths, the source to detector separation required, and the resolution capabilities do not appear to be well quantified. This is an issue of spatial resolution, and within deeper structures the effect of photon scattering must be addressed.

3.5 Spatial Resolution and Imaging of Parameters and Structures

3.5.1 Photon Scattering

Pulse oximetry devices determine oxygen saturation by measuring the change in the absorptive properties of the tissues. However, there are actually two processes which affect how light is transmitted through or reflected from the tissue: 1) absorption of photons, and 2) scattering of photons. The scattering of photons is extensively reviewed by Kessler et al., 1992. Because of scattering the photon path cannot be easily determined, and standard image reconstruction methods cannot simply be used.

To understand the migration of photons in scattering media, several models for simulating the transport of light, have been used. For example, Monte Carlo methods have been applied, where the paths of many photons are individually calculated based on random computations. This requires large computation to obtain enough photons for adequate simulation. As an alternative, the migration of photons can be modeled as a diffusion process (Bruce, 1993, Graber, 1992, Aronson, 1992). Several studies have compared Monte Carlo simulation to estimation of the dif-

fusion equations, and found the results to be consistent (Haselgrove et al., 1991; Madsen et al., 1991). Comparison of these simulations to experimentally measured results in phantom media has found consistent (Haselgrove et al., 1991) or slightly varied (Madsen et al., 1991) results.

3.5.2 Image Estimation

Detected photons can be loosely placed into two categories: 1) ballistic or unscattered photons, and 2) highly scattered photons. Ballistic photons have taken an almost direct route from source to detector, while highly scattered photons have taken an indirect route, scattering among many particles.

Physiological tissue is, in general, highly scattering, so that scattering of photons is more dominant than absorption of photons. Two approaches have generally been proposed and investigated for optical imaging in a scattering medium such as subsurface tissue:

1) separation of ballistic (unscattered) components from scattered components to allow image analysis based on absorptive characteristics only (Benaron et al., 1992), or
2) analysis of the scattered light to reconstruct an image based on a model which relates scattering to optical properties of the tissue.

Both methods will require an implementation of multiple detectors and/or sources, which can provide a measurement of a reflected (or transmitted) field.

The first approach uses time resolved methods to perform separation of unscattered components from scattered components. Time-of-flight measurements can be used to perform a time-gating function, rejecting photons which arrive after a certain window of time due to scattering delay. The effectiveness of this approach seems to be limited to small thicknesses or depths, because the time-gated signal decreases exponentially with depth.

In the second approach, however, by modeling the scattering of photons as a diffusion process, for example, the scattering field can be utilized for image reconstruction to greater depths. While simulation of photon migration based on a given model (the forward problem) can be readily addressed, reconstruction of an image based on the measured light (the inverse problem) is much more difficult.

A variety of methods have been proposed for reconstruction of the image. Weighting functions which estimate individual absorber contributions to the measured light at various detector locations have been studied (Barbour et al., 1992). An iterative perturbation function (Wang et al., 1992) and neural networks (Schlereth et al., 1992) have also been suggested. Other methods include applying the concept of importance used in reactor theory (Barbour et al., 1991), and the Moore-Penrose generalized inverse relation (Arridge et al., 1991).

It is worth noting that tomographic imaging for identification of structural features, has been proposed using optical coherence tomography (OCT) (Fugimoto et al., 1994; Crease 1993). This method applies an optical signal to the physiological medium, compares the reflected signal to a reference signal (reflected off a reference mirror) and looks at the interference. Coherent interfer-

ence occurs when the distance from the reflecting surface in the medium equals the distance from the reference mirror. This method has shown application for tomographic imaging of the structure of the eye, and of the skin (up to 3mm depth) for identification of tumors.

3.6 Current Applications and Devices

Transmission pulse oximetry devices are currently used in a wide variety of clinical, and other applications, for monitoring oxygen saturation. Devices currently available include finger and ear clip devices. Studies have compared pulse oximetry measurement of oxygen saturation (SpO_2) to direct arterial measurement from blood sample (SaO_2) (Miyasaka et al., 1987). In many situations results demonstrated good correlation between SpO_2 and SaO_2. However, inaccuracies due to blood flow limitations (i.e. peripheral vasoconstriction) (Lawson et al., 1987), and other physiological conditions (Cysewska-Sobusiak, 1993) have been sited and examined.

Reflectance pulse oximetry devices have more recently been studied for use on the forehead and demonstrate effective measurement of oxygenation (Mendelson et al., 1988). Some prototype devices have incorporated heaters to improve the reflected signal strength, or pressure and contact sensors to reduce the effects of probe placement (Osawa, Niwa, 1993). Use of the reflectance devices on the forearm and calf, where the reflected signal is weaker, has also been demonstrated (Mendelson, McGinn, 1991). And, the application of optical oximetry to brain tissue has been widely studied (Pan et al., 1993; Hielscher et al., 1993; Chance, 1992).

Clinical application and testing of a commercial reflectance device for use on the forehead (INVOS 2910, Somanetics Corp., Troy, MI) has been reported (Dujovny et al., 1992; Lewis et al., 1992). This device incorporates two detectors, one farther away from the light source, for deeper measurement of regional cerebral oxygenation. A study demonstrated that oxygenation measurement using this device had no dependency on age or sex of the patient, but was dependent on the skin color (Dujovny et al., 1992). Clinical applications of this device which have been reported (Lewis et al., 1992) are: 1) during surgery (carotid endarectomy, cardiopulmonary bypass during aortic arch repair, circulatory arrest during posterior fossa aneurysm repair, and hypothermia during AV fistula repair), 2) during episodes of hypoxia in adults, and 3) for measurement of IR dye injected into cranium.

The extension of these oximetry devices to include measurement of some other relevant parameters has been reported in various studies. This includes measurement of total Hb concentration (Faris et al., 1994; Schmitt et al., 1992), cerebral blood volume (CBV) (Wickramasinghe et al., 1994; Hielscher et al., 1993), glucose (Crease, 1993; Marquardt et al., 1993; Ward et al., 1989), and others. Quantification of these parameters requires estimation or actual computation of the optical pathlength (as previously discussed). Blood flow measurements are also obtainable by using laser Doppler methods (Wickramasinghe et al., 1994; Liepsch et al., 1993; Mendelson, Ochs, 1988). While many parameters beyond oxygenation (and blood flow) have the potential to be non-invasively monitored by optical methods, such devices are not currently available for use in the clinical environment.

Other potential devices which have been suggested, using non-invasive optical techniques, include an optical stethoscope which may provide for detection of sub-audible circulatory func-

tion (Hong, Fox, 1993). Tracking of dyes using non-invasive optical methods may also provide advantages, such as for measuring ICG clearance to assess liver function (Awazu et al., 1991).

3.7 Comparison of Commercial Oximeters

Different pulse oximeter models can be compared using methods-comparison studies in which one uses two methods to measure the same variable. The standard for pulse oximetry comparison is in vitro saturation measurements from arterial blood samples. Correlation coefficients are good measures of association but do not give a complete view of performance. The mean and standard deviation of the difference between the two methods of measurement are preferred and recommended by Altman (Altman, Bland, 1983). The mean of the difference is defined as the bias and the standard deviation is termed precision. Bias is a good indicator of systematic over- or underestimation of quantification while precision is a representation of random error or variability. Accuracy is dependent on the algorithms invoked, thus model and software version are both important in assessing the performance of a device. There have been many studies to compare the relative merits of the various models of pulse oximeters. One such study (Ralston et al., 1991) is represented below (Table 2).

Brand	Saturation >80% Bias (precision)	Saturation <80% Bias (precision)
Datascope Accusat	-0.3% (1.9)	-7.1% (3.2)
Datex Satlite	+0.0% (2.0)	+1.4% (1.5)
Invivo 4500	-0.3% (1.8)	-0.6% (4.9)
Nellcor N-200	+0.8% (1.7)	-5.5% (3.5)
Nonin 8604D	+1.4% (1.8)	+8.8% (4.8)
Novametrix 505	+0.7% (1.9)	-8.1% (4.3)
Ohmeda 3700	-1.0% (2.5)	-5.3% (6.2)
Ohmeda 3740	-0.1% (2.8)	-5.5% (1.0)
Physio-Control 1600	+0.0% (1.9)	-6.0% (6.9)
Radiometer Oximeter	-1.5% (1.8)	-6.7% (3.2)
Sensormedics Oxyshuttle	-0.3% (1.8)	-0.4% (1.8)
Simed S-100	+0.1% (2.2)	+1.8% (1.6)
Spectramed Pulsat	+0.7% (1.6)	-3.4% (3.2)

Table 2: Accuracy of 13 pulse oximeters using finger probes on patients in the ICU. Values are expressed as mean (SD). From Ralston et al., 1991.

Table 3 lists select manufacturers of pulse oximeters. Care must be taken when choosing the appropriate sensor and for the most part sensors may not be interchanged with pulse oximeters. Transmittance sensor manufacturers often store the peak wavelengths of the LEDs in the connector of the cable assembly. The oximeter must be capable of detecting the wavelength and calibrating the instrument accordingly.

Company	Model	Accuracy - SpO_2	Rate Accuracy	Power Requirements	Weight	Price
BCI	3040			12 hr battery backup	2.25 lbs.	1095.00
	3100/3101					1475.00 1870 (w/ EKG)
	3301			24.5 hrs. cont. runtime	9 ounces	695.00
Criticare	SPO_2T 503S					995.00
	503	70-100% 40-70%		10 hours w/ back-light; 120 VAC~60Hz	1.8 lbs	
Medical Research Laboratories	MRL Oximeter Monitor	81-100% 70-80%		120V, 60Hz	6 lbs	
Nonin	8500 Hand Held	70-100% +/- 3% of full scale	+/- 3% +/- 1 digit	6 AA 100 hours	5 ounces 10 w/batteries	1095 1195 w/memory
Sensormedics	Sat-Track	70-100%		120V, 60Hz	2.5 lbs	
SiMed	S-50 S-100e	70-100% 50-70%	+/- 3% +/- 1 digit	120V,60Hz 2 hrs. with 12 hr. charge	7.5 lbs	

Table 3: List of commercial pulse oximeters.

4.0 Summary of Phase I Design Efforts

The Phase I effort was aimed at establishing the feasibility of a device for measurement of deep tissue oxygenation, developing an optimum design, and quantifying the capabilities the device. The performed literature review established the rationale and focus for the extensive series of design efforts required to achieve this goal. First, in order to analyze the interaction between light and tissue, the properties and characteristics of tissue must first be well understood. Thus, an accurate model for physiological tissue was established, which served as the basis for subsequent simulations and analysis of light transport in tissue.

Next, to analyze the interaction between light and tissue and to evaluate advanced methodologies for measurement of deep tissue oxygenation, we developed comprehensive computational models that accurately represent the migration of photons through physiological tissue. Extensive simulations were then performed to predict the transport of light through the tissue, and the resulting light measured on the surface. After characterization of this light-tissue interaction, further simulations allowed for evaluation and analysis of the advanced methodologies for measurement of deep tissue.

To fully demonstrate and quantify the capabilities for measurement of deep tissue, we then examined a two layer model for tissue. Pattern recognition methods (specifically, artificial neural networks) were implemented to reconstruct layered information in the unknown layered medium. The procedure and results of each of these design efforts will be elaborated, in detail, in the following sections.

In addition, as part of this Phase I effort we surveyed the potential for measurement of additional parameters, beyond the intended oxygen saturation, with a non-invasive optical sensor. Incorporation of these additional measurements into a single, multi-function device would provide a more comprehensive assessment of physiological condition, in a cost-efficient manner.

4.1 Physiological Tissue Characteristics

Physiological tissue can be viewed as a multi-layer medium, with absorption and scattering coefficients describing each layer. This representation allows for simulation of the propagation of light through tissue using computational models.

4.1.1 Wavelength Significance

In the UV range absorption in tissue is primarily due to proteins and nucleic acids. In the visible range the primary absorbers are: Hb, HbO_2, Melanin, Bilirubin, and Beta Carotene. As the wavelength increases above 600nm and into NIR range absorption by these specific chromophores decreases and the absorption by H_20 begins to increase. In the IR range the absorption by H_2O is then dominant.

Within the transition stage from 600 nm to 1300 nm absorption due to the specific chromophores (hemoglobin, etc.) is decreased while absorption from H_20 is still small. Total absorption is therefore at its lowest in this range (600-1300 nm). This allows for the most amount of light penetration into the tissue. In high pigmented tissue (such as the liver) a photon within this wavelength range will travel an average of 2 mm before absorption. In low pigmented tissue (such as the brain) a photon within this wavelength range will travel an average of several centimeters before absorption. Within this range optical scattering is high and much larger than absorption, yielding a greater amount of reflected light.

4.1.2 Multi-layer Skin Characteristic

The skin consists of three layers: stratum corneum, epidermis, and dermis. The stratum corneum is a very thin layer (10-20 μm) of dead cells. It has a refractive index of about 1.55 and is not highly scattering. The epidermis is about 50-200 μm thick and has a refractive index of about 1.5. The primary absorber of the epidermis, in the visible and NIR spectrum, is melanin. Absorption (μ_a) and reduced scattering coefficients (μ_s') are on the order of 0.1 mm^{-1} and 1 mm^{-1} respectively. Due to small thickness, absorption and scattering of the stratum corneum and epidermis will generally have minimal effect on light transport through the skin, relative to the remaining structures, for deep tissue measurement.

The dermis layer is about 1-3 mm thick, with a refractive index of 1.4. The dermis consists of

about 70% H_20 and 20% collagen, containing blood, capillaries, sweat and sebatious glands, nerves, and lymphatics. Significant chromophores/absorbers of the dermis, in the visible and NIR spectrum, include hemoglobin, beta carotene, and bilirubin. Absorption (μ_a) and reduced scattering (μ_s') coefficients are on the order of 0.01 mm^{-1} and 1 mm^{-1} respectively. Below the dermis, subcutaneous tissue is comprised of 60-85% lipid (fat), 5-30% H_20, and has a width of several millimeters. Fat cells are 25-200μm in size, and are less absorbing than the skin layers.

The following data have been stated as representative of typical human physiological tissue:

1) Hemoglobin Extinction Coefficients:

<u>at 754 nm:</u>

ε_{Hb}=0.058 $mm^{-1}mM^{-1}$

ε_{HbO2}=0.035 $mm^{-1}mM^{-1}$

<u>at 840 nm:</u>

ε_{Hb}=0.039 $mm^{-1}mM^{-1}$,

ε_{HbO2}=0.045 $mm^{-1}mM^{-1}$

where absorption coefficient $\mu_a=\varepsilon[C]$, with [C]=absorbing concentration.

2) Typical concentration of hemoglobin ~ 0.1 mM

3) Typical reduced scattering coefficient μ_s' ~ 1 mm^{-1}

4.1.3 Modeling Other Structures

Non-invasive optical measurement of physiological parameters requires transport of light through the skin, but may also involve transport through other media. Other media may include muscle (in deep tissue measurements) or the skull (for cerebral measurements). These media can be modeled as additional layers to the skin model.

4.2 Experimental Testing

Tests were performed on human tissue to assess actual absorption levels, and to compare obtained results with diffusion analysis predictions of intensity versus distance from the source. Measurements were performed on the forearm of eight different human subjects, using a prototype sensor developed in Phase I that allows for variation of the source-to-detector distance.

Two different LED sources were used, one for each of the two different wavelengths required for the sensor (Stanley DN304: 850nm; Stanley NR513: 720nm). A simple photodetector (Burr-Brown OPT101) was used for measurement of reflected light at varying distances from the source. A sine wave supply with frequency of 1kHz was used to apply an AC (intensity modulated) light signal to the tissue.

Subject	Attenuation Factor (λ=850 nm)
1	$10^{-1.03}$/cm
2	$10^{-1.13}$/cm
3	$10^{-1.05}$/cm
4	$10^{-0.84}$/cm
5	$10^{-0.91}$/cm
6	$10^{-0.89}$/cm
7	$10^{-0.79}$/cm
8	$10^{-0.87}$/cm

Table 4: Experimental test results using prototype sensor.

Measured light levels for each subject were plotted versus distance from the source. For all cases the logarithm of reflected light was linear as a function of distance, which agrees with the diffusion model and simulations. Computation of the slope of this function yields the attenuation per unit distance from the source, which is shown in Table 4, for λ=850 nm. Tests using the second LED, λ=720 nm, were performed only on subjects 1 and 4 (due to a longer time required to acquire the component), yielding an attenuation of $10^{-1.13}$/cm and $10^{-0.79}$/cm, respectively.

The results demonstrate that there is an attenuation of about one order of magnitude (10^{-1}) per centimeter from the source for all subjects. This agrees with diffusion analysis results of the assumed typical value for tissue absorption and scattering coefficients stated in scientific literature (μ_a=0.005 mm^{-1}, μ_s=1 mm^{-1}), as illustrated in Figure 3.

In addition to these measurements, the effect on tissue absorption due to the restriction of blood was examined. Measurement was taken on the forearm of one person before, during, and after a brief period of blood restriction using a cuff on the upper arm. Measurements taken at about 2 cm from the source indicated a drop of 20-35% of the light intensity during blood restriction, with subsequent return after release of the cuff.

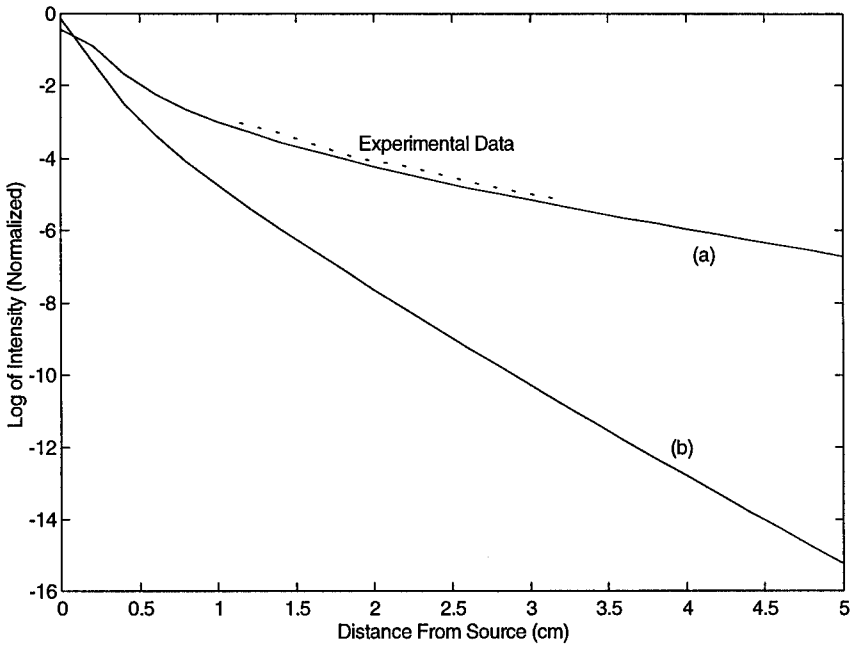

Figure 3: Illustration of reflected light intensity versus distance from the source. Curves (a) and (b) were computed from the diffusion equation using (a) typical characteristics for tissue: μ_a=0.005, μ_s=1, (b) assumed worst case values: μ_a=0.03, μ_s=3. Experimental data from subject 3 (dashed line) fits closely with typical tissue characteristics.

4.3 Model For Light Transport - MC and Diffusion

Computational models for the transport of light through tissue were implemented on a PC platform using Matlab for Windows software. In the models, the optical medium is represented by a 2 dimensional matrix of cells with programmable size and incremental distance per cell. The two dimensions represent linear distance from the source (i.e. x-direction) and depth into the tissue (i.e. z-direction). Characteristics of the medium are described by an absorption matrix that provides the absorption coefficient for each cell. In this way a multiple-layer or highly detailed medium can be described. The model currently assumes a uniform, definable scattering coefficient. Two separate models were constructed using 1) Monte Carlo (MC) analysis and 2) diffusion analysis. Each are individually elaborated next.

4.3.1 Monte Carlo Model

The Monte Carlo (MC) technique simulates the path of many individual photons to provide an indication of the total photon migration. A given photon is injected into the medium at the source location, and then for each cell of the medium that the photon passes through, absorption or scattering is randomly determined based on probabilities. These probabilities are computed from the absorption coefficient of the given cell and the scattering coefficient.

When an absorption event occurs that photon path is then terminated, and a record of the absorption location is stored. When a scattering event occurs the direction of the photon is changed based on probable scattering angle. This model uses a distribution for the scattering angle that is moderately forward directed to more accurately simulate scattering in actual physiological tissue.

When a photon exits the medium (transmission, reflection, or exiting to the sides) a record of the exit location is stored. In addition, when a photon is reflected (i.e. it exits from the same surface it entered) the maximum depth that the photon traveled into the tissue is recorded. This information helps provide an indication of the depth sampled for different source to detector distances.

A drawback of the MC model is that simulation of a sufficient number of photons requires a large computational time. For example, on a pentium 100MHz PC simulation of 50,000 photons, which provides suitable measurements only for small distances from the source, required more than 3 hours.

4.3.2 Diffusion Model

The diffusion model represents photon migration as a diffusion process. Several studies have compared diffusion and MC simulations to experimental measurements and shown that both methods closely mimic the actual behavior of light transport. The diffusion model constructed is based on published techniques (Haselgrove et al., 1991). This approach uses iterative calculations of the diffusion process over small increments of time to provide a time-course of photon migration through the tissue. The computation time required for diffusion simulation is much less than that for MC simulation with sufficient photons.

4.3.2.1 Theory

The isotropic diffusion equation (which assumes uniform scattering) describes the migration of photons as follows:

$$\frac{n}{c}\frac{\partial}{\partial t}\Phi(r,t) - D\nabla^2\Phi(r,t) + \mu_a\Phi(r,t) - S(r,t) = 0$$

where $\Phi(r,t)$ is the photon flux at position r and time t, D is the diffusion coefficient, μ_a is the absorption coefficient, c is the speed of light, n is the refractive index of the medium, and $S(r,t)$ is the light source. Assuming isotropic, uniform scattering with the reduced scattering coefficient $\mu_s' >> \mu_a$ the diffusion coefficient is estimated by $D=1/3\mu_s'$.

The time course of reflected light at a distance d from an impulse source can be described as the product of a scattering term and an absorption term:

$$R(d,t) = (scattering...term)\cdot(absorption...term) = S(d,t)\cdot e^{-\frac{\mu_a ct}{n}}$$

Diffusion theory allows for approximation of the scattering term, S(d,t), which can then be further

simplified:

$$S(d,t) = \left(4\pi D\frac{c}{n}\right)^{-3/2} z_0 t^{-5/2} \exp\left(-\frac{r^2+z_0^2}{4\pi D\frac{c}{n}t}\right) = kt^{-5/2}$$

where $z_0=1/\mu_s'$ and k depends on scattering coefficient, μ_s, and the distance d. This approximation is valid after the initial increase in reflected light, following the source impulse, after which light then decays as $t^{-5/2}$. The time course of reflected light then becomes:

$$R(d,t) = kt^{-5/2}\exp\left(-\frac{\mu_a ct}{n}\right)$$

This formula illustrates that the initial behavior of $R(d,t)$ is dominated by the scattering term and later behavior is dominated by the absorption term. The $\log(R(d,t))$ will approach a straight line with slope equal to $-\mu_a c/n$. The time course of reflected photons therefore indicates the absorption of the media sampled.

4.3.2.2 Iterative Calculations

The isotropic diffusion equation is used as the basis for performing a series of iterative calculations over small increments of time, to model the migration of photons. An initial condition is set for a photon source at t=0. Successive iterations compute the probability of photon location at the time t+Δt:

$$\Phi_s(d, t+\Delta t) = \{\Phi_s(d,t)*K(d)\}\{1-A(d)\}$$

where $\Phi_S(d,t)$ is the probability distribution that a photon emitted from a source, s, at time t=0 will be found at the position d at time t; * represents convolution; $K(d)$ is the point spread function of photons in a time Δt; and $A(d)$ is the absorption matrix which accounts for the absorption of photons in time Δt. The point spread function is defined by:

$$K(d) \propto \exp\left\{\frac{-d^2}{4Dc\Delta t}\right\}$$

with $K(d)$ normalized by:

$$\sum K(d) = 1$$

Using this procedure, iterative calculations provide the time course of photon migration throughout the medium.

4.3.2.3 Probable Path Calculation

The model constructed can also compute the probable path of photons arriving at a distance d

from the source within a chosen time period. Probable paths are computed from the probability distributions of photon location, $\Phi_s(r,t)$. The probability, $\Psi_{sd}(r,T)$, that a photon emitted from the source passes through a point r and then arrives at a detector at position d at time T is calculated by:

$$\Psi_{sd}(r, T) = \int_o^T \Phi_s(r, t)\Phi_d(r, T-t)dt$$

where $\Phi_d(r,t)$ is the probability distribution of a photon emitted from the detector location. This equation can be computed by a simple limited convolution. Based on this equation, the model constructed allows for computation of the probable path for photons arriving at a chosen detector distance within a chosen period of time. The probable path is dependent on both the distance from the source and the time of arrival.

4.3.3 Verification of Models

4.3.3.1 Monte Carlo Simulations

MC simulations were carried out for several different conditions. A uniform scattering coefficient μ_S=40 mm^{-1} was assumed, with scattering angle computed from a probability distribution with forward tendency. The case of uniform absorption was first considered: μ_a=0.1 mm^{-1} (note this value is somewhat higher than expected for typical tissue). Simulations were carried out on 50,000 photons, with a medium size of 10x10 mm and resolution of 0.01 mm per cell (yielding 1000x1000 cells).

Figure 4a shows the histogram of photons reflected versus distance from the source. The distribution is gaussian in form with mean=0, as expected. The location of photon absorptions within the medium, for this simulation, is shown in Figure 4b. This information provides an indication of the migration of photons, yet it is important to note that because these photons were absorbed within the medium they are not detectable on the surface.

For photons that were detected on the incident surface, the maximum depth of penetration is shown in Figure 4c. At small distances from the source, the majority of photons reflected have traveled a short distance into the medium. At larger distances there are less photons reflected, but they generally travel deeper.

Figure 4d shows the average maximum depth, for reflected photons, at each incremental distance. The increase in variability as distance increases is due to fewer photons at larger distances which do not provide a large enough sample size, given the simulation of 50,000 photons. These plots show that there is a distinct relationship between the distance and depth sampled. This relationship is also dependent upon the absorption coefficient.

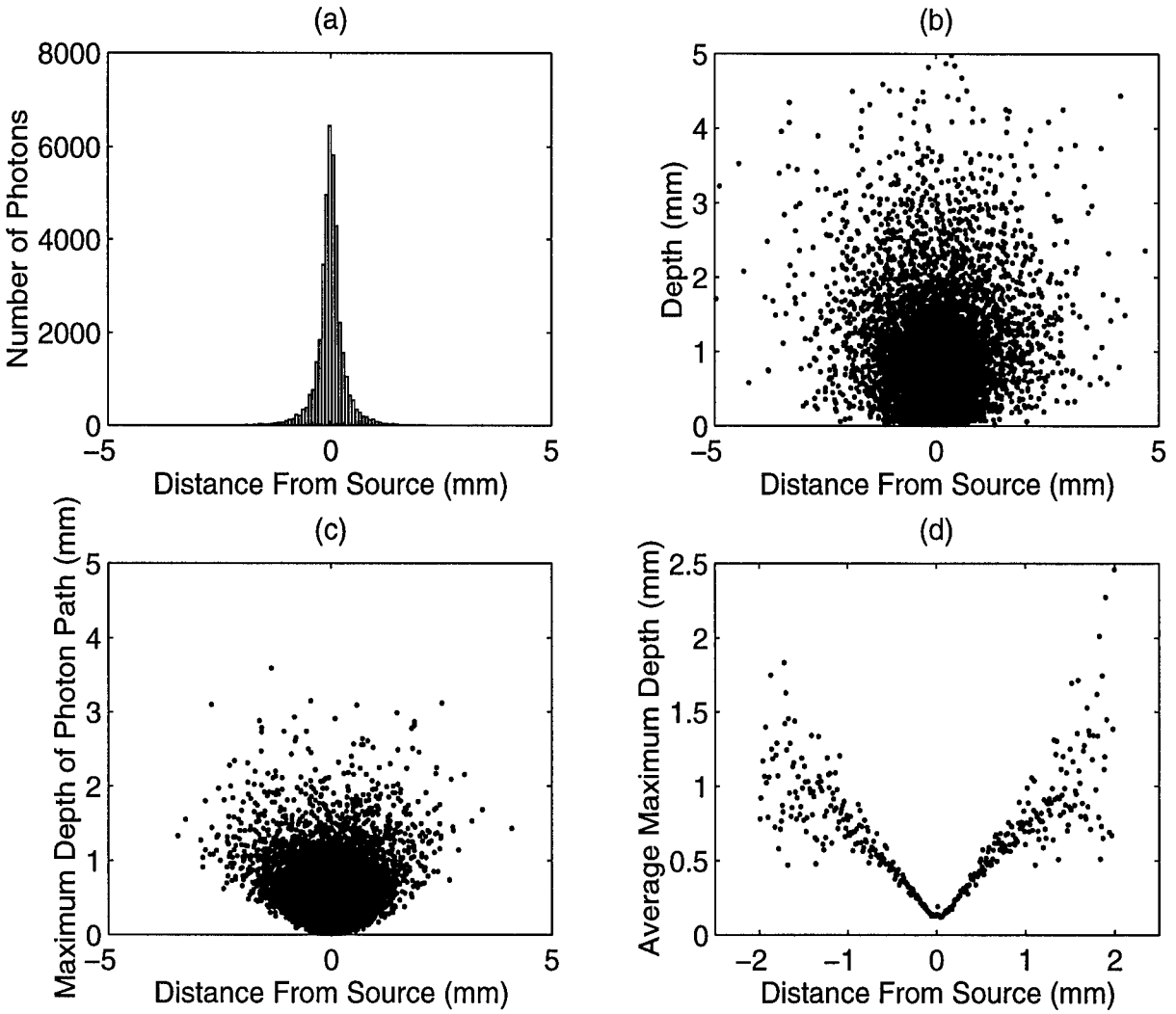

Figure 4: a) Histogram of reflected photons from MC simulation of 50,000 photons; b) Plot of photon absorption locations from MC simulation of 50,000 photons; c) Maximum depth of penetration for reflected photons from MC simulation of 50,000 photons; d) *Average* maximum depth of penetration for reflected photons from MC simulation of 50,000 photons. μ_a=0.1mm^{-1}, μ_s=40mm^{-1}.

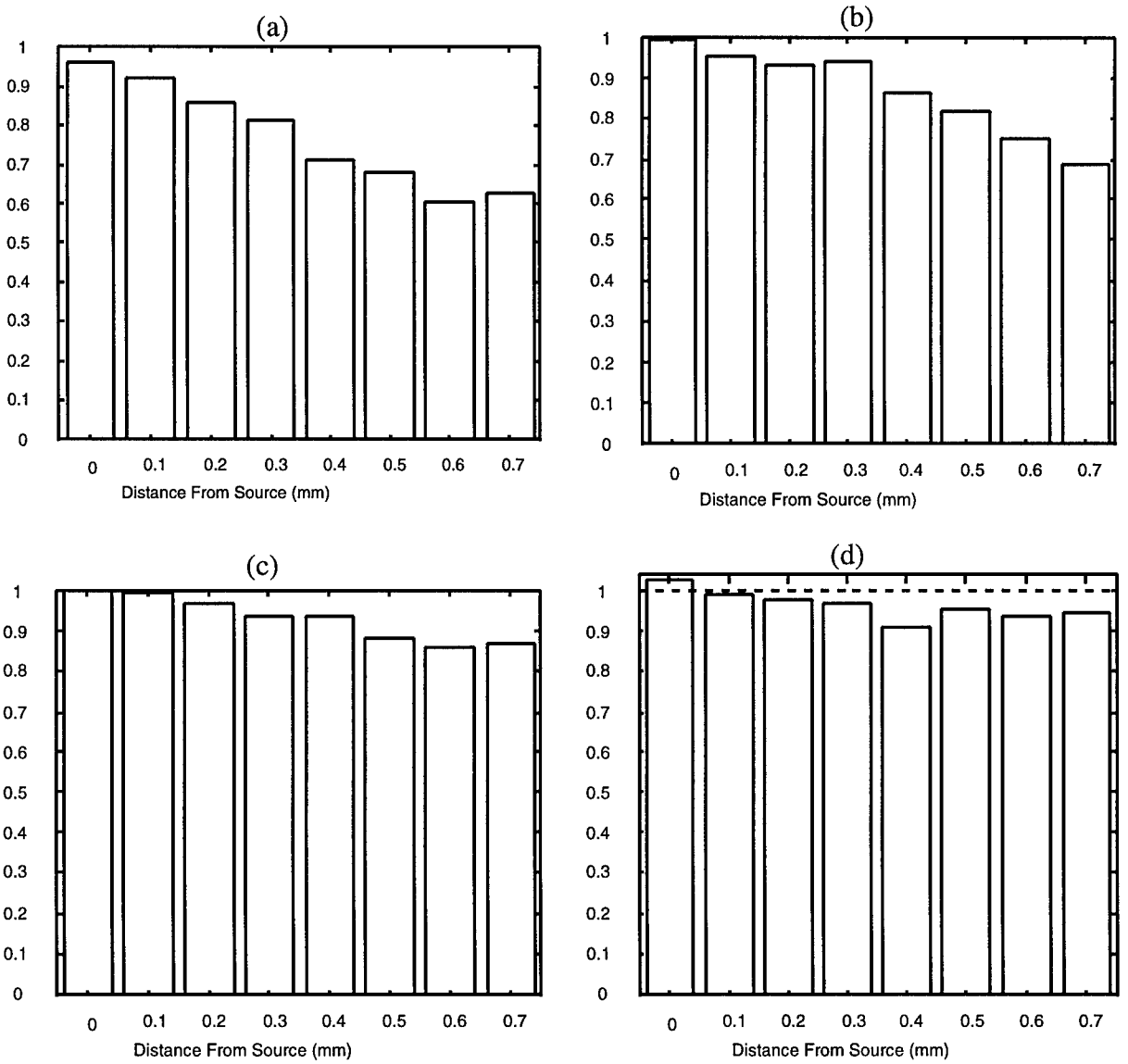

Figure 5: Number of reflected photons at incremental distance from the source, with high absorption band at a) 0.2mm depth, b) 0.4mm depth, c) 0.6mm depth, d) 0.8mm depth, based on MC simulation of 50,000 photons (μ_a=0.1 mm^{-1}, except in band μ_a=1 mm^{-1}). Values are normalized by the number of reflected photons from simulation in the homogeneous medium (i.e. no band).

To illustrate the effect due to depth variations, additional simulations were performed with a band of increased absorption at various depths within the μ_a=0.1 mm^{-1} medium. For these simulations a band of 0.1 mm thickness with absorption coefficient μ_a=1 mm^{-1} was added to the homogeneous medium (μ_a=0.1 mm^{-1}) at one of 4 different depths: 0.2 mm, 0.4 mm, 0.6 mm, and 0.8 mm. For all cases, the reflected light at 0.1 mm increments (i.e. possible detector sites) from the

source was computed and normalized by the amount of light at that distance given no absorption band.

Results are shown in Figure 5. An absorption band at 0.2 mm depth affects the amount of light reflected at all detector distances. At 0.4 mm depth the absorption band affects the amount of light at distances of 0.1 mm and greater. As the depth of the band increases further, the detectors do not see a significant change until increasingly greater distances from the source.

4.3.3.2 Diffusion Simulations

Diffusion simulations were performed on a medium of size 5 mm long by 5 mm deep, and incremental resolution 0.1 mm per cell (yielding a matrix of size 50 x 50). Medium characteristics include absorption coefficient μ_a=0.1, and a uniform scattering coefficient approximately equivalent to that used for the performed MC simulation (μ_s'=5, where μ_s' is a reduced scattering coefficient which accounts for scattering angle). Iterative calculations were carried out from t=0 to 200pS, with Δt=1pS. Figure 6 illustrates the time course of photons arriving at two different detector sites (1 mm and 2 mm from the source). A plot of the logarithm of this time-course (Figure 7) illustrates that the decay approaches a straight line with slope independent of detector distance, and proportional to μ_a, as expected.

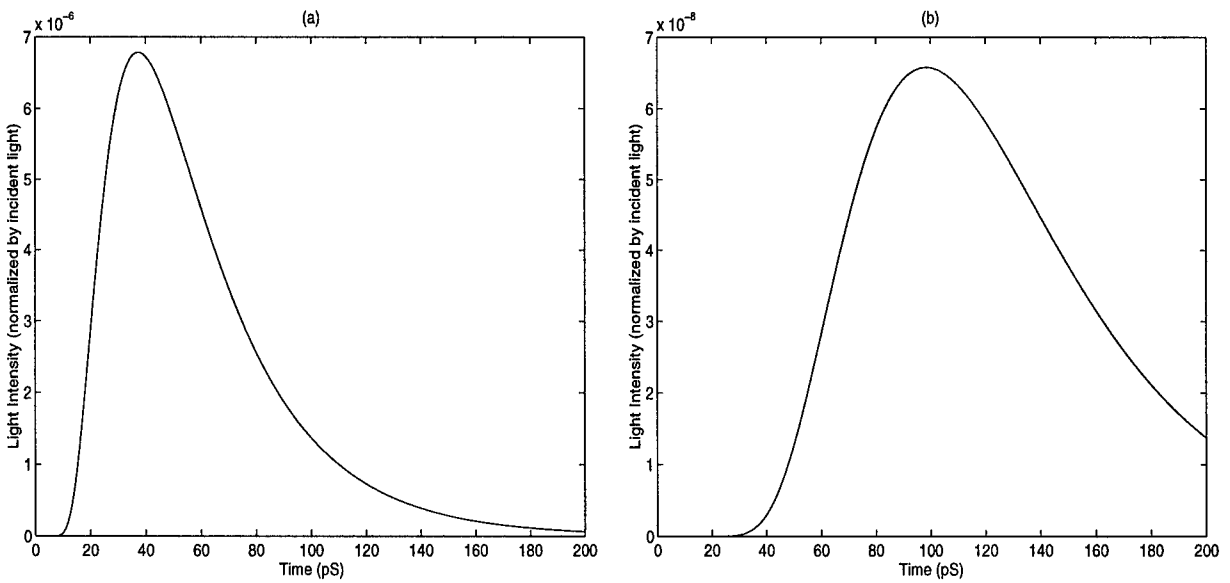

Figure 6: Time course of photons detected a) 1 mm from the source, and b) 2 mm from the source, using diffusion simulation.

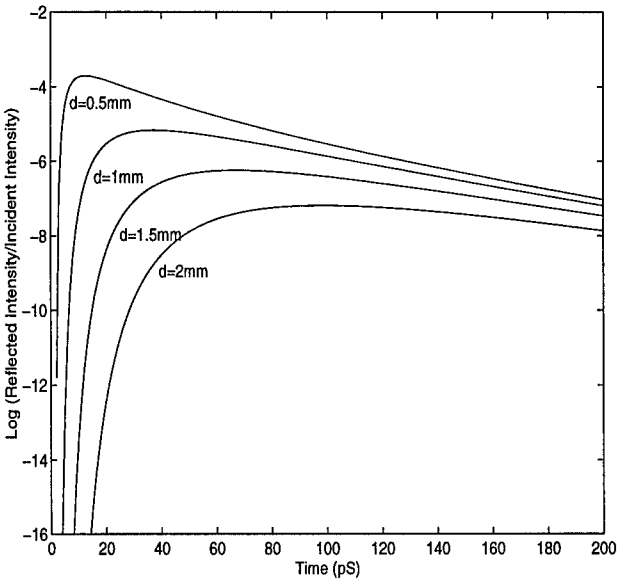

Figure 7: Log of time course of reflected photons at various distances from the source. All signals approach a straight line with slope proportional to μ_a.

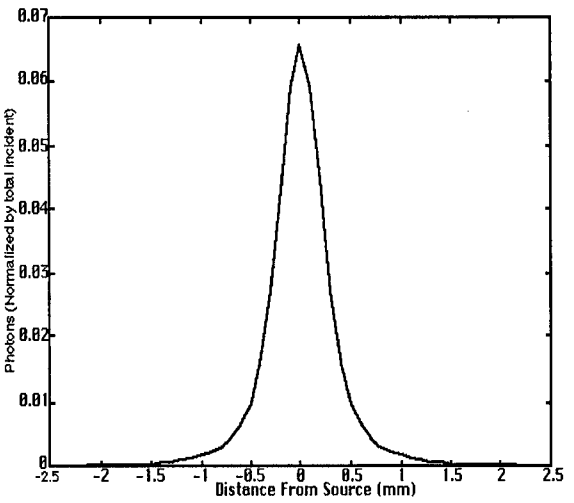

Figure 8: Reflected photons versus distance from the source from diffusion simulation, normalized by total incident photons. The distribution has the same gaussian form seen from the MC simulations.

The total number of photons reflected at each incremental distance from the source was also computed. Figure 8 shows the relationship of total photons reflected (during 1 to 200ps) versus distance from the source. The diffusion simulation demonstrates the same gaussian-form distribution seen in the MC simulation (see Figure 4a).

Results from calculation of the probable photon paths for a distance of 1 mm and 2 mm from the

source are shown in Figure 9 for various time intervals. These plots show that the photon path is dependent on both the distance and the time of arrival. In addition, with increased distance or time, there is increased dispersion/spreading of the photon path. Increased dispersion may yield decreased resolution capabilities.

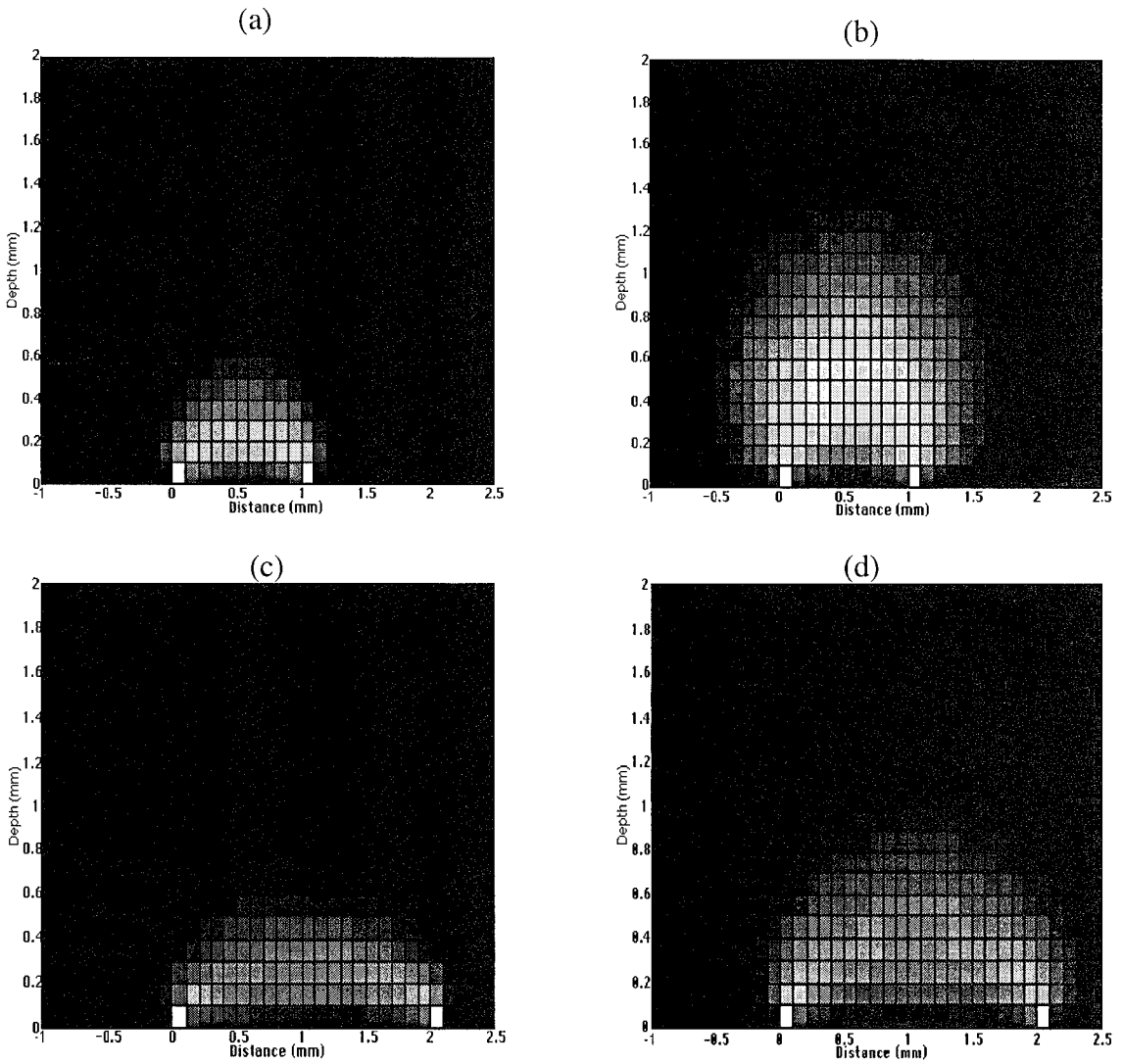

Figure 9: Probable path of photons arriving a) *1 mm* from the source during a time period of *1 to 50pS* after source impulse; b) *1 mm* from the source during a time period of *151 to 200pS* after source impulse; c) *2 mm* from the source during a time period of *1 to 50pS* after source impulse d) *2 mm* from the source during a time period of *151 to 200pS* after source impulse.

4.4 Results of Simulations and Analyses for Optimum Design

In the above simulations for validation of the computational models, the applied absorption coefficients are slightly larger than would be seen for physiological tissue (due to inaccurate data at the outset of the Phase I project). Subsequent simulations, aimed toward the evaluation and development of an optimum design, are based on absorption and scattering characteristics representative of actual physiological tissue (as discussed in section 4.1 and the following sections).

Simulations were performed using the developed diffusion-based model described in section 4.3. Simulations were aimed at determining the characteristics of light and tissue interactions, evaluating advanced methodologies for deep tissue measurement, and demonstrating the capabilities for deep tissue measurement.

Important characteristics of light-tissue interaction, elaborated in sections 4.4.1-4.4.3, are:

1) intensity of reflected light versus distance from the source,
2) depth of photon travel as a function of distance from the source, and
3) depth of photon travel as a function of transit time.

Advanced methodologies identified include the time-resolved (pulsed source) and the frequency domain (intensity modulated source) techniques. Evaluation of these two methods for the capability to perform deep tissue measurements is reported in sections 4.4.4-4.4.5. Depth measurement capabilities are demonstrated by performing simulations in a two layer model for tissue, and an artificial neural network technique is implemented for reconstruction of the layered data. These analyses are reported in sections 4.4.6-4.4.7.

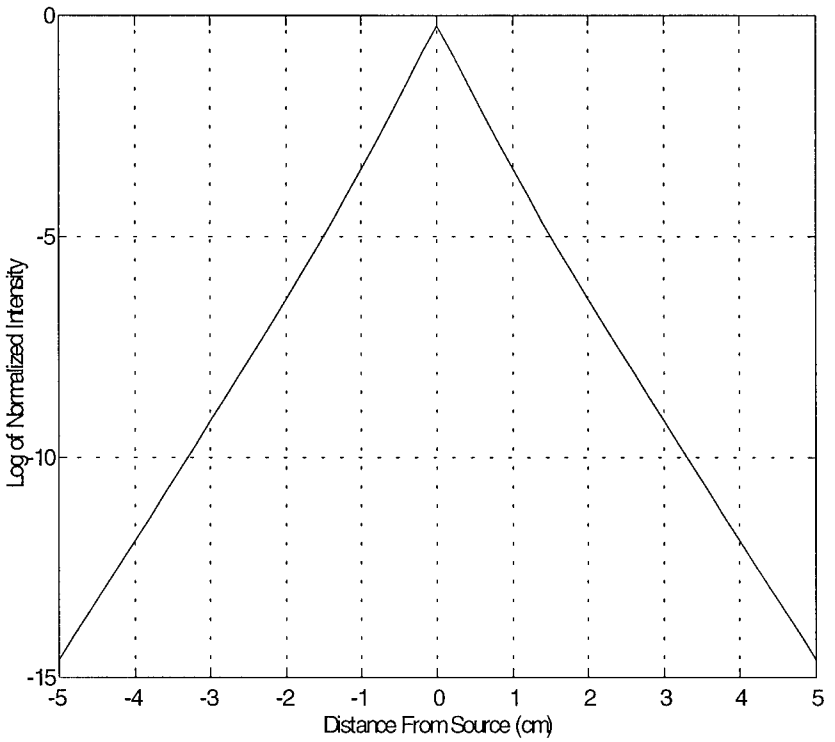

Figure 10: Reflected light intensity versus distance from the source under assumed worst case conditions (μ_a=0.03 mm^{-1}, μ_s=3 mm^{-1}), based on diffusion simulation.

4.4.1 Reflected Light Intensity versus Distance From Source

Given the typical concentration of hemoglobin in tissue under normal conditions, and assuming that absorption is due primarily to hemoglobin, we would expect an absorption coefficient of μ_a ~

0.005 mm^{-1} for wavelengths near 800 nm. However, hemoglobin concentrations can vary significantly among different conditions, and other substances may contribute to the total absorption. In particular, with low levels of oxygenation-- where it can be most important to provide accurate measurements-- tissue absorption will increase (for λ_1<800 nm) due to the larger absorption coefficient of deoxygenated hemoglobin. Based on literature data we assumed worst case (maximum), for skin tissue around 800 nm, to be μ_a=0.03 mm^{-1}, $\mu_s' = 3\ mm^{-1}$

Given worst case values for absorption and scattering, simulations were performed to assess the attenuation of light through tissue as a function of distance from the source. Figure 10 illustrates that the log of reflected light is approximately linear as a function of distance. At a distance of 5 cm from the source the injected light has been attenuated by a factor of about 10^{-15}. ***Given emitter and detector capabilities, these results suggest that adequate light will be measurable at a distance of up to 5 cm for the worst case values of absorption and scattering.*** With lower absorption and scattering values adequate light will be measurable at distances greater than 5 cm from the source. For example, with typical values μ_a=0.005 mm^{-1} and $\mu_s' = 1\ mm^{-1}$ an attenuation of only about 10^{-7} is observed at 5 cm from the source.

4.4.2 Depth of Photon Travel versus Distance From Source

Probable photon paths were computed from the diffusion model, using the method described in section 4.3. Figure 11 illustrates the different paths taken by photons detected at different distances from the source, with μ_a=0.03 mm^{-1}, $\mu_s' = 3\ mm^{-1}$. By computing the probable photon path for light arriving at different distances from the source, the depth sampled as a function of distance was evaluated. Results demonstrate that the average and standard deviation of the depth sampled, shown in Figure 12, both increase with increasing distance from the source.

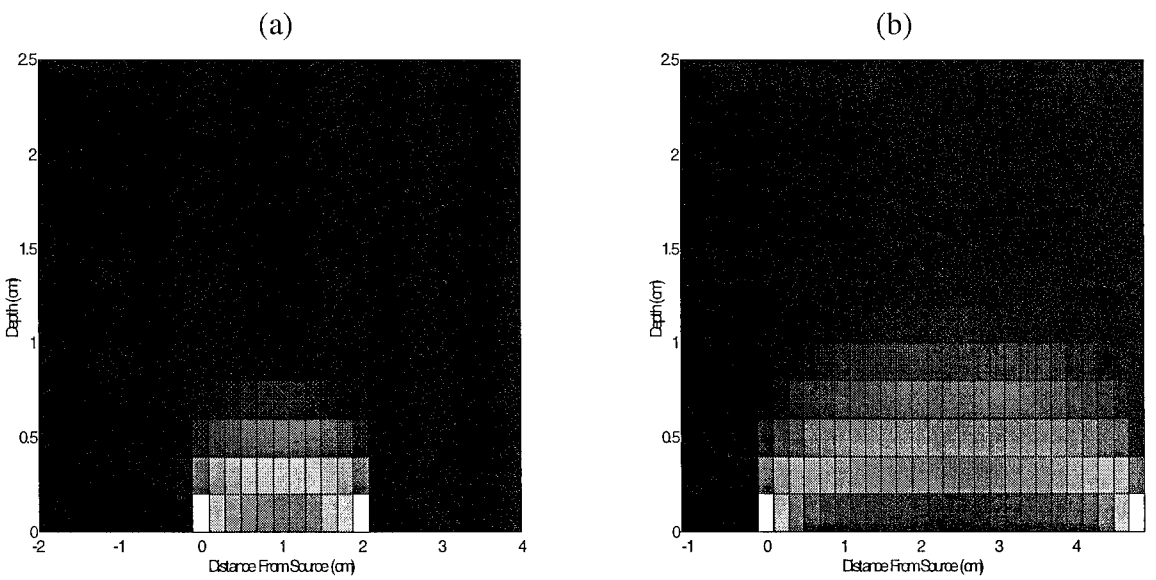

Figure 11: Probable path of photons arriving at a) 2 cm and b) 4.8 cm from source.

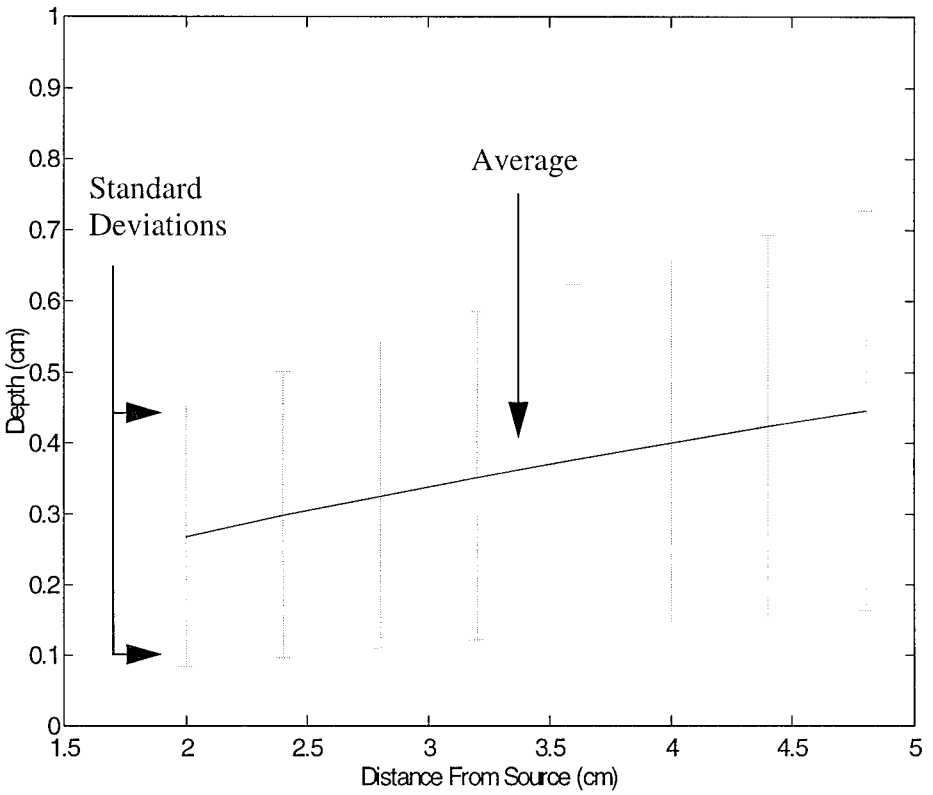

Figure 12: Average and standard deviation of depth of photon path as function of distance.

In Figure 10 it was suggested that reflected light will be measurable at distances up to 5 cm or more from the source. Figure 12 indicates that at 5 cm from the source, the reflected photons have sampled an average depth of 4.5 mm into the tissue, with the edge of the standard deviation envelope at a depth of 7.5 mm. Detection of the reflected light at incremental distances from the source may allow for reconstruction of tissue characteristics along the edge of this envelope, or deeper.

4.4.3 Depth of Photon Travel versus Transit Time

Probable photon paths indicate that the path of photon migration is also a function of the time of arrival at the detector site. Figure 13 illustrates the different paths taken by photons arriving at a given distance (4 cm) from the source at different times, with μ_a=0.03 mm^{-1}, $\mu_s' = 3\ mm^{-1}$. The average and standard deviation of the depth sampled, shown in Figure 14, both increase with increasing time of photon travel.

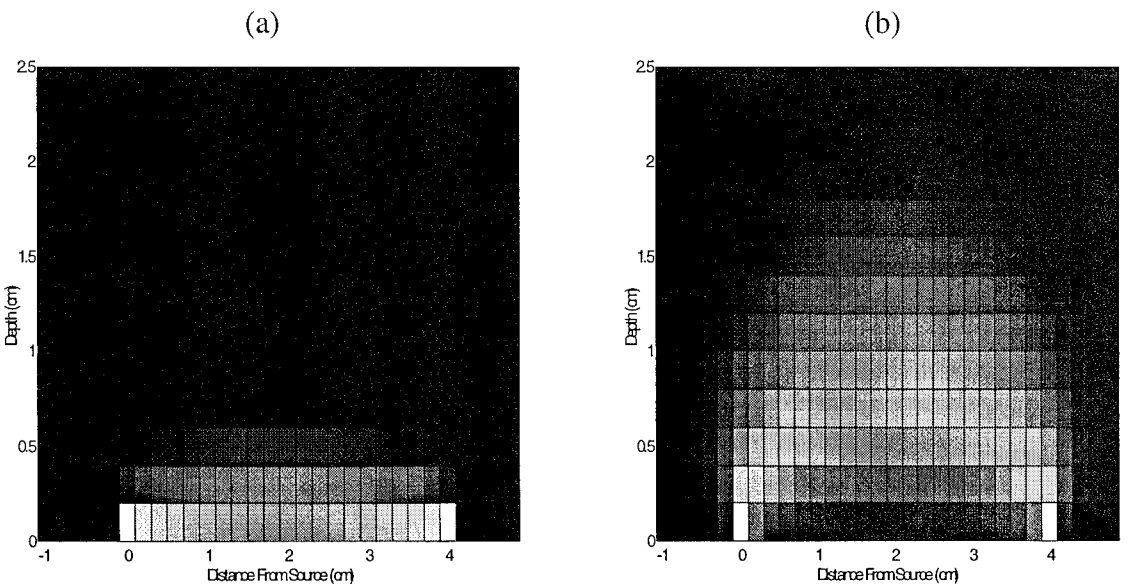

Figure 13: Probable path of photons arriving 4 cm from the source, during a) 0-.5 ns, and b) 4.5-5 nS, after source pulse.

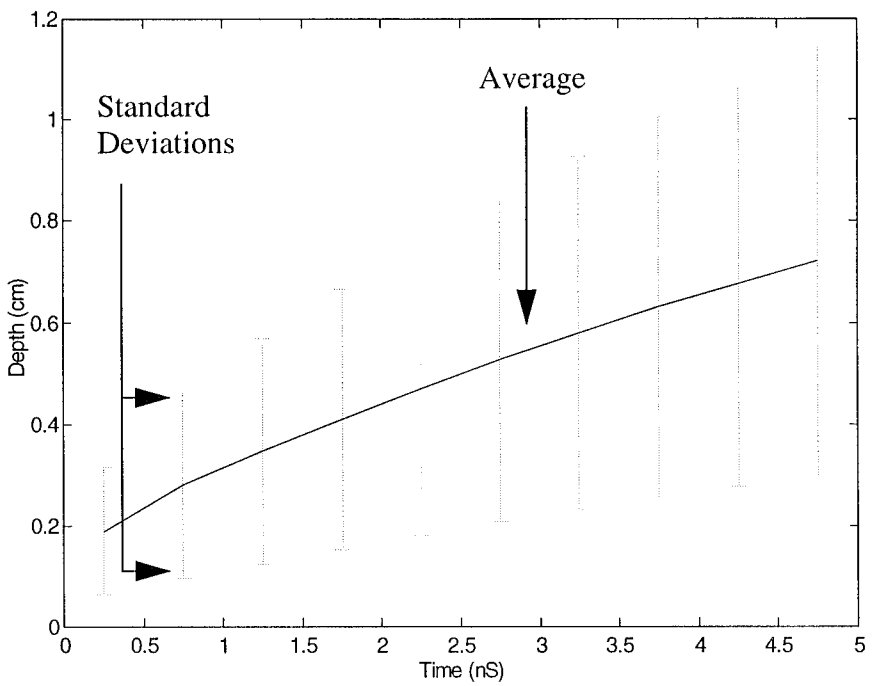

Figure 14: Average and standard deviation of depth of photon path as a function of time.

These results suggest that the pulsed time-resolved or time-gated methods may allow for selection of photons which have sampled different depths. The plots might further suggest, on first inspection, that time-gating may allow for deeper measurement than by use of different detector distances alone, yet this is not necessarily true. By restricting measurement to photons arriving within a given period of time, the signal level will be much smaller.

For instance, Figure 15 illustrates the time-course of photons arriving at a distance of 4 cm from the source. At 2.5 ns the signal level is attenuated to about 10^{-15}, approaching an unmeasurable level. For this time of arrival (2.5 ns) at 4 cm from the source the average of the sampled depth and edge of the standard deviation envelope are about 5 mm and 8 mm respectively (see Figure 14). These values are about the same as for total photons (over all time) arriving at a distance of 5 cm from the source (see Figure 12), the distance at which reflected intensity reaches ~10^{-15}. Thus, the time-gating method appears to reach approximately the same limitations for detection of adequate photons which have traveled to a given depth.

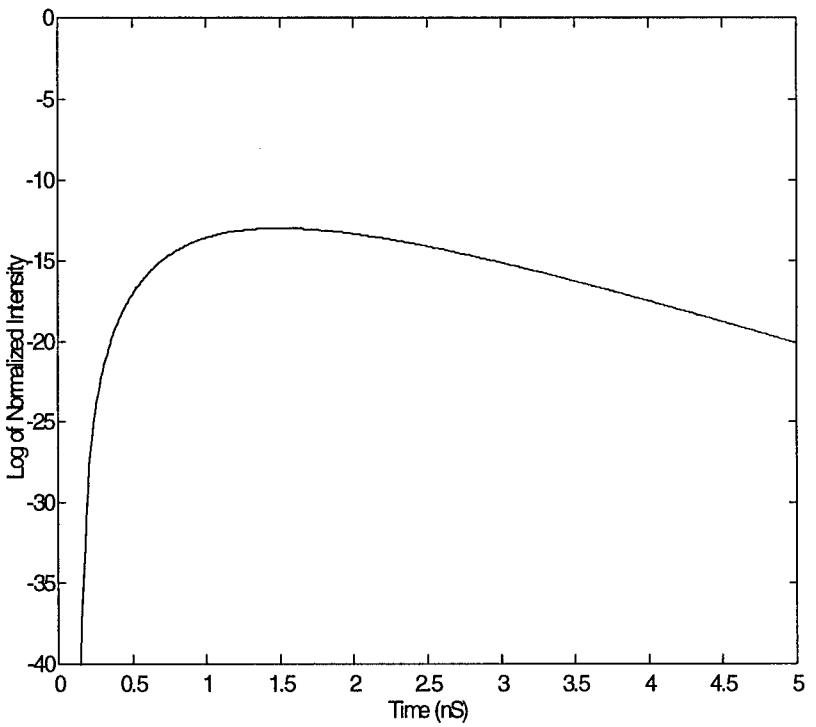

Figure 15: Reflected intensity of light arriving at a distance of 4 cm from the source, following the source pulse.

4.4.4 Time Resolved Measurement of the Absorption Coefficient

Diffusion analysis demonstrates that by injecting a short pulse of light, the absorption coefficient of a medium can be measured from the time course of reflected photons. As discussed in section 4.3.2, the log of reflected light over time will approach a straight line which is proportional to μ_a. Figure 16 shows the time course of reflected photons arriving at detector distances up to 5 cm from the source, for a medium with μ_a=0.03 mm^{-1}, μ_s' = 3 mm^{-1}. These plots illustrate that at 5 nS after the injected pulse of light, the reflected signals are attenuated by 10^{-18} to 10^{-22}, and are therefore unmeasurable.

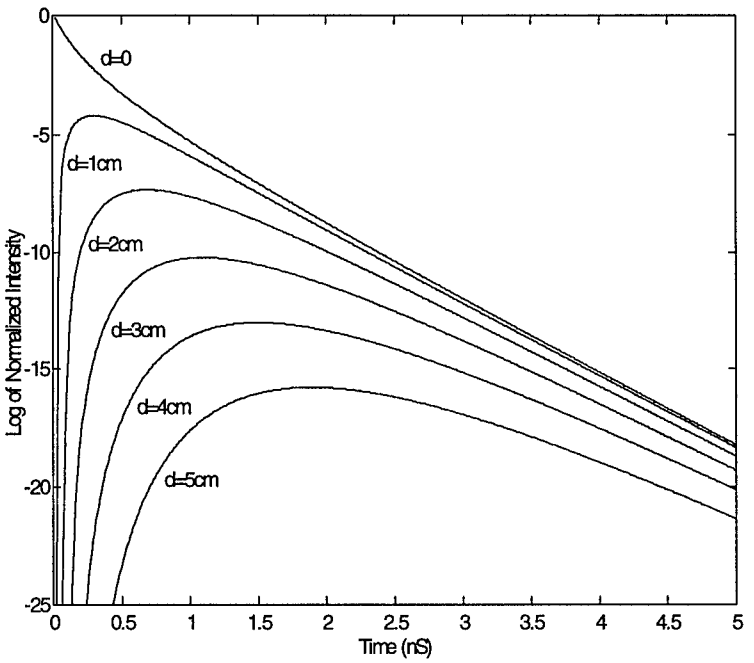

Figure 16: Time course of photons arriving at different distances from the source.

Calculation of the absorption coefficient from the slope of the time course of reflected light, at times between 0 and 5 nS, is shown in Figure 17. This figure demonstrates that at 5 nS after the injected pulse of light, the signals detected at a distance of 2 cm or more from the source have still not reached close enough to the straight line behavior proportional to μ_a. These signals do not approach the straight line behavior until after 5 ns, when the light has attenuated below measurable levels.

Accurate computation of μ_a (such as within 5%) using the pulsed time-resolved method, under these conditions, is therefore not possible at detector distances greater than 2 cm from the source. As a result, the capability for measurement to large depths will be greatly restricted when using the time-resolved method, since deep measurement requires accurate measurement at large distances from the source.

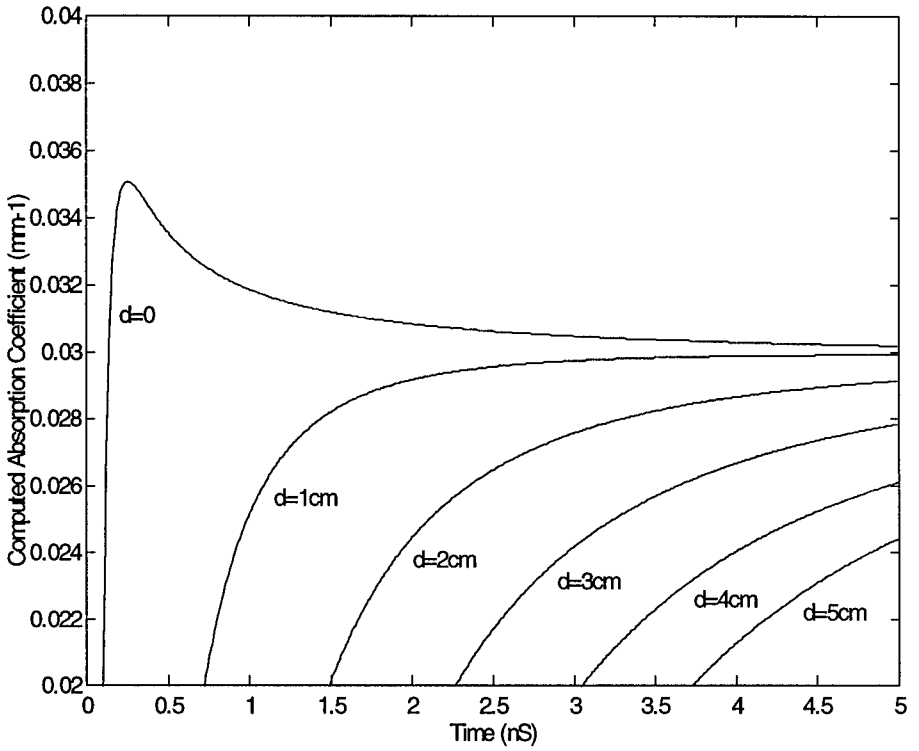

Figure 17: Computation of absorption coefficient, over time, from the time resolved waveforms.

4.4.5 Frequency Domain Measurement of the Absorption Coefficient

An alternative method for computation of the absorption coefficient is to apply an intensity modulated signal. The signal attenuation and the phase shift as a function of detector distance then allow for measurement of the absorption and scattering coefficients (Fantini et al., 1995). Specifically, the slope of the detected DC signal, AC signal, and phase versus distance from the source are dependent upon the absorption and scattering coefficients. For semi-infinite geometry this relationship is not precisely linear, but with appropriate calculations can be treated as such (Fantini et al., 1994). Measurement of two of these three functions thus allows for determination of both the absorption and scattering coefficients.

Figure 18 illustrates the reflected light, at various detector distances, due to a 100 MHz intensity modulated signal. The relationship of the DC signal and phase shift versus detector distance is shown in Figure 19. Using the appropriate calculations (Fantini et al., 1994) the absorption coefficient is computed from the slope of the DC and phase signals (as a function of distance), at distances from 0 to 5 cm from the source (shown in Figure 20).

Since the diffusion approximation is not valid in the immediate vicinity of the light source, computation of μ_a is not valid for small distances from the source. However, results indicate that this

method allows for accurate computation of the absorption coefficient from about 1.5 cm out to 5 cm or more from the source, therefore providing measurement to greater depths.

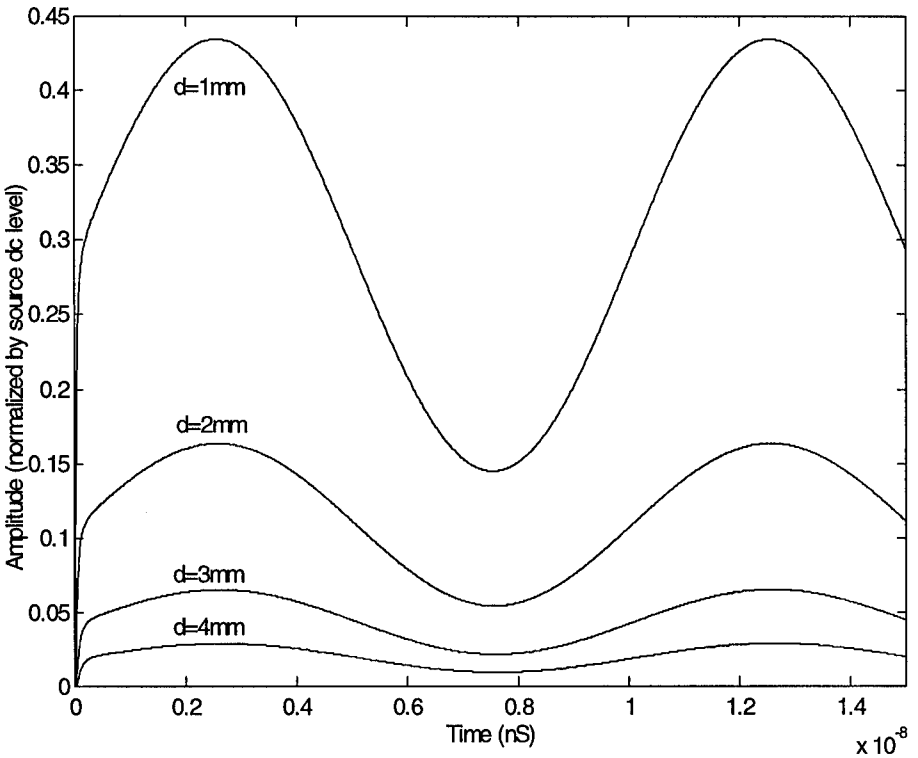

Figure 18: Reflected light at different distances from the source due to a sinusoidal intensity modulated source.

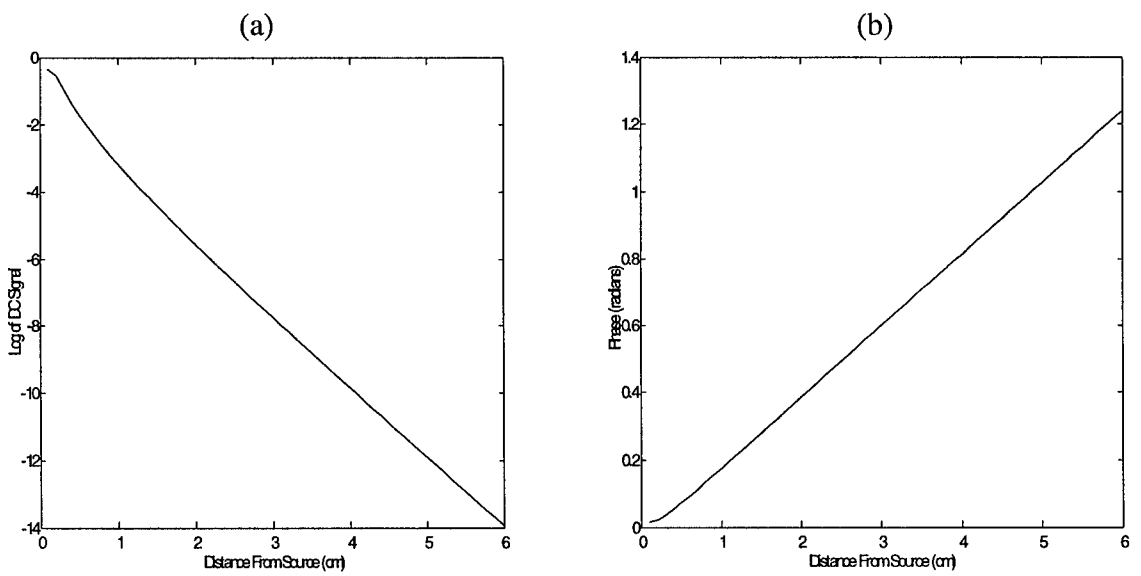

Figure 19: a) DC and b) phase shift of reflected light, as a function of distance, due to an intensity modulated source.

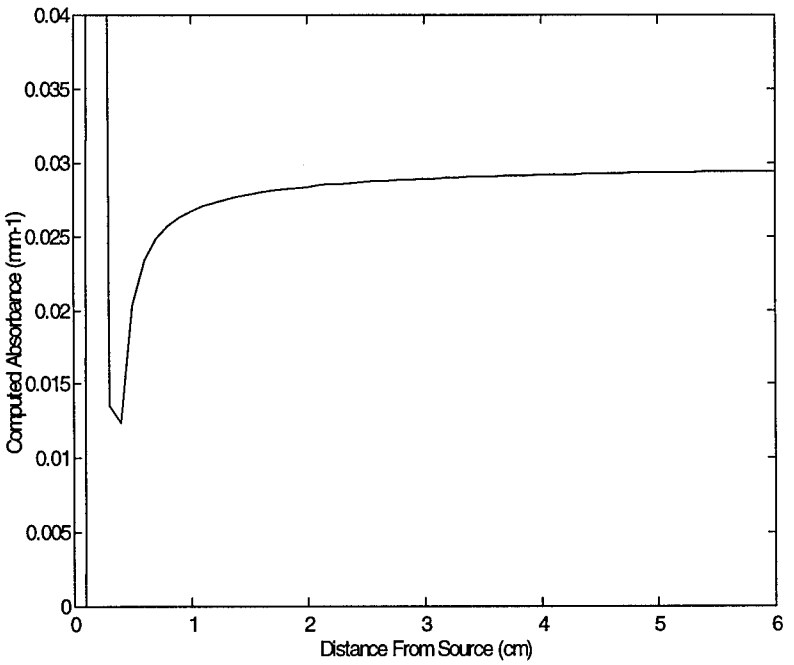

Figure 20: Frequency domain computation of absorption coefficient (μ_a=0.03 mm^{-1}).

4.4.6 Capabilities for Depth Measurement Using the Frequency Domain Method

In a non-homogeneous medium, as expected for tissue, the absorption coefficient is no longer a uniform, single variable. However, despite the highly complex structure of tissue, it may be viewed as a multiple layer system. With multiple layers of different absorptions, the number of unknown variables which must be determined becomes increasingly large. Table 5 shows the total number of unknown variables, where n is the number of layers.

Variable(s)	Number
# of layers (=n)	1
μ_a of each layer	n
μ_s of each layer	n
refractive index of each layer	n
depth of each boundary between layers	n-1
Total:	4n

Table 5: Number of unknown variables in a multiple layer medium.

An unknown number of layers can make the problem difficult, and even a small number of layers yields too many variables to account for within the scope of this Phase I effort. Nevertheless, we

can make some valid assumptions to reduce the number of unknown variables, and demonstrate the capability for resolution of depth variations. The following assumptions were made:

1) scattering coefficient, μ_s, is constant across all layers ($\mu_s' = 3\ mm^{-1}$)

2) refractive index is constant across all layers (r.i. = 1.4)

3) # of layers (n) = 2

These assumptions maintain a valid analysis for the following reasons:

1) μ_s and μ_a are computed individually from the phase and DC information at varying distances from the source. Therefore a value of μ_s within the range of typical tissue will not affect measurement of μ_a. (μ_s will affect the amount of light reflected, which determines the distance from the source up to which light is measurable).

2) The refractive index determines the velocity of light in the tissue, and has a small range (about 1.3 to 1.5) in tissue.

3) While physiological tissue may have a highly complex structure, it can be modeled by a layered structure. In many cases, a two-layer structure can be sufficient, and multiple layers may be represented by a single layer. For example: a) skin layer and subcutaneous tissue layer, b) skin and blood vessel, c) skin/skull and brain tissue, d) skin/subcutaneous and muscle, e) skin/subcutaneous and liver. The two layer model allows for determination of the relationship between spatial variations in reflected light on the surface and depth variations in tissue absorption, which may then be expanded to more layers.

Given the above assumptions, the following unknown variables remain:

1) μ_a of surface layer

2) μ_a of deep layer

3) depth of boundary between the two layers

These three parameters are therefore those which we need to determine, based on the pattern of reflected light. Figure 21 illustrates this two layer model, with the three unknown variables.

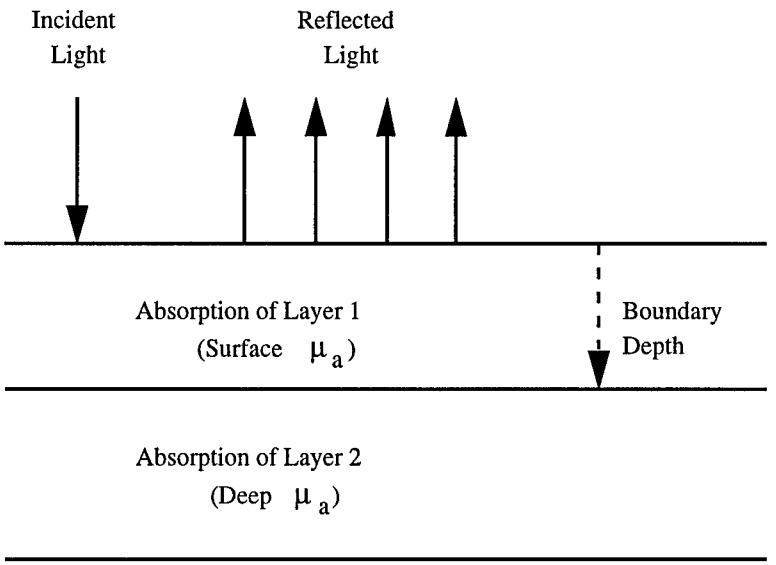

Figure 21: Illustration of the two layer model with three unknown variables: surface μ_a, deep μ_a, and boundary depth.

To examine the effect each variable has on the pattern of reflected light, we performed simulations which vary one variable at a time, while the others remain unchanged. This yields the following three analyses, each with two different conditions:

1) surface μ_a=varied, deep μ_a=constant, boundary depth=constant
   a) surface μ_a < deep μ_a
   b) surface μ_a > deep μ_a

2) deep μ_a=varied, surface μ_a=constant, boundary depth=constant
   a) surface μ_a < deep μ_a
   b) surface μ_a > deep μ_a

3) Boundary depth=varied, surface μ_a=constant, surface μ_a=constant
   a) surface μ_a < deep μ_a
   b) surface μ_a > deep μ_a

Using the methodology discussed in section 4.4.5 for frequency domain computation of the absorption coefficient, μa was computed for each of the above simulations. Figure 22 shows the computed μ_a curves (versus distance from the source), illustrating the effect of each varied parameter. Distinct variations in the computed μ_a curves are seen due to variations in the three variables (surface μ_a, deep μ_a, and boundary depth).

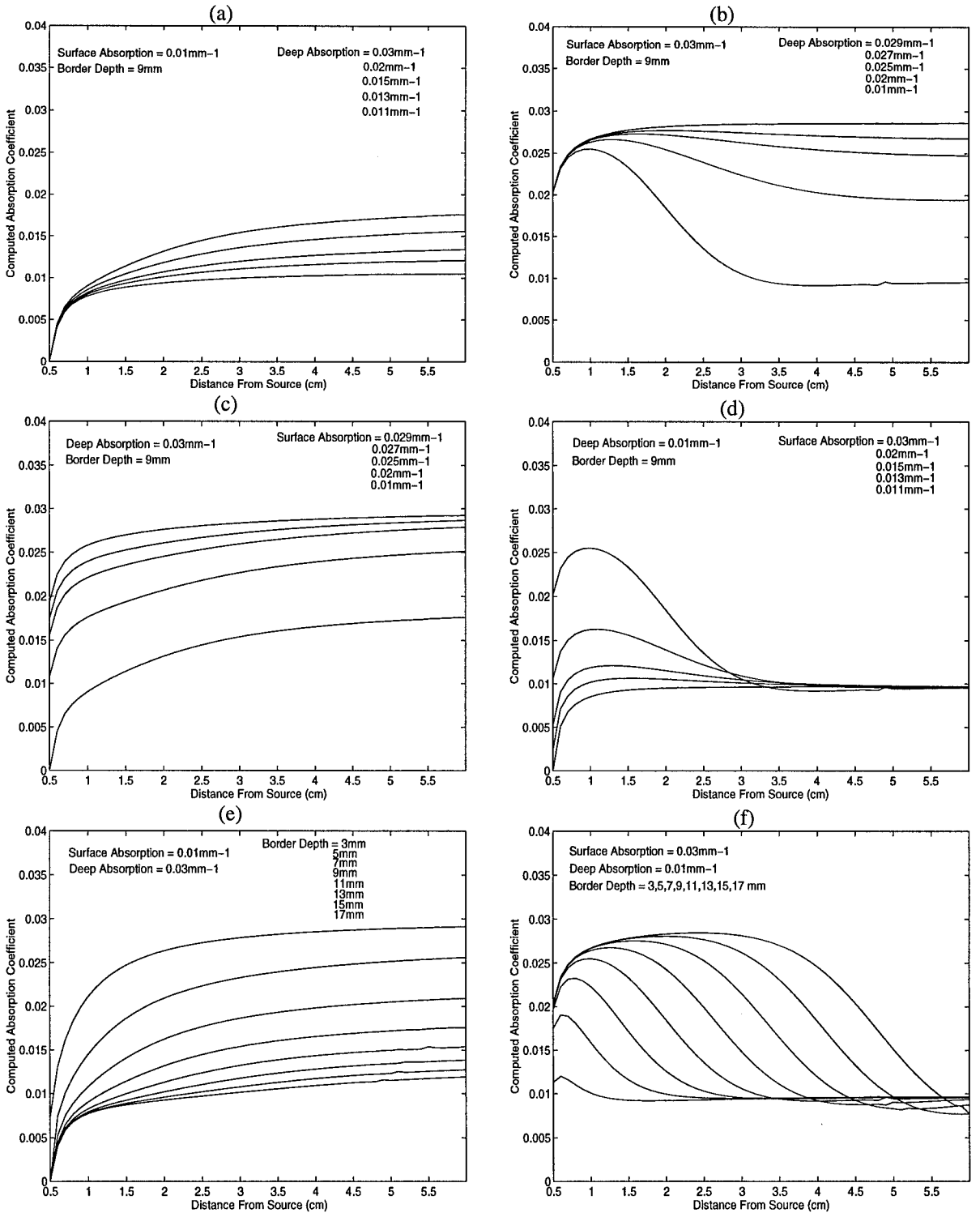

Figure 22: Computation of absorption coefficient using the frequency domain method under each of six different conditions for the two layer medium. In each plot one unknown variable is varied, as indicated above and described text.

For example, in subplot:

a) Deep absorption is varied, surface absorption < deep absorption

•computed absorption varies, particularly at large distances from source

b) Deep absorption is varied, surface absorption > deep absorption

•computed absorption varies at large distances from source, same at very short distances

c) Surface absorption is varied, surface absorption < deep absorption

•computed absorption varies at all distances from source

d) Surface absorption is varied, surface absorption > deep absorption

•computed absorption varies at small distances from source, same at large distances

e) Border depth is varied, surface absorption < deep absorption

•computed absorption varies at all distances from the source

f) Border depth is varied, surface absorption > deep absorption

•computed absorption varies at increasing distances from source with increasing depth

Thus, it is clear that variations in the unknown variables are indeed reflected in the computed μa curve. However, the given problem requires definition of this complex relationship, so that for an unknown medium each of the variables can be determined.

To review, the complete process, using the frequency domain method, is as follows:

1) An intensity modulated source is applied to the medium (tissue);
2) Reflected light is measured at varying distances from the source;
3) DC and phase shift of reflected light, as a function of distance, are measured;
4) The absorption coefficient, μ_a, is computed as a function of distance, using the DC and phase shift information;
5) The unknown variables (surface μ_a, deep μ_a, border depth) are calculated from the computed μ_a curve.

It is this last step which requires determination of the complex relationship between the unknown variables and the computed μ_a curve. For the purpose of this phase I effort, we constructed an artificial neural network, and trained it to learn this relationship. Details and results of this implementation are discussed in the next section.

4.4.7 Neural Network Determination of Absorptions and Boundary Depth

Artificial neural networks are mathematical structures, based on the interaction between physio-

logical neurons, which can perform a variety of computational functions. One particular function is the ability to perform pattern recognition. A neural network can be trained to learn a desired relationship by supplying sample data and the corresponding desired output. Ideally the neural network generalizes the appropriate relationship and is able to derive the appropriate output for any given input vector.

Here we apply neural network pattern recognition methods to determine the relationship between the computed absorption coefficient as a function of distance (from the frequency domain measurement) and the corresponding two layer structure of the measured medium. By training an artificial neural network, results indicate the distinctness of the relationship and the corresponding sensitivity to layered absorption.

Vector #	Surface μa (mm^{-1})	Deep μa (mm^{-1})	Border Depth (mm)	Vector #	Surface μa (mm^{-1})	Deep μa (mm^{-1})	Border Depth (mm)
1	.010	.011	9	24	.030	.010	9
2	.010	.013	9	25	.010	.030	11
3	.010	.015	9	26	.030	.010	11
4	.010	.020	9	27	.010	.030	13
5	.011	.010	9	28	.030	.010	13
6	.013	.010	9	29	.010	.030	15
7	.015	.010	9	30	.030	.010	15
8	.020	.010	9	31	.010	.030	17
9	.020	.030	9	32	.030	.010	17
10	.025	.030	9	33	.010	.030	19
11	.027	.030	9	34	.030	.010	19
12	.029	.030	9	35	.010	.020	13
13	.030	.020	9	36	.020	.010	13
14	.030	.025	9	37	.015	.025	13
15	.030	.027	9	38	.025	.015	13
16	.030	.029	9	39	.020	.030	5
17	.010	.030	3	40	.030	.020	5
18	.030	.010	3	41	.015	.025	5
19	.010	.030	5	42	.025	.015	5
20	.030	.010	5	43	.015	.025	16
21	.010	.030	7	44	.025	.015	16
22	.030	.010	7	45	.015	.025	19
23	.010	.030	9	46	.025	.015	19

Table 6: Simulation conditions for neural network training set.

A set of vectors was compiled from the simulation results discussed in the previous section (section 4.4.6), which examine the effect of the three unknown parameters in the assumed two layer model (surface μ_a, deep μ_a, border depth). These vectors, containing the computed μ_a as a function of distance from the source (based on the frequency domain method), were applied as training inputs to a neural network. Table 6 lists the conditions of each simulation included in the training set.

The neural network implemented is illustrated in Figure 23, and has the following structure:

Inputs = 55, corresponding to the computed μ_a value at 1 mm increments from the source (6-60 mm)

Hidden Layer Neurons = 75

Outputs = 3, corresponding to each unknown variable: surface μ_a, deep μ_a, boundary depth

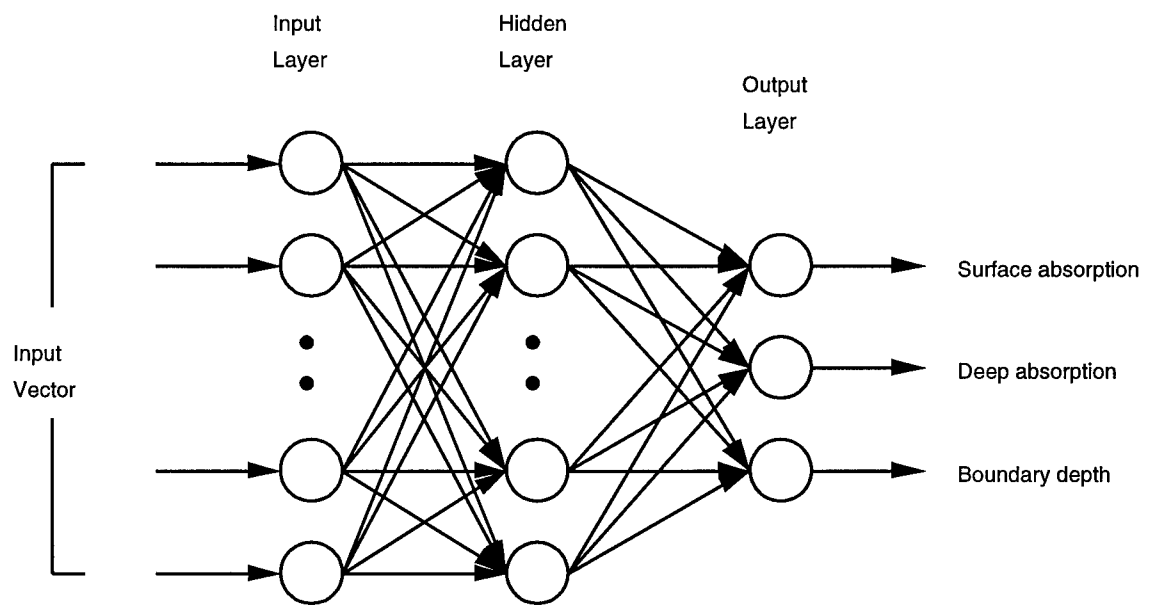

Figure 23: Illustration of the neural network structure.

By applying the computed μ_a vectors to the neural network, and training it to provide the correct output for the absorption of each layer, and the depth of the boundary, the neural network learns the complex relationship.

Results of the neural network implementation are shown in Table 8, which lists the error achievements for the training process, as well as for some additional test cases (i.e. not in training set) which were applied to the trained network. Table 7 lists the simulation conditions for the 3 test vectors.

Vector #	Surface μ_a (mm^{-1})	Deep μ_a (mm^{-1})	Border Depth (mm)
1	0.018	0.026	12
2	0.023	0.012	12
3	0.013	0.024	6

Table 7: Simulation conditions for neural network test vectors.

	Training Set (46 vectors)	Test Set (3 vectors)
Variable	Standard Deviation Error	Error (absolute value)
Depth	0.5510 mm	0.14, 0.9, 1.24 mm
Surface Absorption	0.00073 mm-1 (2-7%)	0.001, 0.0009, 0.0029 mm-1
Deep Absorption	0.0015 mm-1 (5-15%)	0.0004, 0.0015, 0.0019 mm-1

Table 8: Neural network results for reconstruction of layered medium.

These results demonstrate that the relationship between computed absorption as a function of distance, and layered variations is distinct and determinable. Given the conditions of the training set vectors with boundary depths up to 2 cm, the results demonstrate the ability to make measurements up to 2 cm deep. Simulations were performed with the second layer at depths greater than 2 cm deep; however, when it was attempted to include these cases in the neural network training set, the learning process was slow and conversion to minimal error levels was uncertain.

To improve upon the achieved performance further training and a larger training set (for increased generalization capability) may be beneficial. However, the artificial neural network, while suitable for testing in the scope of phase I project, is not the best approach for this particular problem due to its inherent binary (1 or 0 output) nature. For our study, we utilized the neural network to provide a range of possible output values (normalized within the scale of 0 to 1), which works against the strengths of the neural network. Other methods of pattern recognition, which could be implemented within the scope of a Phase II project, may therefore prove more effective.

4.5 Potential Expansion for Multi-parameter Measurement

4.5.1 Tissue Pigments

Kessler (1992) lists the following pigments as contributing to the optical properties of tissue: Hemoglobin (oxy- and deoxy-); Myoglobin (oxy- and deoxy-); Cytochromes aa_3,b,c; Flavopro-

teins, Pyridinnucleotides; and Melanin. Measurement of these pigments may allow for diagnostic indicators of physiological status.

Hemoglobin

Pulse oximetry devices typically measure the change in absorption due to systolic pulsation at two different wavelengths to determine the ratio of oxygenated to deoxygenated hemoglobin. However, measurement of the total hemoglobin can allow for a more accurate measurement of oxygenation, and itself can provide valuable information about physiological status.

Measurement of total hemoglobin has been proposed by using a different set of wavelengths than used for the oxygenation measurement. By using two NIR wavelengths each in isobestic regions for oxy- and deoxy-hemoglobin (i.e. 800 nm and 1300 nm), total hemoglobin is measured (Schmitt et al., 1992). Thus, a 3-wavelength design would be capable of measuring both oxygenation, hemoglobin and total hemoglobin. In this case absolute quantization of total hemoglobin requires knowledge of the pathlength.

Alternatively, time-resolved (with pulsed source) or frequency domain (intensity modulated source) methods allow for quantification of the absorption coefficient. This then allows for quantification of hemoglobin concentrations, using two wavelengths.

Myoglobin

Myoglobin possesses similar optical characteristics to those of hemoglobin. Like hemoglobin, it has distinct absorption spectra for the oxygenated versus deoxygenated state, with specific isobestic wavelengths where absorption is independent of the oxygenation state. This may allow for the measurement of the oxygenation state of myoglobin, which can be important for example during muscle activity, using a two (or more) wavelength system.

Cytochrome aa_3

Cytochrome aa_3 can be a useful diagnostic indicator because of its role in the mitochondrial respiratory chain. Specifically, the oxidation state of cytochrome aa_3 can be indicative of the delivery of oxygen to the cells. Similar to hemoglobin and myoglobin, the absorption spectrum of cytochrome aa_3 is dependent on this oxidation state. This can allow for measurement of cytochrome aa_3 oxidation using similar optical methods. Wickramasinghe et al. (1994) describe a three wavelength system for measurement of HbO_2, Hb, and cyt aa_3.

Melanin

Information on the quantity and location of melanin in the skin can provide useful diagnostic information. Optical absorption by melanin is large in the visible region but decreasing into the IR region. As indicated by the dependency of pulse oximetry measurement on melanin, melanin absorption can be significant in the NIR region used for the pulse oximeter. Determination of melanin concentration may therefore prove useful for improving the accuracy of oxygenation measurement, as well.

Flavoproteins and Pyridinnucleotides

Several specific substances may fall into this category. These may have specific diagnostic value by themselves or may contribute interference to measurement of other substances, so that knowledge of their quantity may prove useful.

4.5.2 Chemical Concentrations

Glucose

Measurement of glucose can be useful for a variety of applications including diabetic monitoring. Studies have demonstrated the measurement of glucose concentrations in blood samples using optical (NIR wavelength) methods (Marquardt et al., 1993, Ward et al., 1989). Glucose has a characteristic absorption spectrum in the range of 2.0-2.5 μm, however interference occurs due to proteins which have a strong absorption in this range. Least squares analysis and filtering methods have been used to provide more accurate determination of glucose concentration. Marquardt et al. indicate that the 2.27 μm glucose absorption band provides most of the reliable glucose information.

Another reported study employed polarimetric techniques to measure the rotation of polarized light through a test cell and through the aqueous humor of an extracted eye (Cote et al., 1992). Rotation of the polarized light is linearly related to the concentration of glucose in the optical medium. Adaptation of these methods for non-invasive measurement of glucose in vivo may prove effective.

Water Content

A change in the tissue fluid balance can occur due to various physiological disorders or conditions. For instance, there is an increase in water content with inflammation or trauma. Tissue reflectance has been shown to change (within the range of about 500 nm to 1400 nm) with different fluid levels, due to absorption by water (Tsai et al., 1993). Correlation of absorption changes to water content changes may therefore be possible. Tsai suggests the use of 1300 nm wavelength, an isobestic point for hemoglobin, where the oxygenation state will not influence measurement.

pH

Optical measurement of pH (hydrogen ion activity) has been studied using either a luminescent or an absorptive indicator. A luminescent indicator is excited by a given wavelength, and then emits light at a second wavelength dependent on the pH level. This method requires a strong intensity of light for excitation, and the resulting emission is generally weak. An absorptive indicator, on the other hand, changes absorption with the pH level. An absorptive indicator (compound 5-91, containing azo chromophore) has been developed (Wolthuis et al., 1992) with the desired characteristics for physiological measurement; compound 5-91 has sensitivity in physiological range 6.8-7.8 pH and an absorption peak at 625 nm.

O_2 Consumption

This parameter has been identified as potentially beneficial to monitor, yet relevant literature on non-invasive optical measurement was not found. However, this parameter may be able to be computed from the non-invasive optical measurement of hemoglobin oxygenation and/or cytochrome aa_3 oxidation states.

CO_2, Bicarbonate, Metabolic ions (K^+, Na^+, $Ca2^+$, Mg^{2+})

These substances have been identified as potentially beneficial to monitor, yet relevant literature on non-invasive optical measurement was not found. Optical properties of these substances would require further investigation.

4.5.3 Other Parameters

Temperature

Thermal imaging techniques to measure temperature differences in physiological tissue utilize the ratio of absorption at two different optical wavelengths, which is dependent on temperature. Optimum wavelengths for this measurement are those at which transmission through the epidermis, and absorption by the blood vessels, is maximum. Wavelengths around 1.2 μm and 1.7 μm have been suggested for meeting these criteria. Methods for intravascular measurement of temperature detect reflected light through an absorptive filtering lens which changes absorption properties dependent on temperature (Wolthuis et al., 1993).

Blood Flow (BF)

Methods for non-invasive optical monitoring of blood flow include laser Doppler flowmetry systems which are currently commercially available. These systems measure the velocity of blood particles by detecting the Doppler shift in reflected light, to determine blood perfusion. An example of such a system is the MEDPACIFIC Model LD 5000 Laser Doppler perfusion monitor (MEDPACIFIC Corp., Seattle, WA). One study has reported the simultaneous application of this system with oximetry measurement in a single optical probe. In addition, studies have demonstrated the calculation of cerebral blood flow (and blood volume) based on the non-invasive optical measurement of hemoglobin (Wickramasinghe et al., 1994).

Blood Volume (BV)

Studies have demonstrated the determination of cerebral blood volume based on measurement of total hemoglobin concentration (Wickramasinghe et al., 1994). This calculation assumes that total Hb is equal to the sum of deoxy-Hb and oxy-Hb, and that Hematocrit is known: CBV=100*Y / H*R, where CBV=cerebral blood flow, Y=change in total Hb, H=hematocrit, and R=cerebral to large vessel packed cell ratio. Application of this methodology to measurement of blood volume contained within other regions may also prove effective.

Substance/Parameter	Potential Wavelength(s)
Hemoglobin oxygenation	2 λ system: 645-780 nm, 820-950 nm
Total Hemoglobin	2 λ system: 800, 1300 nm, or time-resolved/frequency domain methods
Hb, HbO_2, and cytochrome aa_3	3 λ system: 775, 845, 904
Glucose	2270 nm
Water Content	1300 nm (or other isobestic point for Hb)
pH	625 nm
Temperature	1200 nm, 1700 nm
Blood Flow	Laser Doppler: ~630 nm; or computed from Total Hb
Blood Volume	computed from Total Hb

Table 9: List of some substances/parameters and potential wavelengths for non-invasive optical monitoring.

4.6 Summary

The Phase I design effort involved a comprehensive series of efforts which established the capability for measurement of deep tissue oxygenation, and yielded detailed specifications and requirements for the device. To summarize, we:

1) Performed an extensive review of state of the art technology and ongoing research
2) Determined the optical properties of physiological tissue, including experimental validation
3) Developed computational models for simulation of light transport in tissue
4) Performed extensive simulations to characterize light-tissue interaction
5) Evaluated advanced methodologies for deep tissue measurement
6) Demonstrated capabilities for deep tissue measurement using the frequency domain method
7) Implemented a pattern recognition scheme for reconstruction of a layered medium

Results indicate that the best approach for measurement in deep tissue is the frequency domain methodology. Extensive analyses demonstrated and quantified the capability of this technique for measurement of deep tissue. This was most evident by application of the neural network for reconstruction of absorption in the layered medium. ***Analyses indicates that the designed sensor will be capable of measuring hemoglobin concentration and oxygen saturation, up to 2 cm deep.***

5.0 Detailed Phase II Design

The Phase I design effort established the feasibility of the proposed sensor, determined the best technical approach, and helped detail requirements for the complete device. As determined through the Phase I design efforts, the Phase II system will meet the following needs:

1) Frequency domain implementation: The Phase I effort performed a comparison between pulsed time-domain techniques and continuous-wave sinusoidally modulated frequency domain techniques. The frequency domain techniques were shown to be far superior when the goal is to perform deep tissue examination. This is primarily due to the CW (continuous wave) nature of the signal, which allows for long integration periods of the signals of interest to increase the signal-to-noise ratio. For this methodology, the signals of interest are the DC level of the incident radiation and the phase shift between the received and transmitted signals.

2) Resolution of spatial variations in light detected on the surface: Phase I analyses indicate that spatial variations in reflected light along the tissue surface contain information on the deep layered structure of the tissue. For high resolution of these variations, and therefore high resolution of depth variations, an array of detectors with small incremental distances is required. This aspect is key to the unique design which has been developed to allow distinction of layered information and measurement within deep tissue.

3) Interpretation scheme for extracting layered information: In spite of the short time duration and lack of substantial resources imposed by the typical Phase I effort, the development team managed to construct an advanced pattern recognition scheme to automatically extract layered information from the simulated results (namely the absorption of each of the two layers and the depth of the second layer). The Phase II instrument will build upon this work, resulting in a sensor that robustly performs this quantitative operation.

5.1 Design Overview

The process for the designed system is as follows:

1) An intensity modulated source is applied to the medium (tissue);

2) Reflected light is measured at incremental distances from the source;

3) DC and phase shift of reflected light, as a function of distance, are measured;

4) The absorption coefficient, μ_a, is computed as a function of distance, using the DC and phase shift information;

5) The unknown variables (surface μ_a, deep μ_a, border depth) are calculated from the computed μ_a curve;

6) Oxygenation and hemoglobin concentrations are derived from absorption coefficients.

Figure 24 illustrates the block diagram for the frequency domain implementation. Main components of the system include: driving circuitry, light source, detector array, DC signal measurement, phase shift measurement, and signal processing and computation. Each component is elaborated next.

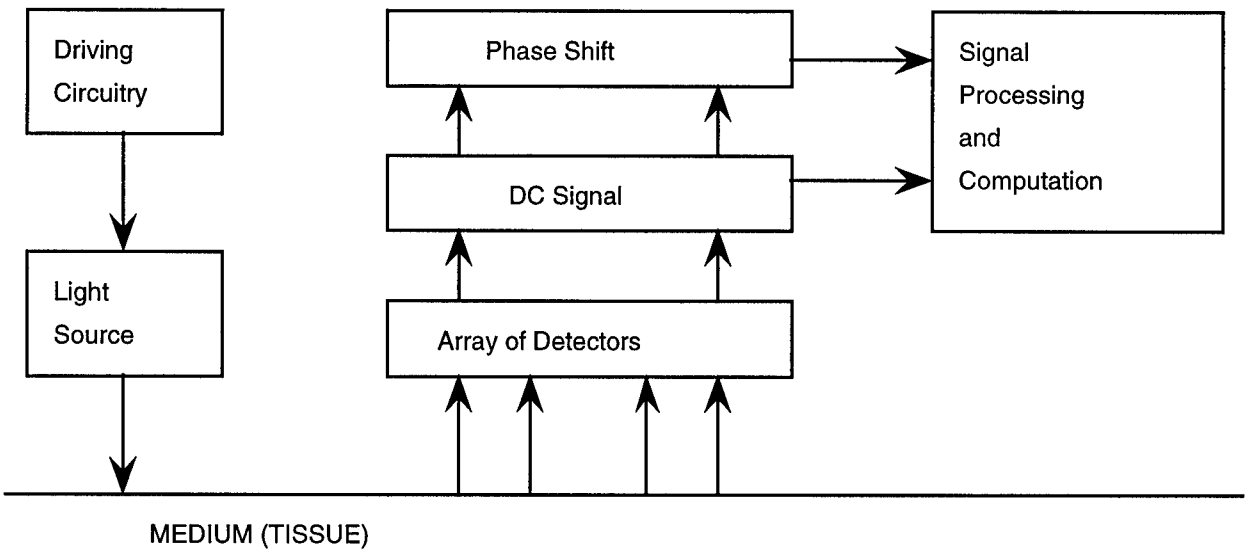

Figure 24: Block diagram of sensor design.

5.1.1 Driving Circuitry

The driving circuitry generates a sine wave supply voltage to the light source for producing an intensity modulated light signal. Modulation frequency of the light source will be in the range of 10-50 MHz. Current through the LEDs is maximized to provide a maximum amount of radiant light intensity, without exceeding device limitations (e.g. for typical candidate sources, the current through the source cannot exceed 100mA). The driving circuitry also provides the capability for automatic switching between the two required wavelengths.

The drive circuitry must provide a stable current drive to each of the LEDs. Preferably it will produce 100% modulation depth with minimum phase noise and distortion at the required frequency. Distortion can be minimized by making sure that the LED does not cutoff and that the current is a pure sine wave. A typical drive circuit would be like that shown in Figure 25.

In this circuit, the current through the diode is equal to one half the AC and DC voltages divided by the resistor, R_S. The values of the DC must be at least half of the AC peak-to-peak amplitude to avoid cutoff. The operational amplifier must be able to drive the required current at the desired frequency with margin to spare in order to maintain linear operation. This particular stage must be well isolated from all noise or external modulation sources. The DC supply is usually provided by a DAC (digital to analog converter) with a stable reference, while the AC signal is an input from the frequency synthesizer. The frequency synthesizer will typically be located some distance from the sensor. Details of the frequency synthesizer are elaborated next.

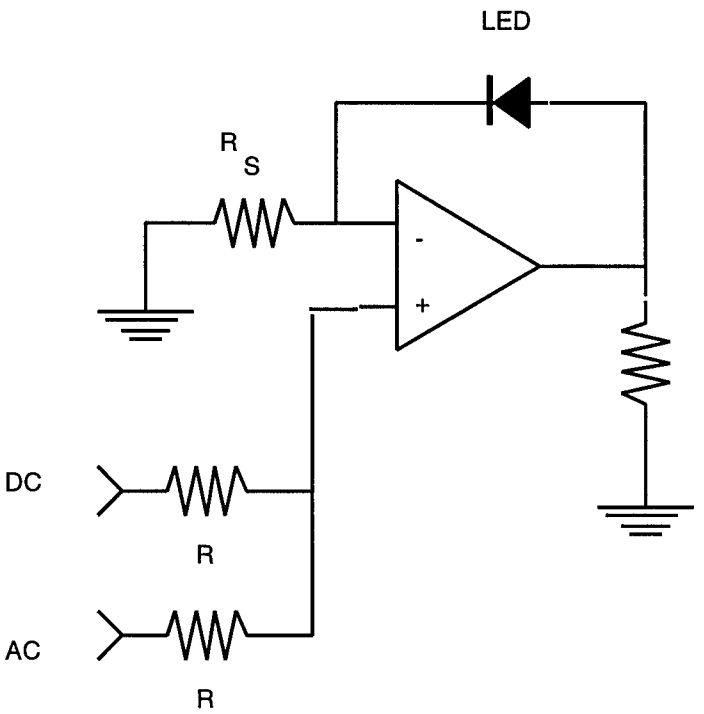

Figure 25: Current drive for LED illumination source.

5.1.2 Frequency Synthesizer (FS)

There are several ways to implement a frequency synthesizer for this sensor. The major determining factors are the number of frequencies and the noise performance. The number of frequencies depends on the modulation, demodulation and phase measurement technique. The required noise performance depends on the sensitivity of the required phase measurement. Frequency synthesis, itself, can be quite complex. A typical FS design includes 12 steps as outlined below.

Step 1. Frequency Plan. Based on considerations such as spurious outputs, phase noise, and/or switching time, a preliminary frequency plan is developed (i.e. multi- or single loop, digital, fractional etc.).

Step 2. Intermodulation Products. Intermodulation products generated from mixers or multipliers must be evaluated and eliminated from any critical bands.

Step 3. Preliminary Filter Design. A preliminary filter design is performed to establish the feasibility of reducing out of band spurious outputs to the required levels.

Step 4. Phase Noise. A preliminary phase noise analysis is performed to determine whether or not the phase-noise requirement can be met with the selected approach and commercially available references.

Step 5. Block Diagram. A preliminary detailed block diagram is prepared upon successful completion of steps 1-4.

Step 6. Radio-frequency Power Levels. The designer must now establish input and output power levels for each block in the diagram.

Step 7. Leakage of RF signals. Expected leakage of RF signals through circuits-- such as the local oscillator leakage to the output of the mixer-- is identified, power levels estimated, magnitudes of possible spurious combinations and modifications made to the block diagram as necessary, including additional filters, or isolation amps.

Step 8. Discrete FM sidebands. Based on the FM sideband requirements, tolerable limits at each stage in the design are established, estimates are made, and measures taken to meet requirements. Particular problems occur when power supplies feeding the voltage controlled oscillators are not properly designed.

Step 9. Schematic Diagram. Upon completion of steps 1-8 a preliminary schematic is prepared.

Step 10. Packaging. The synthesizer is divided into modules as necessary for elimination of RF pickup. Connectors and cables are identified as well as overall distribution of power and signal routing.

Step 11. Schedule. A schedule is prepared with milestones based on availability of resources, labor estimates, and availability of parts.

Step 12. Circuit Design. Detailed hardware design and construction.

Some important practical considerations include cost and size. There are certain components that are in volume manufacture and hence are very cheap. This is particularly true for filters at 455 KHz, 10.7 MHz and 70 MHz. Recently, many new highly integrated RF components have emerged to support the boom in cellular phones and other wireless products. These are all considerations that must be taken into account during the design process.

In the case of the proposed instrument, the most likely approach is to use a two frequency approach where one frequency is used to drive the LED and a second frequency is used to translate the phase and amplitude information down to lower frequency where it is easier to process. For example, one might use 10.7 MHz as the modulation frequency, 10.69 as the local oscillator giving 0.01 MHz or 10 Khz as the baseband frequency. Phase and amplitude measurements are then made on this 10 KHz signal and averaged to further reduce noise resulting in an update of about 100 Hz. A typical block diagram for such a system is shown in Figure 26.

The phase/frequency detector and dividers are typically part of a low cost integrated circuit (IC). The 1 MHz oscillator is a very common but high performance frequency reference. Isolation amps can be as simple as an emitter follower.

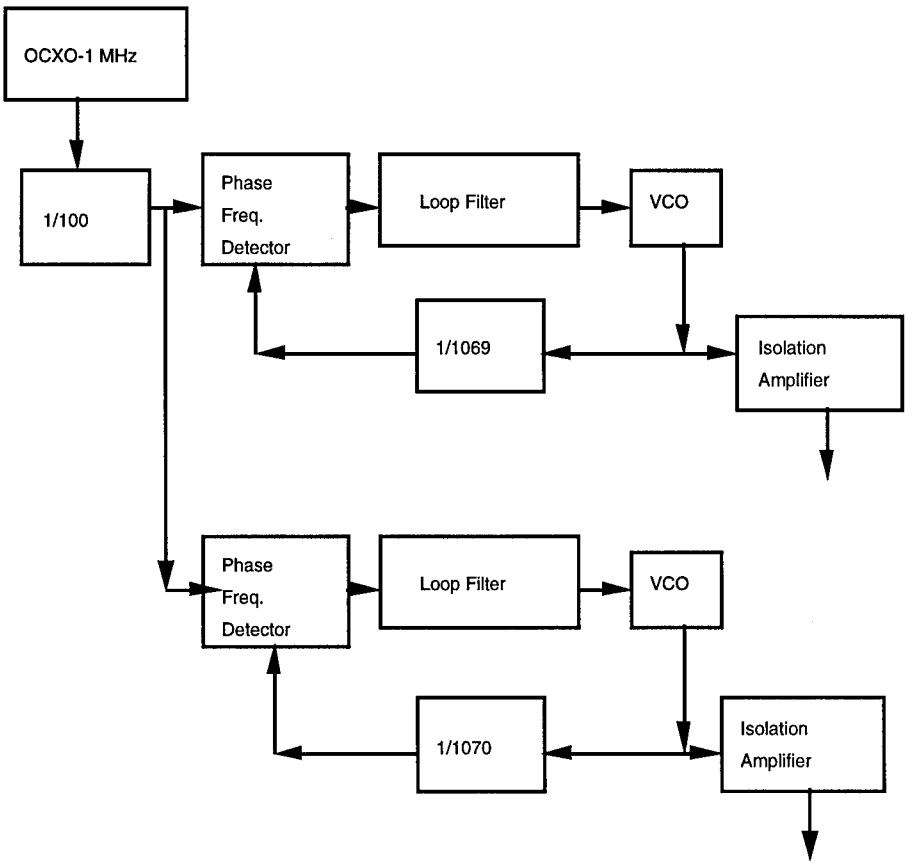

Figure 26: Two loop, dual frequency synthesizer block diagram.

5.1.3 Light Source

Light source options include lasers, LEDs (Light Emitting Diodes), and lamps. *LEDs were chosen for this applications because they are low cost, safe, and meet the performance characteristics required for a frequency domain implementation.* Components were selected to provide wavelengths within the required range: λ_1=820-880 nm and λ_2=710-760nm. The sources must also be capable of modulation at the desired frequency. The components used for testing during this Phase I effort meet these requirements: Stanley LED NR513: 720nm; Stanley LED DN304: 850nm, and are included in the Phase II design.

5.1.4 Detectors

Options for light detectors include diodes, PIN Diodes, APDs (avalanche photo-diodes), PMTs (photo-multiplier tubes), and CCDs (charge coupled devices). *PIN diodes were chosen because they provide the optimum trade-off between speed, sensitivity, cost, and size for this application.* Detectors will be placed at 1 mm increments, ranging 0.6 to 6 cm from the light source.

The detector module must have a preamplifier drive circuit. The preferred type of preamplifica-

tion circuit depends on the type of detector. Photoconductive detectors are typically biased and AC coupled to a low impedance amplifier. Photovoltaic detectors are typically coupled to the input of a transimpedance amplifier as shown in Figure 27. In this case, the photons generate a current that flows in to a virtual ground node and through the feedback resistance R_F which sets the transimpedance gain. Ideally, the photodiode and amplifier are immediately adjacent to one another to eliminate noise pickup and reduce input capacitance which acts as a significant current shunt at higher frequencies causing a reduction in signal and an increase in the noise. Unfortunately, large arrays of detectors with integrated preamplifiers are not common or low cost in part because there are few applications that require it. However, there are many applications that would benefit from it.

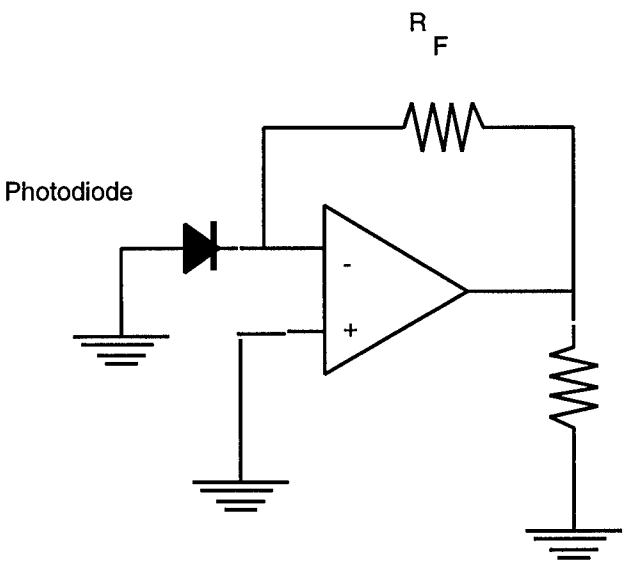

Figure 27: Detector coupled to a transimpedance amplifier.

In the Phase II prototype, we will probably examine two approaches. The first approach will use an array of discrete detector elements, such as that shown in Figure 28, tightly coupled to a surface mount or (chip on board) array of preamps each with separate output and RF processing chain or multiplexer. A second approach is to use discrete diodes and amplifiers such as those shown in Figure 29. This latter approach allows the use of higher performance detector/preamps, however, the packaging density is low and the cost is high.

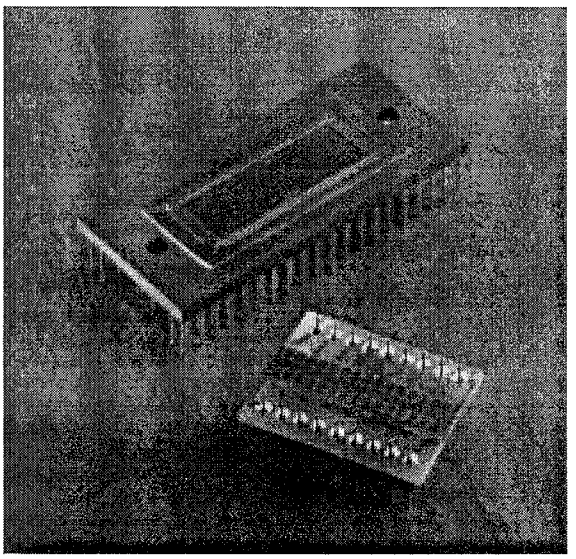

Figure 28: Example of array of discrete detector elements on surface mount/chip.

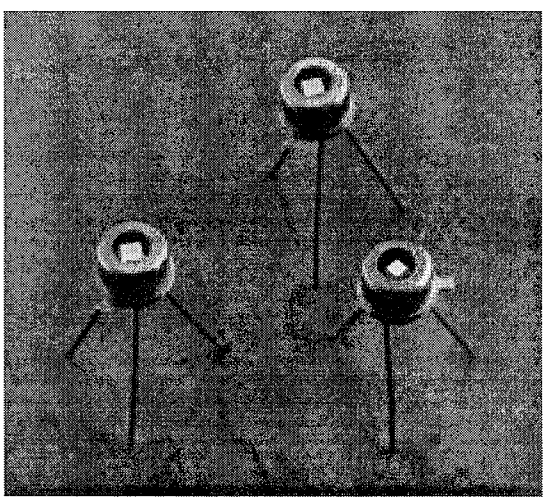

Figure 29: Example of discrete diode detectors

5.1.5 DC and Phase Shift Measurements -- Demodulation

This system function consists of the circuitry required for making the DC and phase measurements of reflected light signals along the detector array. Sensitivity of these measurements determines the sensitivity which can be obtained for computation of the absorption coefficient, hemoglobin concentration, and oxygenation.

The DC and phase shift signals must also be processed through signal conditioning circuits and analog-to-digital conversion, for input to the software platform, where signal processing and parameter computation are performed.

The measurement of the DC, AC amplitudes and phase shift relative to the reference of a sine wave can be accomplished in many ways. One technique is to digitize the output at a fast rate relative to the frequency and then use the Discrete Fourier Transform (DFT) to obtain this data. Because the signal is a pure sine wave this should work reasonably well, however the phase accuracy is approximately equal to 2π divided by the square root of a quantity which is half the number of samples per cycle times the signal to noise ratio. Thus for the given sensor application, where high phase accuracy is required at low frequencies, one must take many samples per cycle per detector resulting in considerable computation.

Another alternative is to use analog techniques to do the same thing. For example, the sine wave can be prefiltered into DC and AC components. The AC part can be input to a precision rectification circuit after adequate amplification and power measured as the square of the input, while the DC input can simply be measured directly. This technique will work well if the frequency to be measured is sufficiently large relative to the measurement frequency so that it can be readily separated from the DC component. Logarithmic amplifiers can also be used to measure signal power both at frequency and at DC if properly post filtered.

Phase measurements can be made in many ways, as well. The most common way is to use a limiter on the sinusoidal input to generate edges corresponding to zero crossings of the sine wave. These crossings are then compared against their reference counterpart. The method of comparison can be a digital count or an amount of charge or a sequence of varying pulse widths that when properly filtered are proportional to the phase. Each of these techniques will be studied more closely in the early part of the Phase II design.

5.1.6 Signal Processing and Computation

The measured DC and phase signals are digitized (A/D conversion) and then input to a separate analysis system. A wide variety of signal processing operations must be performed to arrive at the final computation of physiological parameters: oxygenation, oxyhemoglobin, deoxyhemoglobin and total hemoglobin. These operations include signal conditioning of the DC and phase signal, noise filtering, antialiasing filtering, complex feature extraction, and pattern recognition methodologies.

The exact calculation of a physiological parameter, such as hemoglobin concentration, relies on the instantaneous value of the phase difference between the source and received signals. Improperly designed filters can easily alter the instantaneous phase value measured at the receiver. Filter algorithms must therefore be carefully designed, tested, and implemented to ensure accurate phase measurements.

Computation of physiological parameters will include tissue absorption coefficients, hemoglobin concentrations, and tissue oxygenation levels. Calculation of the absorption coefficient from the measured DC and phase signals in the semi-infinite medium is derived in published literature (Fantini et al., 1994). From the absorption coefficient, measured at each of the two different wavelengths, concentrations of Hb and HbO_2, and oxygen saturation are computed based on the following formulas:

$$[HbO_2] = \frac{\mu_a^{\lambda_1}\varepsilon_{Hb}^{\lambda_2} - \mu_a^{\lambda_2}\varepsilon_{Hb}^{\lambda_1}}{\varepsilon_{HbO_2}^{\lambda_1}\varepsilon_{Hb}^{\lambda_2} - \varepsilon_{HbO_2}^{\lambda_2}\varepsilon_{Hb}^{\lambda_1}}$$

$$[Hb] = \frac{\mu_a^{\lambda_2}\varepsilon_{HbO_2}^{\lambda_1} - \mu_a^{\lambda_1}\varepsilon_{HbO_2}^{\lambda_2}}{\varepsilon_{HbO_2}^{\lambda_1}\varepsilon_{Hb}^{\lambda_2} - \varepsilon_{HbO_2}^{\lambda_2}\varepsilon_{Hb}^{\lambda_1}}$$

$$SaO_2 = \frac{[HbO_2]}{[Hb]+[HbO_2]}100\ \% = \frac{\varepsilon_{Hb}^{\lambda_2}\mu_a^{\lambda_2}/\mu_a^{\lambda_1}}{\varepsilon_{HbO_2}^{\lambda_2} - \varepsilon_{HbO_2}^{\lambda_2} + (\varepsilon_{HbO_2}^{\lambda_1} - \varepsilon_{Hb}^{\lambda_1})\mu_a^{\lambda_2}/\mu_a^{\lambda_1}}100\ \%$$

where $\mu_a^{\lambda_1}$ and $\mu_a^{\lambda_2}$ are the computed absorption coefficients at each wavelength, and ε are the hemoglobin extinction coefficients for HbO_2 and Hb at each wavelength, λ_1 and λ_2.

In addition, algorithms for reconstruction of the layered structure and deep tissue information will be developed. This will involve identification and implementation of advanced techniques for pattern recognition. In the Phase I project neural network techniques were studied, which demonstrated a capability to reconstruct a layered structure up to 2 cm deep. However, while the neural network approach was suitable for study in the scope of the phase I project, it is not the best approach for this problem due to its inherent binary (1 or 0 output) nature. For instance, we utilized the neural network to provide a range of possible output values (normalized within the scale of 0 to 1), which works against the strengths of the neural network.

In addition, the neural network implemented in Phase I is computationally expensive. Activation functions involved with neural summations at node entities are inherently costly nonlinear transcendental functions. The size of the neural network was rather large as well. Other methods for pattern recognition, which can be implemented within the scope of the Phase II project, will be studied and tested in order to both advance the capability beyond the neural network approach implemented in the Phase I system and result in a computationally more efficient solution.

The software development process will also establish the operational platform, address compatibility, integrate algorithms, optimize computational performance and speed, and implement the required code. Diagnostic test procedures will validate the performance of the software subsections and complete design.

5.1.7 Packaging

The requirements of each functional block will be integrated into the complete hardware system, and fabricated to meet the design package specifications. Packaging design is critical to meeting the goals for reliability, sensor size, ease-of-operation, and cost. Fabrication procedures must also be taken into account. The optical components must be mounted and aligned to ensure con-

sistent performance over a broad range of factory conditions. The electronics must be packaged in a ruggedized chassis that will reliably meet the demands of the shop floor.

Figure 30 shows the sensor packaging and source/detector configuration. Approximate dimensions are: length=7 cm, width=1.8 cm, thickness=1.3 cm. Final Phase II Sensor dimensions will be minimized while maintaining maximum capabilities for deep tissue measurement and easy application and attachment to the body.

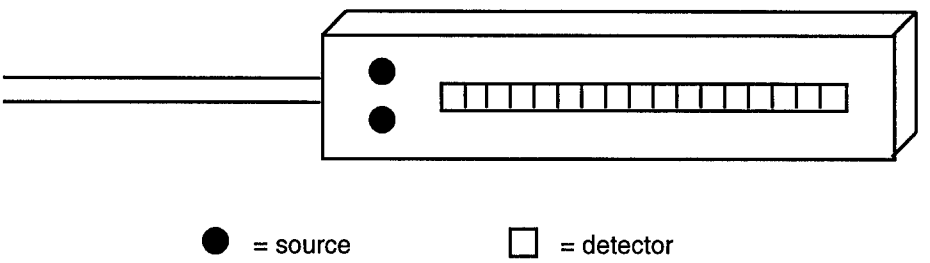

Figure 30: Illustration of Sensor Package

5.2 Design Characteristics

A sound engineering design for an instrumentation quality sensor factors in a number of desired properties that the end product should possess. These include those listed below:

Reliability	Accuracy	Sensitivity	Low Cost
High Resolution	Non-invasiveness	Ease-of-use	Small size
Speed	Versatility	Remote capability	

The sensor engineering methodology employed by Cybernet Systems Corporation starts with a system specification process that ensures that these issues are factored into the final solution. The following subsections briefly discuss each of the properties listed above and their impact on the Phase II design presented herein.

Reliability

Reliability implies a device which ensures consistent performance throughout time and use. This characteristic is achieved through selection of quality components and materials. The design must also account for operation under all possible conditions and endure the effects of extensive use. Fabrication techniques and packaging design play a significant role in achieving this desired property.

Accuracy

Accuracy of the device refers to an ability to provide measurements indicative of the actual tissue

values. This performance will depend on several design parameters including the specific design methodology implemented, tolerance levels of components, calibration techniques, application conditions, and signal to noise levels. Simulation and evaluation results from Phase I indicate performance capabilities of the designed methodology. Other contributing factors, related to specific application conditions will be further identified through the Phase II testing process.

Sensitivity

The sensitivity of measurement refers to the smallest amount of change which the device can discern. This performance will depend on several design parameters including the specific design methodology implemented, tolerance levels of components, calibration techniques, application conditions, signal to noise levels, and computational procedures. Simulation and evaluation results from Phase I indicate performance capabilities of the designed methodology. Other contributing factors, related to specific application conditions will be further identified through the Phase II testing process.

Low Cost

Cost of the device is determined by the required components, materials, and fabrication process for the chosen implementation. The frequency domain implementation utilized in the designed sensor allows for a low cost solution because LEDs (rather than ultra-fast lasers) can be used. Cost is obviously one of the most important factors in determining the eventual commercial potential of the Phase II device. Therefore, this factor will be examined very closely in Phase II to glean as much of a potential foothold in commercialization of the result. As is always the case in Cybernet System Corporation efforts, however, this desire for commercial success will not affect the delivery of a Phase II solution that satisfies *all* of the sponsor's requirements.

High Resolution

For the project at hand, this refers to high resolution of spatial differences in reflected light. This resolution corresponds to resolution of depth variations and is dependent upon implementation of the detector array. Specifically, the number and spacing between the detector components determines the resolution. Phase I analyses indicate that 1 mm spacing adequately supplies the required level of resolution.

Non-invasiveness

Non-invasiveness of the methodology is important for safe and practical implementation in the emergency medical treatment setting. This requirement is satisfied through the sole use of optical measurement only. It should be emphasized once again that the intended sources and detector components utilized fall well within the safety standards set by, among others, the American National Standards Institute (ANSI). (See ANSI Standard ANSI Z136.1-1993).

Ease-of-use

Operation of the device should be simple and not interfere with other treatment procedures. Design of packaging, interface requirements, operating procedures, and interface compatibility

ensures easy operation. The device should also be easy to place on the patient or soldier. As a standard for comparison, a pulse oximeter can very quickly be attached to a patient simply by clipping to an earlobe or placing over a finger.

Small size

Due to portable application and attachment issues, minimization of sensor size is important. This characteristic is limited by component sizes, and the packaging design. The largest contributing factor for the designed sensor is the size of the required detector array. Since deep tissue assessment requires measurement at large distances from the source, there is a tradeoff between sensor size and measurement depth. However, attenuation of light through the tissue will restrict the distance at which adequate light will be measurable. This characteristic therefore defines the maximum depth of measurement and the corresponding minimum sensor size.

Speed

The time required for acquisition of the computed physiological parameters depends on the invoked methodology, the applied computational algorithms, and the analysis platform. There is generally some level of tradeoff between speed and accuracy, as averaging of multiple measurements can be performed to reduce errors due to random noise fluctuations. Application areas will need to be investigated in the Phase II to see if certain situations have different constraints than others. For example, in extreme trauma situations having a fast measurement may take precedence over having a more accurate measurement.

Versatility

This characteristic encompasses all aspects relevant to applicability of the sensor to the large number of medical applications.

5.3 Sensitivity Analysis

As part of the Phase I design effort, a comprehensive sensitivity analysis was performed to determine the sensitivity of computed parameters to variable design parameters and to measurement noise. This analysis allows determination of optimum design parameters and the measurement sensitivity required to achieve the desired sensitivity for the computed parameters.

5.3.1 Analysis methodology

The analysis was performed by imposing specific sensitivity requirements on each of the three computed parameters:

[Hb]: Concentration of deoxy-hemoglobin

$[HbO_2]$: Concentration of oxy-hemoglobin

SaO_2: Oxygen saturation of hemoglobin (oxygenation)

Relevant design parameters which were included in the analysis are:

dr: precision of detector location, r

$d\lambda$: precision of light source wavelength, λ

df: precision of modulation frequency, f

Δr: distance between detectors (at r_i and r_{i+1}) used for slope computation

Noise parameters which were included are:

η_{Udc}: measurement noise in DC signal, U_{dc}

η_ϕ: measurement noise in phase shift signal, ϕ

The performed sensitivity analysis resulted in computation of the maximum allowable error in the DC and phase shift measurements required to achieve a desired sensitivity for the computed parameters. These maximum errors are defined as follows:

σ_{Udc}: error in DC measurement

σ_ϕ: error in phase measurement

To compute the maximum error values, σ_{Udc} and σ_ϕ, the following process was implemented:

1) Establish desired sensitivity values for the computed parameters (i.e. $dSaO_2$=1%)

2) Propagate this constraint through a series of calculated partial differentials, from the computed parameter down to the design and/or measurement parameter (i.e. $dSaO_2$-->σ_{Udc})

3) Determine constraint on the design/measurement parameter required to meet the desired sensitivity for the computed parameter (i.e. σ_{Udc}<0.038%)

For example, to propagate the desired constraint from $dSaO_2$ (the imposed sensitivity for oxygen saturation) down to σ_{Udc} and σ_ϕ (the allowable error in DC and phase shift measurements), the following series of equations are followed:

$$dSaO_2 = \frac{\partial SaO_2}{\partial \mu_a^{\lambda_1}} d\mu_a^{\lambda_1} + \frac{\partial SaO_2}{\partial \mu_a^{\lambda_2}} d\mu_a^{\lambda_2}$$

$$d\mu_a^{\lambda} = \frac{\partial \mu_a^{\lambda}}{\partial n} dn + \frac{\partial \mu_a^{\lambda}}{\partial S_{dc}} dS_{dc} + \frac{\partial \mu_a^{\lambda}}{\partial S_\phi} dS_\phi$$

$$dS_{dc} = \frac{\partial S_{dc}}{\partial U_{dc}(r_{i+1})} dU_{dc}(r_{i+1}) + \frac{\partial S_{dc}}{\partial U_{dc}(r_i)} dU_{dc}(r_i)$$

$$dS_{\phi} = \frac{\partial S_{\phi}}{\partial \phi(r_{i+1})} d\phi(r_{i+1}) + \frac{\partial S_{\phi}}{\partial \phi(r_i)} d\phi(r_i)$$

$$dU_{dc}(r) = \frac{\partial U_{dc}(r)}{\partial r} dr + \frac{\partial U_{dc}(r)}{\partial \lambda} d\lambda + \eta_{Udc} = \sigma_{Udc}$$

$$d\phi(r) = \frac{\partial \phi(r)}{\partial r} dr + \frac{\partial \phi(r)}{\partial \lambda} d\lambda + \eta_{\phi} = \sigma_{\phi}$$

In the above equations, the following additional definitions apply:

$dSaO_2$=imposed sensitivity for oxygen saturation

μ_a^{λ}=absorption coefficient at wavelength λ

n=index of refraction

S_{dc}=slope of (logarithm of) reflected DC light signal

S_{ϕ}=slope of reflected phase signal

$U_{dc}(r)$=DC level of reflected light signal at distance r from source

$\phi(r)$=phase shift of reflected light signal at distance r from source

Partial differentials are calculated from the series of equations used to compute the final parameter (SaO_2, [Hb], or [HbO_2]) from the measured DC and phase signals (U_{dc}, ϕ). The form of these equations for the example above (sensitivity of SaO_2) is as follows:

$$SaO_2 = f(\mu_a^{\lambda_1}, \mu_a^{\lambda_2})$$

$$\mu_a^{\lambda} = f(f, n, S_{dc}, S_{\phi})$$

$$S_{dc} = f(U_{dc}(r_{i+1}), U_{dc}(r_i))$$

$$S_\phi = f(\phi(r_{i+1}), \phi(r_i))$$

SaO_2 is a function of the absorption coefficient at each wavelength (see section 5.1.6 for exact equations). μ_a is computed from the slope of the DC and phase signals (as derived in Fantini et al., 1994) and is also dependent upon the modulation frequency, f, and index of refraction, n. Slope of the DC signal (phase signal), S_{dc} (S_ϕ), is computed from the difference between DC (phase) signal of two adjacent detectors, at locations r_i and r_{i+1}. $U_{dc}(r)$ is the measured DC signal at position r, whose accuracy will depend on precision of the detector location, dr, precision of the wavelength, $d\lambda$, and noise level of the DC measurement, η_{Udc}. $\phi(r)$ is the measured phase shift signal whose accuracy will depend on precision of the detector location, dr, precision of the wavelength, $d\lambda$, and noise level of the phase measurement, η_ϕ.

Specific values for the required partial differentials are computed from the derived formulas based on typical characteristics (for absorption and scattering) of tissue (see section 4.1).

5.3.2 Analysis Results

The performed sensitivity analysis examined maximum allowable measurement errors given: 1) different imposed constraints for sensitivity of the computed parameters, and 2) different distances for detector separation.

Table 10 shows results for imposed sensitivity on SaO_2, Table 11 shows results for imposed sensitivity on $[HbO_2]$, and Table 12 shows results for imposed sensitivity on [Hb]. Maximum allowable measurement errors are of the same order of magnitude for each of the computed parameters, to achieve the same level of sensitivity (i.e. SaO_2=1%, [Hb]=1% of [total Hb], $[HbO_2]$=1% of [total Hb], with an assumed [total Hb]=0.1 mM).

Imposed Sensitivity	Distance Between Detectors for Slope Calculation	Required Measurement error for DC Signal	Required Measurement error for Phase Shift
$dSaO_2$	Δr	σ_{Udc}	σ_ϕ
1 %	1 mm	< 0.038 %	< 0.000068 radians
10 %	1 mm	< 0.38 %	< 0.00068 radians
1 %	10 mm	< 0.38 %	< 0.00068 radians
10 %	10 mm	< 3.8 %	< 0.0068 radians

Table 10: Measurement error requirements due to imposed sensitivity on SaO_2 of 1% and 10%, with detector separations of 1 and 10 mm.

Imposed Sensitivity	Distance Between Detectors for Slope Calculation	Required Measurement error for DC Signal	Required Measurement error for Phase Shift
$d[HbO_2]$	Δr	σ_{Udc}	σ_ϕ
.001 mM	1 mm	< 0.030 %	< 0.000054 radians
.01 mM	1 mm	< 0.30 %	< 0.00054 radians
.001 mM	10 mm	< 0.30 %	< 0.00054 radians
.01 mM	10 mm	< 3.0 %	< 0.0054 radians

Table 11: Measurement error requirements due to imposed sensitivity on $[HbO_2]$ of 0.001 mM and 0.01 mM, with detector separations of 1 and 10 mm. With the assumption of total hemoglobin concentration of 0.1mM these sensitivities correspond to 1% and 10% of total hemoglobin concentration.

Imposed Sensitivity	Distance Between Detectors for Slope Calculation	Required Measurement error for DC Signal	Required Measurement error for Phase Shift
d[Hb]	Δr	σ_{Udc}	σ_ϕ
.001 mM	1 mm	< 0.036 %	< 0.000064 radians
.01 mM	1 mm	< 0.36 %	< 0.00064 radians
.001 mM	10 mm	< 0.36 %	< 0.00064 radians
.01 mM	10 mm	< 3.6 %	< 0.0064 radians

Table 12: Measurement error requirements due to imposed sensitivity on [Hb] of 0.001 mM and 0.01 mM, with detector separations of 1 and 10 mm. With the assumption of total hemoglobin concentration of 0.1 mM these sensitivities correspond to 1% and 10% of total hemoglobin concentration.

Results indicate that the maximum measurement errors, σ_{dc} and σ_ϕ, for the desired sensitivity (ideally 1%) are achievable, yet aggressive, most particularly for the phase measurement. Contributing factors to σ_{dc} and σ_ϕ include precision of detector location, precision of the wavelength, and measurement noise. Measurement noise will likely be the largest contributing factor.

An important characteristic indicated by the sensitivity analysis is that higher sensitivity can be achieved through use of a larger separation distance between detectors used for slope measure-

ments. This is due to the fact that better measurement of the slopes for the DC and phase signals can be made with a greater detector separation-- under the assumption of uniform slope as viewed from the two detectors.

However, the designed sensor has been developed for application to multiple-layer structures, where reconstruction of the layered information is performed. This technique requires high resolution of spatial variations in the reflected light, and therefore close detector spacing. Thus, there will be some tradeoff between sensitivity to the computed parameter, and resolution of depth variations. However, the design will allow for optimization of any compromise between the two capabilities.

For instance, keeping a small incremental distance between detectors, yet measuring the slope between larger distances, can allow for maintaining high resolution of spatial information while providing sensitive measurement. This will produce some smoothing of the spatial information, but reconstruction of the layered information using pattern recognition methods may be unaffected. This characteristic would deserve further study during the Phase II project.

It is also important to note that the sensitivity analysis performed is indicative of a single measurement. The sensor methodology developed in this Phase I, however, is based on a large number of measurements at many locations along the length of a detector array. These measurements are then processed through pattern recognition techniques for reconstruction of layered information. As a result, the sensitivity performance will be based upon many measurements, and will also depend upon the capabilities of the pattern recognition process. In particular, a large number of measurements can allow for compensation of measurement noise (due to the averaging effect), and therefore improve sensitivity. Furthermore, pattern recognition methods are, in part, aimed towards extracting desired information from noise.

Calibration techniques can also be implemented if required to help improve sensitivity performance. For example, error in the DC and phase measurements will be affected by variations in the exact wavelength of light and the precise location of detectors, as determined by the specific components and individual fabrication. Calibration of each constructed sensor to account for the precise wavelength of the LED and location of detectors can minimize these errors. Since calibration is generally undesirable, it will be avoided if possible.

The Phase II implementation will require a challenging sensor design to achieve the phase shift measurements which are required, but the task is feasible. A variety of techniques to enhance the sensitivity of phase shift measurements will be able to be addressed within the scope of the Phase II project.

6.0 Regulatory Requirements for the Phase II System and Related Medical Devices

In 1938 the Federal Food, Drug, and Cosmetic Act passed and the Food and Drug Administration (FDA) became authorized for the first time to regulate medical devices in order to assure their safety. At this point in time no pre-market approval was required for devices. Under Dr. Theodore Cooper, a committee was formed to examine problems associated with medical devices.

New concepts for legislation were introduced by the "Cooper Committee" after reporting that problems with medical devices had resulted in 10000 injuries and 751 deaths in the previous ten-year period.[1]

May 28, 1976 President Ford signed into law the Medical Device Amendments to complement the previous Act. The purpose of the Amendments is to ensure that medical devices are safe and effective and properly labeled for intended use. The FDA now has the authority to regulate devices during most phases of their development, testing, production, distribution, and use. Devices and drugs are treated as separate entities. Products that are not metabolized or are not dependent upon being metabolized in order to achieve their major intended purpose are to be regulated as devices and not drugs. There are approximately 1700 types of medical devices being regulated under this legislation. Device categories include:

1.Over-the-Counter Devices - devices that can be purchased by the consumer without a prescription;
2.Prescription Devices - devices for which adequate directions for use cannot be devised in order to permit lay persons to use the device safely and effectively unless under the supervision and direction of a practitioner;
3.Investigational Devices - devices still in developmental stages and used on human subjects only for purposes of developing safety and effectiveness data;
4.Custom Devices - devices ordered from a manufacturer by health professionals to conform to their special needs or those of an individual patient and not generally available to or generally used by other practitioners; and
5.Critical Devices - devices as defined in the Good Manufacturing Practice (GMP) regulation that are life-sustaining, life-supporting or intended to be implanted into the human body and whose failure can be reasonably expected to result in a significant injury.[2]

6.1 Control categories

There are three control categories that vary in degree of regulation necessary to provide reasonable assurance of safety and effectiveness. Assessment of Classes I, II, or III will be extremely important to medical device developers. Examples of devices similar in nature to our Phase II device follow:

Cardiovascular - Monitoring Devices:[3]

Section	Device	Class
870.2050	Biopotential amplifier and signal conditioner	II
870.2060	Transducer signal amplifier and signal conditioner	II
870.2300	Cardiac monitor (including cardiotachometer and rate alarm	II
870.2360	Electrocardiograph electrode	II
870.2700	Oximeter	II

1. Federal and Drug Administration. Regulatory Requirements for Medical Devices: A Workshop Manual. 1989;. HHS Publication FDA 89-4165.
2. Federal and Drug Administration. Regulatory Requirements for Medical Devices: A Workshop Manual. 1989;. HHS Publication FDA 89-4165.

Section	Device	Class
870.2910	Ear oximeter	II
870.2920	Impedance plethysmograph	II
870.2910	Radiofrequency physiological signal transmitters and receivers	II
870.2920	Telephone electrocardiograph transmitters and receivers	II

Neurology - Diagnostic Devices:[1]

Section	Device	Class
882.1310	Cortical electrode	II
882.1320	Cutaneous electrode	II
882.1330	Depth electrode	II
882.1340	Nasopharyngeal electrode	II
882.1350	Needle electrode	II
882.1400	Electroencephalograph	II
882.1410	Electroencephalograph electrode/lead tester	II
882.1420	Electroencephalogram (EEG) signal spectrum analyzer	I
882.1540	Galvanic skin response measurement device	II
882.1560	Skin potential measurement device	II
882.1835	Physiological signal amplifier	II
882.1845	Physiological signal conditioner	II
882.1855	Electroencephalogram (EEG) telemetry system	II

It is noted that the devices which are most similar in nature to the device Cybernet Systems Corporation will market are the oximeters, which are listed as Class II devices. There are no Class III indications. Class designation from the FDA will determine the requirements that must be met before distribution of the device, within the U.S., may begin.

6.2 Establishment Registration

Domestic establishments engaged in the manufacture, preparation, propagation, compounding, assembly, or processing of medical devices intended for human use and commercial distribution register their establishment with the FDA on Form FDA 2891. Manufacturers and other specified processors of devices must register using this protocol.

Form 2892 is also required to list devices by generic category/classification name. Manufacturers of finished medical devices and manufacturers of components or accessories sold to the end-user are required to submit this form. This action will be performed during the proposed Phase II effort.

---

3. Food and Drug Administration. Classification of Cardiovascular Devices. Federal Register, 5 February 1980 Code of Federal Regulations.
1. Food and Drug Administration. Classification of Neurological Devices. Federal Register, 4 September 1979. Code of Federal Regulations.

6.3 Pre-market Notification: 510(k)

Manufacturers intending to market a new or significantly modified device are required to submit a pre-market notification to the FDA in order to establish substantial equivalence (SE) in terms of safety and effectiveness to a device already on the market in the U.S. prior to the May 28, 1976 enactment date of the Amendments or to a device marketed after that date that has been determined substantially equivalent.

Pre-market notification is meant to:

- Identify new devices that must be placed automatically into Class III and undergo pre-market approval (PMA) or reclassification before they are marketed.
- Classify new devices; A not substantially equivalent (NSE) new device is in Class III, and a substantially equivalent (SE) new device is in the same regulatory class as the device to which it is found equivalent.
- Achieve marketing equity by allowing manufacturers of new devices that are SE to pre-amendments devices to market their devices without facing any greater regulatory burdens than faced by manufacturers of the pre-amendments devices.

Pre-market notification must be submitted to the Center for Devices and Radiological Health (CDRH) at least 90 days before introducing the device into interstate commerce or otherwise holding or offering the device for commercial distribution. CDRH determines whether the device is substantially equivalent (SE) to a device that was or is being marketed based on the information submitted by the manufacturer in the pre-market notification and other information available to the FDA.

After determination of a device performing the same function, comparison can be made regarding the safety and effectiveness of the new device. If differences in the devices do not raise safety and effectiveness questions the device is designated SE. It may be necessary to provide actual test data to demonstrate SE. If the device is considered to be of moderate concern the FDA may request additional information on the software development process. *The purpose of data, such as clinical data, for a pre-market notification submission is to demonstrate that the device is SE in performance to the pre-amendments device.* Final determination of substantial equivalence is left to CDRH. If the device is found to be not substantially equivalent it is automatically classified into Class III and unless reclassified is subject to pre-market approval. If the manufacturer disagrees with the agency decision a petition may be filed for reclassification of the device into Class I or Class II. FDA will accept petitions for review only if there is sufficient data to justify the request.

No formal form is necessary for pre-market notification; however, "510(k) notification" should be contained in the cover letter. If additional information is requested from the reviewers, the 90 day time period stops and begins upon resubmission. This will occur each time additional information is requested. For this reason, providing all documentation to substantiate the manufacturers claim is advisable to expedite the notification period. A summary statement of safety and effectiveness information should be included or alternatively it should be stated that the this information will be made available upon request.

Recommended format for notification 510(k):

The name of the device (both trade, common or usual and classification name.)

The establishment registration number. If not yet registered, a statement to this effect is sufficient.

The class of the device (if known), or a statement that the class is not known, indicating the appropriate panel.

Action taken to conform to any applicable FDA Special Controls for a Class II device, if a special control has been issued.

Proposed labels and labeling for the device, including any advertisements sufficient to describe the intended use of the product. Proposed labeling is sufficient.

Adequate summary of any information known about the device's safety and effectiveness or a statement that such information will be made available upon request by any person.

A statement (with accompanying data) indicating how the device is similar to and/or different from other comparable products that are already in commercial distribution.

We expect that the device proposed in this project will be classified as Class II (i.e. functionally equivalent to existing physiological monitoring devices and oximeters). Thus, we plan a clinical testing and trial task described in Section 7.0 to collect supporting data for this contention (and thus to support 510(k) application for a commercial version of the device).

6.4 510(k) Summaries and Other Considerations

Companies must decide upon submission of a 510(k) summary or statement. 510(k) summaries submitted in pre-market notifications are intended in part for public disclosure. The FDA will make publicly available a list of all premarket notifications submissions for which SE determinations have been made and will provide information as to whether a summary or statement was submitted as part of the application. This information is most accessible through FOI (Federal Information Services) which will assess fees per request.

Companies wishing to retain a shield from public disclosure may apply for confidentiality under the follow conditions:

The device is not on the market.

The intent to market the device has not been previously disclosed.

The firm requests in its 510(k) that FDA treat the submission of the firm's intent to market as confidential information.

Requests must state that:

The intent to market the device in confidential.

The intent to market has not been revealed.

The confidentiality of the firm's intent to market has been protected by the firm.

The firm will notify FDA when the intent to market the device is disclosed or the device is put on the market.

The firm understands the prohibition against submitting false information to the Governments.

The ISO9000 series of international standards for Quality Management and Quality Assurance are currently being applied to the medical community in the form of the new GMP guidelines draft document.[1] These new GMP standards, which all medical manufacturers will be required follow, are based on the ISO Series. The Proposed Revisions of the Current Good Manufacturing Practice (CGMP) Regulations was released in the Federal Register November 23, 1993.[2] These standards, which must also be adhered to for successful worldwide commercialization of the technology proposed in this project, are further discussed in the Phase I final report in Section 7.

7.0 Phase II Experimental and Clinical Trials

The Phase I design effort and simulations establish the capability for deep tissue measurement, and specify optimum design parameters for the sensor. However, while tissue properties have been accurately modeled, physiological characteristics are highly complex and variable. It is therefore important to perform experimental testing of the designed sensor early during the Phase II project, in both test materials and actual physiological tissue. This will provide feedback on the performance of the sensor and allow for optimization of the final Phase II device. This testing process will also identify issues related to specific applications and clinical operability of the device.

7.1 In House Test Procedures

A number of test procedures will performed in house by Cybernet Systems Corporation to evaluate the performance of the early prototype sensor. This testing process will include measurement of absorption coefficients in phantom structures and test solutions or materials. This methodology is commonly used throughout the scientific and medical community for validation of optical sensor performance. Test solutions and materials will be obtained which represent typical characteristics found in physiological tissue. Several commonly used substances among the research community that have well quantified absorption and scattering characteristics are commercially available, such as 'IntraLipid' (Kiba Vitrum Inc., Alameda, CA). Customized production of materials which possess layered absorption structures may also be necessary, for demonstration of the sensor's capability to resolve layered information.

In addition to measurements in phantom and test materials, we will perform some simple tests of sensor performance in human tissue to demonstrate measurement of the physiological parameters under normal conditions. This process will also identify application and attachment issues for

1. Federal and Drug Administration. Regulatory Requirements for Medical Devices: A Workshop Manual. 1989;HHS Publication FDA 89-4165.
2. Food and Drug Administration. Medical Devices; Current Good Manufacturing Practice (CGMP) Regulations; Proposed Revisions; Request for Comments. Federal Register, 23 November 1993. Code of Federal Regulations 21CFR Part820.

measurement of different tissues and at different locations. Furthermore, measurements taken simultaneously with a pulse oximeter will provide a basis for comparison with an established methodology. Indications of sensor performance during conditions of reduced levels of hemoglobin concentration and oxygenation can also be obtained through the use of a blood pressure cuff to momentarily reduce perfusion.

7.2 Experimental Test Procedures - Outside source

In addition to the in house test procedures, it is important to comprehensively evaluate performance of the device under the conditions of abnormal hemoglobin and oxygenation values which will be seen during trauma. The required procedure will need to create varying levels of tissue oxygenation and hemoglobin concentration in a highly controlled manner. As a result, animal testing is required, which will be performed by an outside source.

In the Phase I study we identified sources which have the facilities and expertise to perform the required animal testing. These potential sources include contacts Cybernet has established with the Johns Hopkins University, the University of Michigan Hospital, local commercial testing facilities, or possible DoD participation (as discussed during Phase I with DoD representatives from the Walter Reed Army Institute of Research). Final selection of the source for execution of these experimental tests will be performed early in the Phase II project to ensure adequate preparation and testing time.

To meet the Phase II testing requirements a valid protocol capable of comprehensively evaluating and qualifying the designed sensor must also be established. This will involve creating varying levels of tissue oxygenation and hemoglobin concentration in the animal. Measurements of hemoglobin concentration and oxygenation will then be performed simultaneously using the designed sensor and an established technique. Specific details of the protocol include selection of the animal species, and preparation procedures appropriate for the required testing. Oxygenation levels can be varied in a controlled manner through administration of specific inspired gas mixtures, in the intubated and anesthetized animal.

Established measurement techniques for determination of oxygenation and hemoglobin concentrations, which can be compared to measurements from the designed sensor, include standard arterial blood gas analysis. Of particular importance is the limited response time of blood gas measurement, which may complicate the ability to perform simultaneous equivalent measurements. The need for measurement of localized values is also very important for establishing the depth resolution capabilities of the developed sensor. Tissue pO_2 electrodes, placed directly in the tissue to be measured, may offer a solution to both of these concerns, by providing faster response time and highly localized measurement. However, calibration of measurement to reflect an oxygen saturation value may be difficult. Care must also be taken to ensure that the two measurement techniques do not interfere with each other.

Coordination of the testing effort through the outside source will performed by Cybernet Systems Corporation to ensure that all these requirements are addressed, critical timelines are kept, and complete documentation of the results is prepared.

7.3 Performance evaluation

The testing procedures performed in phantom materials, human tissue, and under the animal protocols will produce a large amount of valuable data for evaluation. Subsequent analysis will be performed, providing a comprehensive evaluation of the sensor performance. Specifically the following analyses will be performed

1) Correlation of measurement results in test materials with the known properties of the material:

This process will identify performance characteristics of the methodology and sensor implementation in the idealized medium. As result, factors due to physiological conditions and variability will not be represented. This allows for identification of performance issues related specifically to the measurement technique and implemented design, not to physiological factors, so that optimization to the design identified.

2) Correlation of measurement results in human tissue with pulse oximetry measurements:

This process will identify performance characteristics of the sensor in physiological tissue, and allow for comparison to pulse oximetry measurement. It is important to be aware that pulse oximetry devices have inherent inaccuracies themselves and are limited to peripheral measurement only.

3) Correlation of measurement results from animal testing with established measurement techniques:

This process will identify performance characteristics of the sensor in physiological tissue under the abnormal conditions which will occur during trauma. This will allow for quantification of accuracy specifications of the device over the complete range of intended operating conditions.

The results of this complete evaluation will produce comprehensive specifications on the device performance, including accuracy, sensitivity, acquisition time, etc. In addition, issues relevant to the clinical implementation, such as ease-of-use and versatility will be identified. Opportunities for improvement of the performance will be determined and the sensor design updated.

8.0 Conclusion

The work presented herein represents an extensive series of efforts towards the development of an optical sensor for measurement of oxygenation within deep tissue. This Phase I project established feasibility of the developed concept, and prepared detailed design requirements for a Phase II prototype. Analyses indicate that the device will meet the intended goal, by providing measurement of tissue oxygenation up to 2 cm deep. Furthermore, the designed sensor will also provide measurement of oxy- and deoxy-hemoglobin concentrations up to 2 cm deep.

As a result of this Phase I effort, realization of a device for measurement of deep tissue oxygenation now becomes a sensor development task, as proposed for the Phase II project.

The benefits offered by the proposed sensor will be significant, as there is currently a great need

for non-invasive, portable techniques for measurement of critical physiological parameters, such as tissue oxygenation, within deep tissue. The device designed in this Phase I addresses this need and extends capabilities beyond current commercial, prototype, and research devices. Specifically, the designed device:

- Uses a reflectance technique for measurement at any location,
- Implements an advanced frequency domain methodology for quantization of hemoglobin concentrations,
- Uses an array of detectors, with small increments in source-to-detector distance, for high resolution of spatial variations in reflected light-- corresponding to resolution of depth variations,
- Implements pattern recognition techniques to reconstruct absorption values in a layered structure up to 2 cm deep.

The proposed device is therefore a uniquely advanced concept which offers capabilities beyond all known commercial, prototype, and research techniques for optical measurement of tissue. It avoids the inaccuracies due to peripheral vasoconstriction by measuring at non-peripheral locations, and provides measurement into deeper tissue. The device also has a greater capability for measuring oxygenation and hemoglobin concentrations within specific physiological structures and systems.

References

Altman DG, Bland JM. Measurement in medicine: The Analysis of Method Comparison Studies. The Statistician 32:307-317, 1983.

Ancoli-Israel S. Ambulatory Cassette Recording of Sleep Apnea. Ambulatory EEG Monitoring edited by John S. Ebersole, Raven Press 1989.

Aronson R. Exact interface conditions for photon diffusion. Physiological Monitoring and Early Detection Diagnostic Methods. Los Angeles, CA, USA., Proceedings of SPIE - The International Society for Optical Engineering v 1641. Publ by Int Soc for Optical Engineering, Bellingham, WA, USA. p 72; 1992.

Arridge SR, van der Zee P, Cope M, Delpy DT. Reconstruction methods for infra-red absorption imaging. Los Angeles, CA, USA., Proceedings of SPIE - The International Society for Optical Engineering v 1431. Publ by Int Soc for Optical Engineering, Bellingham, WA, USA. p 204-215; 1991.

Awazu K, Niwa S, Matsubara H, Namihisa T. An instrument for liver function testing using an optical sensor. IECON Proceedings (Industrial Electronics Conference) v 3. Publ by IEEE, Computer Society, Los Alamitos, CA, USA (IEEE cat n 91CH2976-9). p 2420-2425; 1991

Barbour RL, Graber HL, Aronson R, Lubowsky J. Imaging of subsurface regions of random media by remote sensing. Los Angeles, CA, USA., Proceedings of SPIE - The International Society for Optical Engineering v 1431. Publ by Int Soc for Optical Engineering, Bellingham, WA, USA. p 192-203; 1991.

Barbour RL, H. L. Graber, J. Lubowsky, R. Aronson, B. B. Das, K. M. Yoo, R. R. Alfano, Imaging of diffusing media by a progressive iterative backprojection method using time-domain data. Physiological Monitoring and Early Detection Diagnostic Methods. Los Angeles, CA, USA., Proceedings of SPIE - The International Society for Optical Engineering v 1641. Publ by Int Soc for Optical Engineering, Bellingham, WA, USA. p 24; 1992.

Benaron D, Lennox, M, Stevenson K,. Two-dimensional and 3-D images of thick tissue using time-constrained times-of-flight and absorbance spectrophotometry. Physiological Monitoring and Early Detection Diagnostic Methods. Los Angeles, CA, USA., Proceedings of SPIE - The International Society for Optical Engineering v 1641. Publ by Int Soc for Optical Engineering, Bellingham, WA, USA. p 35; 1992.

Bronzino J. Biomedical Engineering and Instrumentation Basic Concepts and Applications. PWS Publishers 158-164; 171-4, 1986.

Bruce, Neil C., Scattering from dense volumes, Proceedings of the 16th Congress of the International Commission for Optics., Optics as a Key to High Technology Proceedings of SPIE - The International Society for Optical Engineering v 1983 pt 2, p 891-892; 1993.

Burch, Christina L., Suddeath, Lee F. Sevick, Eva M., Localization and quantitative spectroscopy of phosphorescence and fluorescence signals for noninvasive monitoring in tissues, Proceedings of the Conference on Lasers and Electro-Optics. Anaheim, CA, USA. Optical Society of America. IEEE/Lasers and Electro-Optics Society. European Physical Society.

Caplan RA, Ward RJ, Posner K, Chceney FW. Unexpected Cardiac Arrest During Spainal Anesthesia: A Closed Claims Analyusis of Predisposing Factors. Anestestiology 68: 5-11, 1988.

Chance, B. NIR spectroscopy of adult human brain: continuous-light and pulse-light spectroscopy. Physiological Monitoring and Early Detection Diagnostic Methods. Los Angeles, CA, USA., Proceedings of SPIE - The International Society for Optical Engineering v 1641. Publ by Int Soc for Optical Engineering, Bellingham, WA, USA. p 162; 1992.

Chance B, Wang NG, Maris M, Nioka S, Sevid E. Quantitation of Tissue Optical Characteristics and Hemoglobin Desaturation By Time and Frequency Resolved Multi-Wavelength Spectrophotometry. Oxygen Transport to Tissue 14;297-304:1992.

Clark J. The electrocardiogram, Chapter 4 -- The origin of biopotentials. Medical Instrumentation Application and Design edited by John G Webster Houghton Mifflin Company 197-207, 1978.

Cote GL, Fox MD, Northrop RB. Non-invasive optical polarimetric glucose sensing using a true phase measurement technique. IEEE Trans. Biomed. Engin. 1992;39(7):752-6.

Crease, Robert P., Biomedicine in the age of imaging, Science; v 261 n 5121 Jul 30 1993.

Cui W, Kumar C, Chance B. Experimmental study of migration depth for the photons measured at sample surface. Los Angeles, CA, USA., Proceedings of SPIE - The International Society for Optical Engineering v 1431. Publ by Int Soc for Optical Engineering, Bellingham, WA, USA. p 180-191; 1991.

Cysewska-Sobusiak, Anna. Utilization of spectrophotometric technique in noninvasive detection of hypoxemia impendence, Holography, Interferometry, and Optical Pattern Recognition in Biomedicine III. Los Angeles, CA, USA., Proceedings of SPIE - The International Society for Optical Engineering v 1889 1993. Publ by Society of Photo-Optical Instrumentation Engineers, Bellingham, WA, USA. p 48-57, 1993.

Delpy DT, Cope M, Van der Zee P, Arridge S, Wray S, Wyatt J. Estimation of Optical Path Length. Phys Med Biol 33;1433-42:1988.

Dujovny, Manuel M. D., Lewis, Gary D., Vinas, Federico M. D., Ausman, James I. M. D., Silva, Hugo M. D., Flemming, James M., Cerebral oxygen saturation as a function of age, sex, and skin, color., Physiological Monitoring and Early Detection Diagnostic Methods. Los Angeles, CA, USA., Proceedings of SPIE - The International Society for Optical Engineering v 1641. Publ by Int Soc for Optical Engineering, Bellingham, WA, USA. p 126-132; 1992.

Fantini S, Franceschini MA, Gratton E. Semi-infinite-geometry boundary problem for light migration in highly scattering media: a frequency-domain study in the diffusion approximation. J. Opt. Soc. Am B 1994;11(10):2128-2138.

Fantini S, Franceschini MA, Fishkin JB, Barbieri B, Gratton E. Quantitative determination of the absorption spectra of chromophores in strongly scattering media: a light-emitting-diode based technique. Applied Optics 1994;33(22):5204-5213.

Fantini S, Franceschini-Fantini MA, Maier JS, Walker SA. Frequency-domain multichannel optical detector for non-invasive tissue spectroscopy and oximetry. Optical Engineering 1995;34(1):32-42.

Faris, F., Doyle, M., Wickramasinghe, Y., Houston, R., Rolfe, P., O'Brien, S., Non-invasive optical technique for intrapartum fetal monitoring: preliminary clinical studies, Medical Engineering & Physics; v 16 n 4 July 1994. p 287-291, 1994.

Fugimoto, J.G., Izatt, J.A., Hee, M.R., Bouma, B., Swanson, E.A., Lin, C.P., Puliafito, C.A., Biological imaging using optical coherence tomography and microscopy, Proceedings of the 5th European Quantum Electronics Conference -Technical Digest 1994. EPS-Quantum Electronics and Optics Division. IEEE. Optical Society of America, IEEE, Piscataway, NJ, USA. p 20-21, 1994

Gilboy NS, McGaffigan PA. Noninvasive Monitoring Of Oxygenation With Pulse Oximetry. J of Emergency Medicine. 1989:15;26-31.

Giunta F, Brandi LS, Mazzanti T, Oleggini M, Tulli G, Cuttano AMR. The Relationships Between Oxygen Delivery and Consumption and Continuous Mixed Venous Oximetery are Predictive Parameters in Septic Shock. Oxygen Transport to Tissue XIV, Edited by Erdmann W and Bruley DF. Plenum Press, NY, 1992.

Godik, E. E., Gulyayev, Yu. V., Human body through the 'eyes of radiophysics'., Telecommun Radio Eng; v 46 n 9 Sep 1991 p 90-99; 1991.

Goldman, L., Kerr, J.H., Laser-induced subsurface imagery 1B transillumination with fiber optics, Physiological Monitoring and Early Detection Diagnostic Methods. Los Angeles, CA, USA., Proceedings of SPIE - The International Society for Optical Engineering v 1641. Publ by Int Soc for Optical Engineering, Bellingham, WA,

USA. p 2-5; 1992.

Graber HL, Barbour RL, Lubowsky J , Aronson R, Das BB, Yoo KM, Alfano RR. Evaluation of steady-state, time- and frequency domain data for the problem of optical diffusion tomography. Physiological Monitoring and Early Detection Diagnostic Methods. Los Angeles, CA, USA., Proceedings of SPIE - The International Society for Optical Engineering v 1641. Publ by Int Soc for Optical Engineering, Bellingham, WA, USA. p 6; 1992.

Haaland DM, Ward KJ, Robinson MR, Eaton RP. Quantitative IR spcectroscopy of flucose in blood using partial least-squares analyses. 7th International Conference on Fourier Transform Spectroscopy, 1989, p. 607.

Haselgrove J, Leigh J, Yee C, Wang N, Maris M, Chance B. Monte Carlo and diffusion calculations of photon migration in non-infinite highly scattering media. Proc. SPIE (1991) Vol. 1431:30-41.

Hielscher, Andreas H., Tittel, Frank K., Jacques, Steven L., Noninvasive monitoring of blood oxygenation by phase resolved transmission spectroscopy, Photon Migration and Imaging in Random Media and Tissues. Los Angeles, CA, USA. SPIE - Int Soc for Opt Engineering, v 1888, p 275-288, Bellingham, WA USA; 1993.

Hong, HynnDae, Fox, Martin D., Optical interferometric sensing of skin vibration, Proceedings of the 15th Annual International Conference of the IEEE Engineering in Medicine and Biology Society. San Diego, v 15 pt 2 1993. Publ by IEEE, IEEE Service Center, Piscataway, NJ, USA. p 894-895; 1993.

Hong, HyunDae, Fox, Martin D., Detection of skin displacement and capillary flow using an optical stethoscope, Proceedings of the 1993 IEEE 19th Annual Northeast Bioengineering Conference. Newark, NJ, USA., p 189-190; 1993.

Kessler M, Frank K, Hoper J, Tauschek D, Zundorf J. Reflection spectrometry. Oxygen Transport to Tissue XIV, Edited by Erdmann W and Bruley DF. Plenum Press, NY, 203-12: 1992.

Klose, Peter H., Lewis, Gary D., Messing, W., Kasperski, Randal, Flemming, James M., Noninvasive infrared cerebral oximetry., Physiological Monitoring and Early Detection Diagnostic Methods. Los Angeles, CA, USA. , Proceedings of SPIE - The International Society for Optical Engineering v 1641. Publ by Int Soc for Optical Engineering, Bellingham, WA, USA. p 202-207; 1992.

Koelink MH, de Mul FF, Greve J. Monte Carlo simulations and measurements of signals in laser Doppler flowmetry on human skin. Proc. SPIE (1991) Vol. 1431:63-72.

Lawson D, Norley I, Korbon G, Loeb R, Ellis J. Blood Flow Limits and Pulse Oximeter Signal Detection. Anesthesiology 1987:67;599-603.

Levine SP, Lowry SR, Puskar MA. Computerized infrared spectral identification of compounds frequently found at hazardous waste sites. Analytical Chemistry 58:1156-62 May '86

Lewis, Gary D., Flemming, James M., Widman, Ronald A., Infrared cerebral oximeter: summary of recent clinical case histories., Physiological Monitoring and Early Detection Diagnostic Methods. Los Angeles, CA, USA, Proceedings of SPIE - The International Society for Optical Engineering v 1641. Publ by Int Soc for Optical Engineering, Bellingham, WA, USA. p 194-201; 1992.

Liem, K. D., Oeseburg, B., Hopman, J. C. W., Method for the fixation of optrodes in near-infra-red spectrophotometry., Med Biol Eng Comput; v 30 n 1 Jan 1992 p 120-121; 1992

Liepsch, Dieter. Poll, Axel. Pflugbeil, Gottlieb. In vitro laser anemometry blood flow systems. Proceedings of SPIE - The International Society for Optical Engineering v 2052 1993. Publ by Society of Photo-Optical Instrumentation Engineers, Bellingham, WA, USA. p 163-178;1993

Luebbers, D.W. Chemical in vivo monitoring by optical sensors in medicine. Sensors and Actuators, B: Chemical; v B11 n 1-3 Mar 1 1993. p253-262; 1993

Madsen SJ, Patterson MS, Wison BC, Park YD, Moulton JD, Jacques SL. Time-resolved diffuse refectgance and transmittance studies in tissue simulating phantoms: a comparison between theory and experiment. Los Angeles,

CA, USA., Proceedings of SPIE - The International Society for Optical Engineering v 1431. Publ by Int Soc for Optical Engineering, Bellingham, WA, USA. p 42-51; 1991.

Maris MB, Mayevsky A, Sevick EM, Chance B. Frequency-domain measurements of changes of optical pathlength during spreading depression in a rodent brain model. Los Angeles, CA, USA., Proceedings of SPIE - The International Society for Optical Engineering v 1431. Publ by Int Soc for Optical Engineering, Bellingham, WA, USA. p 122-135; 1991.

Marquardt LA, Arnold MA, Small GW. Near-infrared spectroscopic measurement of glucose in a protein matrix. Analytical Chemistry 65:3271-8 Nov 15 '93

McCrae D, Saaski E, Wolthuis R. Development of a medical fiber-optic pH sensor based on optical absorption. IEEE Transactions on Biomedical Engineering 30:531-7, May 1992.

Mendelson Y, McGinn MJ. Skin Reflectance Pulse Oximetry: In Vivo Measruements From the Forarm and Calf. J Clin Monitoring 7;7-12:1991.

Mendelson Y, Kent JC, Yocum BL, Birle MJ. Design and Evaluation of a New Reflectance Pulse Oximeter Sensor. Biomed Instrum Technol 22(4); 167-73: 1988.

Mendelson Y, Ochs BD. Noninvasive Pulse Oximetry Utilizing Skin Reflectance Photoplethysmography. IEEE Trans Biomed Eng 35(10); 798-805:1988.

Mitchell G, Hartl J, Wolthuis R. Development of a dual function sensor system for measuring pressure and temperature at the tip of a single optical fiber. IEEE Transactions on Biomedical Engineering 40:298-302, May 1993.

Miyasaka K, Katayama M, Kusakawa I, Ohata J, Kawano T, Honma Y. Use of Pulse Oximetry In Neonatal Anesthesia. J Perinatology. 1987:7;343-5.

Nishimura S, Tomita Y, Horiuchi T. Clinical application of an active electrode using an operation amplifier. IEEE Transactions on Biomedical Engineering Vol 39 No 10 Oct 1992.

Osawa, Masahiko, Niwa, Shinichiro, Portable diffuse reflectance spectrophotometer for rapid and automatic measurement of tissue, Measurement Science & Technology; v 4 n 6 Jun 1993. p 668-676, 1993.

Pan, L., Amory, D., Li, J.K.-J., Kalatzis-Manolakis, E.S., Improved design of a noninvasive near-infrared brain,oxygenation monitor, Proceedings of the 1993 IEEE 19th Annual Northeast Bioengineering Conference. Newark, NJ, USA. p 31-32; 1993.

Preininger C, Klimant I, Wolfbeis OS. Optical fiber sensor for biological oxygen demand. Analytical Chemistry 66:1841-6 Jun 1, 1994.

Pullerits J, Burrows FA, Roy WL. Arterial Desaturation in Healthy children During Transfer to the Recovery Room. Can J Anaest 34: 470-473, 1987.

Ralston AC, Webb RK, Runciman WB. Potential Errors in Pulse Oximetry. Part I: Pulse Oximeter Evaluation. Anaesthesia 1991:46;202-6.

Riley T, Mounaimne M, Goodman S, Carasea K. Diagnosis of Narcolepsy Using a 24-Hour Portable Recorder. *Postgraduate Medicine* July 82

Schlereth F, Fossaceca JA, Keckler AD, Barbour RL. Imaging in diffusing media with a neural net formulation: a problem in large-scale computation. Physiological Monitoring and Early Detection Diagnostic Methods. Los Angeles, CA, USA., Proceedings of SPIE - The International Society for Optical Engineering v 1641. Publ by Int Soc for Optical Engineering, Bellingham, WA, USA. p 46; 1992.

Schmitt, Joseph M., Zhou, Guan-Xiong, Miller, Justin, Measurement of blood hematocrit by dual-wavelength near-IR photoplethysmography., Physiological Monitoring and Early Detection Diagnostic Methods. Los Angeles, CA, USA. , Proceedings of SPIE - The International Society for Optical Engineering v 1641. Publ by Int Soc for

Optical Engineering, Bellingham, WA, USA. p 150-161; 1992.

Severinghous JW. Continuous Monitoring of Arterial O_2: What's the Quality of the Monitors and Should We Use Them? University of Chicago Continuing Education Use and Interpretation of Monitoring and New Technologies. Sept. 10, 1988.

Shepherd AP,Steinke, JM. Diffusion model of the optical absorbance of whole blood. Journal of the Optical Society of America. A, Optics and Image Science 5:813-22 Jun '88

Shimizu, Koichi, Kitama, Masataka, Mouri, Mitsuhiro, Yamamoto, Katsuyuki, Noninvasive measurement of physiological functions in a living body by transillumination, Proceedings of the IEEE Instrumentation and Measurement Technology Conference 2 1994. p 982-985; 1994, IEEE. The Society of Instrument and Control Engineers, Japan.

Smith PR, Ruiz de Marquez G, Thomason H. Optical analysis of Blood in motion distinguishing absorption from multiple scattering. Optical Biopsy and Fluorescence Spectroscopy and Imaging, 1995, p. 103-108.

Soliman IE, Patel RI, Ehrenpreis MB, Hannallah RS. Recovery Score Do Not Correlate with Post-Operative Hypoxemia in Children. Anest Analg 67:53f-56, 1988.

Svaasand, L.O., Tromberg, B.J., Haskell, R.C., Time resolved reflectance, Proceedings of the 1994 Conference on Lasers and Electro-Optics Europe - Technical Digest. EPS- Quantum Electronics and Optics Division. IEEE. Optical Society of America. IEEE, Piscataway, NJ, USA,94TH0614-8. p 286-287, 1994.

Takatani, Setsuo, Ling, Jian, Optical oximetry sensors for whole blood and tissue, IEEE Engineering in Medicine and Biology; v 13 n 3 Jun-Jul 1994. p 347-357; 1994.

Takatani S, Ling J. Optical Oximetry Sensors for Whole Blood and Tissue. IEEE EMB13(3);347-57:1994.

Tarassenko L, Lee VS. Absorption and multiple scattering by suspensions of aligned red blood cells. Journal of the Optical Society of America. A, Optics and Image Science 8:1135-41 Jul '91

Tompkins WJ, Webster JG. Design of Microcomputer-Based Medical Instrumentation. Prentice-Hall, Inc. 335-9, 1981.

Tsai, Cheng-Lun, Fouke, Janie M., Noninvasive detection of water and blood content in soft, tissue from the optical reflectance spectrum, Photon Migration and Imaging in Random Media and Tissues. Los Angeles, CA, USA., Proceedings of SPIE - The International Society for Optical Engineering v 1888 1993. Publ by Society of Photo-Optical Instrumentation Engineers, Bellingham, WA, USA. p 479-486; 1993

Tyler IL, Tanisira B, Winter PM, Motoyama EK: Continuous Monitoring of Arterial Wxygen Saturation With Pulse Oximetry During Transfer to the Recovery Room. Anest Analg 64: 1108-1112, 1985.

Wang Y, J. Chang, R. Aronson, R. L. Barbour, H. L. Graber, J. Lubowsky, Imaging of scattering media by diffusion tomography: an iterative perturbation approach. Physiological Monitoring and Early Detection Diagnostic Methods. Los Angeles, CA, USA., Proceedings of SPIE - The International Society for Optical Engineering v 1641. Publ by Int Soc for Optical Engineering, Bellingham, WA, USA. p 58; 1992.

Ward KJ, Haaland DM. Robinson MR, Eaton RP. Quantitative IR spcectroscopy of glucose in blood using partial least-squares analyses. 7th International Conference on Fourier Transform Spectroscopy, 1989, Proc SPIE Vol. 1145, p. 607-8.

Wickramasinghe, Yapa A., Rolfe, Peter, Palmer, K., Watkins, S., Spencer, S.A., Doyle, M., O'Brien, S., Walker, A., Rice, C., Smallpeice, C., Development and clinical evaluation of noninvasive near-infrared monitoring of cerebral oxygenation, Proceedings of SPIE - The International Society for Optical Engineering; v 2085 1994. p 29-37, 1994

Wilson BC. Optical Properties of Tissues. Encyclopedia of Human Biology. Academic Press, 1991, Vol. 5: 587-597.

Winter LD, Prokop RA. Venkateswarlu P. Automated molecular absorption spectrometry for determination of fluorine in biological samples.

Wolthuis R, Mitchell G, Hartl J, Saaski E. Development of a dual function sensor system for measuring pressure and temperature at the tip of a single optical fiber. IEEE Trans. Biomed. Engin. 1993;40(3):298-302.

Wolthuis R, McCrae D, Saaski E, Hartl J, Mitchell G. Development of a medical fiber-optic pH sensor based on optical absorption. IEEE Trans. Biomed. Engin. 1992;39(5):531-537.

Received 2/8/2000

DEPARTMENT OF THE ARMY
US ARMY MEDICAL RESEARCH AND MATERIEL COMMAND
504 SCOTT STREET
FORT DETRICK, MARYLAND 21702-5012

REPLY TO
ATTENTION OF:

MCMR-RMI-S (70-1y) 21 Jan 00

MEMORANDUM FOR Administrator, Defense Technical Information Center, ATTN: DTIC-OCA, 8725 John J. Kingman Road, Fort Belvoir, VA 22060-6218

SUBJECT: Request Change in Distribution Statement

1. The U.S. Army Medical Research and Materiel Command has reexamined the need for the limitation assigned to technical reports written for the attached Awards. Request the limited distribution statements for Accession Document Numbers listed be changed to "Approved for public release; distribution unlimited." These reports should be released to the National Technical Information Service.

2. Point of contact for this request is Ms. Virginia Miller at DSN 343-7327 or by email at virginia.miller@det.amedd.army.mil.

FOR THE COMMANDER:

Phylis Rinehart

Encl
as

PHYLIS M. RINEHART
Deputy Chief of Staff for
Information Management